Mechanically stable and environmentally friendly polymer/particle composites for the application as low-fouling coating in the marine sector

Dissertation

zur Erlangung des akademischen Grades
Doktor der Ingenieurwissenschaften
(Dr.-Ing.)
der Technischen Fakultät
der Christian-Albrechts-Universität zu Kiel

Iris Hölken
Kiel
2016

Erstgutachter: Dr. habil. Yogendra Kumar Mishra

Zweitgutachter: Prof. Dr. Lorenz Kienle

Datum der mündlichen Prüfung: 16.09.2016

Abstract

Biofouling, the attachment of marine organisms to surfaces subjected to aquatic environments, is one of the major problems within marine technology. For its prevention, biocide-containing paints were most prevalent up to the beginning of the 21th century. Since the detection of their negative impact on the ecosystem and the resulting prohibition, the development of biocide-free ecofriendly antifouling solutions is strongly required. In this work, novel ecofriendly and durable antifouling coatings on the basis of a two-component thermoset polythiourethane (PTU) have therefore been developed.

Initially, the material properties of PTU are mechanically and chemically characterized with respect to stoichiometric component-variations. Long-term immersion experiments are conducted in two habitats. Further development of PTU towards higher mechanical stability is obtained by incorporation of tetrapodal-shaped ZnO (t-ZnO) micro- and nanoparticles. The filler amount is varied in a wide range and all results are compared to PTU references using commercially available spherical ZnO (s-ZnO) particles. An increase in tensile strength as well as in the adhesion to metal substrates is shown in dependency of the filling factor. Wettability measurements as well as the evaluation of the surface free energy with its polar and dispersive fractions reveal an impact of t-ZnO incorporation. Preliminary immersion experiments show the reduction of marine fouling as a result of increasing t-ZnO incorporation and based on these results, long-term field experiments are realized in two habitats (seawater, freshwater). A residue-free clean-ability is demonstrated after 12 months of immersion.

Furthermore, the well-known fouling-release material silicone is reinforced by t-ZnO in order to enhance the mechanical stability. Tensile strengthening as a function of increasing filler amount is evaluated and the chemical fingerprint is determined accordingly. Immersion experiments are implemented, the reduction of fouling when compared to PTU is demonstrated. The lack of mechanical stability of the silicone/t-ZnO composites is shown by cleaning as it causes significant damages. Consequently, the fouling-release properties of silicones are combined with the mechanical features of PTU by the fabrication of PTU/silicone composites with additional reinforcement by t-ZnO micro- and nanoparticles. The two one-component silicones ETAS and MTAS are chosen for further experiments. Their appropriate amount as well as the stirring time of the components are accordingly characterized. The increase in tensile strength of PTU/silicone composites is shown as a function of t-ZnO filler content. Surface characteristics demonstrate the formation of silicone microdomains on the surface of the composites embedded into the PTU matrix. The wetting behavior underlines the retention of the silicones surface properties. Immersion results from seawater and subsequent cleaning show convincing easy-to clean features for all PTU/ETAS composites. On the other hand, those samples immersed into freshwater demonstrate self-cleaning properties for PTU/ETAS composites filled with ZnO particles of arbitrary morphology.

Kurzfassung

Der Begriff Biofouling beschreibt das Anhaften von Organismen an Oberflächen, die Gewässern ausgesetzt sind. Da dieses Phänomen in der maritimen Technologie ein immenses Problem darstellt, kamen bis Ende des 21. Jahrhunderts biozidhaltige Antifoulingbeschichtungen zum Einsatz, die den Bewuchs erfolgreich verhindern konnten. Nachdem jedoch negative Einflüsse auf das Ökosystem festgestellt wurden, trat ein Verbot für den Einsatz derartiger Beschichtungen in Kraft. Seitdem ist die Entwicklung von umweltfreundlichen Alternativen im Fokus der Wissenschaft. Thema dieser Arbeit war daher die Herstellung eines umweltfreundlichen und langzeitstabilen Antifoulingsystems auf Basis eines zweikomponentigen duroplastischen Polythiourethans (PTU).
Zunächst werden die Materialeigenschaften des PTUs mechanisch und chemisch charakterisiert, wobei der Einfluss von Stöchometrievariationen im Vordergrund steht. Langzeitversuche in zwei verschiedenen Habitaten zeigen das Bewuchsverhalten. Zur Verstärkung des PTU-Systems kommen im Weiteren tetrapodale Zinkoxid (t-ZnO) Mikro- und Nanopartikel zum Einsatz. Der Füllstoffanteil wird über ein breites Spektrum variiert, zudem erfolgt der Vergleich zu kommerziell erhältlichen sphärischen ZnO-Partikeln (s-ZnO). Durch das Einbringen tetrapodalen Partikelin resultiert ein Anstieg der Zugfestigkeit sowie eine starke Verbesserung der Haftungseigenschaften zu Metalloberflächen. Ein Einfluss der t-ZnO Partikel bezüglich der Benetzungseigenschaften sowie der freien Oberflächenenergie und deren polarer und dispersiver Anteile wird aufgezeigt. Vorläufige Studien im Aquarium Geomar ergeben eine starke Bewuchsminderung für mit t-ZnO gefüllte PTU-Proben. Basierend auf diesen Ergebnissen werden Langzeitfeldversuche in Salzwasser und Süsswasser durchgeführt, bei denen der positive Einfluss der t-ZnO Partikel jedoch nicht auftritt. Das Hochdruckreinigen der Proben nach zwölfmonatiger Immersion führt allerdings zu rückstandsfreien Probenoberflächen und demonstriert die hervorragenden Reinigungseigenschaften des PTU. Des Weiteren werden t-ZnO-Partikel in das bekannte fouling-release (FR) Material Silikon eingebracht, um eine hinreichende mechanische Stabilität zu erlangen. Der Anstieg der Zugfestigkeit als Funktion der t-ZnO Partikel wird dargestellt, desweiteren erfolgt eine chemische Charakterisierung. Langzeitfeldversuche in zwei Habitaten zeigen eine Bewuchsminderung auf allen Silikonproben im Vergleich zu PTU. Durch Hochdruckreinigung wird jedoch die unzureichende Stabilität der Silikonproben aufgezeigt da signifikante Schäden an den Oberflächen auftreten. Hieraus ergibt sich der Versuch, die hervorragenden mechanischen Eigenschaften von PTU mit den FR-Eigenschaften von Silikon zu verbinden. Hergestellt werden PTU/Silikon-Komposite, die eine zusätzliche Verstärkung durch tetrapodale ZnO-Partikel erfahren. Die zwei Einkomponentensysteme MTAS und ETAS kommen im Weiteren zum Einsatz. Ein Anstieg der Zugfestigekit durch das Einbringen von t-ZnO kann aufgezeigt werden. Oberflächencharakterisierungen zeigen die Formation von Silikonmikrodomänen an der Oberfläche der PTU/Silikon-Komposite, darüber hinaus verdeutlicht das Benetzungsverhalten den Erhalt der Oberflächeneigneschaften von Silikon auf den Probenoberflächen. Bewuchsstudien mit anschliessender Hochdruckreinigen zeigen überzeugende Reinigungseigenschaften der PTU/ETAS Komposite, desweitern kann ein signifikanter Einfluss der ZnO-Füllpartikel auf den Bewuchs von PTU/ETAS innerhalb der Süsswasserumgebung festgestellt werden.

Contents

List of Figures

Chapter 1

1 Introduction

Biofouling describes the undesired growth of marine organisms on any surface immersed into water [1, 2] (figure 1). It is one of the most important topics in the marine sector as it brings along major challenges with respect to economic and ecologic aspects in shipping [3, 4]. In addition, the efficiency is tremendously impacted [5, 6]. Weight gain resulting from hard fouling elements like barnacles and mussels combined with elevated hydrodynamic drag resistance caused by increased surface roughness lead to additional fuel consumption of up to 40 % [7].

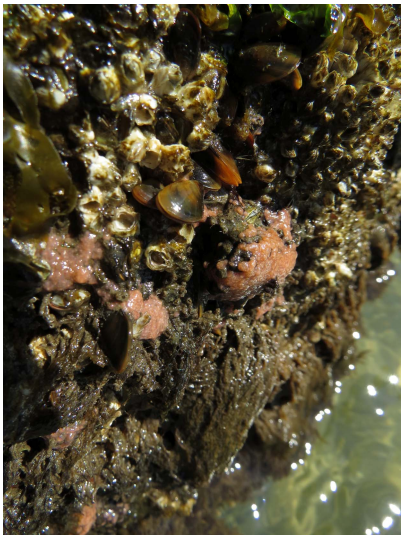

Figure 1: Different fouling species like barnacles and mussels on a stone.

A study by Schultz et al. [8] provides an overview on the costs caused by biofouling of a naval ship hull. Considering the increased fuel consumption, the coating itself arises to an amount of $ 56 M per year [8].

However, not only the increased fuel consumption, the transport costs and the maintenance costs of ships are affected. Greenhouse gas emission as critical environmental pollution is another direct result of biofouling [9, 10]. Furthermore, fouling organisms can spread over large distances which impacts the ecosystem worldwide as species are exchanged and therefore affect the local marine flora and fauna [11, 12]. Besides ships, also stationary maritime structures such as bases for wind turbines or oil platforms are impacted by biofouling, as they suffer from biocorrosion, the materials degradation due to aquatic organisms [7, 13].

With the introduction of tributyltin (TBT)-based antifouling coatings in the 1950s, a convenient solution for the combat of biofouling was provided. The efficiency of these coatings was based on self-polishing polymers which rely on the principle that the polymeric matrix is continuously degraded and thereby releasing toxic additives [14]. However, at the end of the 1970s, investigations on the impact of these biocides on non-target organisms within the marine environment revealed an alarming situation. A study on the embryogenesis and larval state of oysters showed negative influence, as the molluscs suffered from complete lack of reproduction accompanied by the development of cell calcification anomalies even at very low concentrations [15]. Due to these observations, a global regulation was initiated in 2003 which included the complete prohibition of TBT-containing coatings for the marine sector [16, 17, 18]. In 2008, this regulation became valid when the International Maritime Organization (IMO) banned TBT based coatings [19]. A convincing substitute was introduced by copper based systems in combination with organic biocides [20, 21, 22]. But these paints also showed negative impacts on the environment. Consequently they are pending prohibition within the next years [23, 24].

In recent years many research groups focused on the development of ecofriendly antifouling solutions which do not contain any harmful additives. Most prominent are the so-called fouling release (FR) coatings, which rely on the principle that marine organisms cannot adhere properly to their surface. At a certain vessel speed, their attachment to the hull is not strong enough to withstand the arising shear forces and they simply get washed off [25]. Most of these FR properties are based on low elastic moduli polymers with low surface energy [26]. From the materials perspective up to now only fluoropolymers and silicones can fulfill these requirements. As silicones provide outstanding FR features over fluoropolymers, nowadays they are the most prominent ecofriendly antifouling alternatives [27]. On the other hand, the major drawback of FR paints is the lack of mechanical stability including poor adhesion to the substrate. Therefore, the currently available coatings cannot provide long-lasting antifouling protection. As a consequence, the

development of more reliable alternatives is urgently needed [28].
In order to fabricate an antifouling coating which can fulfill the requirements of being non-toxic and simultaneously mechanically stable, a suitable polymer matrix needs to be selected. Besides convincing mechanical features, it should provide stability towards environmental conditions, e.g. UV-light, saltwater and biocorrosion. In addition, it should be processable on a large scale to ensure the desired industrial compatibility. From the polymeric family, polyurethanes offer a great variety of products as their main components isocyanate and dialcohol can be combined in a way that offers the desired characteristics. At first, it is essential that the processing is possible without the utilization of solvents which contain environmentally harmful constituents. In order to ensure UV-stability, aliphatic isocyanates are best suited as they are free from UV-instable aromatic rings [29]. Large scale application is usually conducted via spraying techniques where short curing times are preferable. In this context, high reactivity is provided by sulphur containing dialcohols. An aliphatic solvent-free polythiourethane (PTU) (thiol = -SH group) was therefore used in this work as base material for varying material modifications in order to gain an environmentally friendly antifouling coating.
To obtain additional mechanical stability, the chosen polymeric matrix can be reinforced by additives [30]. It was already shown by Niu et al., that nano- and microstructures from inorganic materials have a strong impact on the mechanical properties of polymeric materials [31]. A remarkable size and shape dependency of the particles on the polymer features was reported. For this reason, zinc oxide filler particles with their enormous spectrum of different nano- and microstructures offer promising reinforcing properties as filler material [32, 33]. Due to the necessity of large-scale production, the recently developed flame-transport synthesis (FTS) [33] enables the fabrication of complex shaped three-dimensional ZnO tetrapodal structures (t-ZnO), which have already proven to be beneficial in a lot of applications. Besides the possibility to combine the two extremely low surface energy polymers silicone and teflon by simple mechanical interlocking mechanisms [34], ZnO tetrapods can also be used to realize self-reporting materials [35] as to name only two prominent examples. In addition, t-ZnO particles have proven to be biocompatible [36].

Another approach of this work is the combination of PTU with different silicone elastomers in order to fabricate phase separating composites. These kind of composites, where the mechanical stability of a robust matrix polymer is combined with the properties of fouling-release surfaces, have already proven to show promising FR features [37]. However, the results were only preliminary and the utilization of the material suffered from the incompatibility with large-scale application.

Aim of this work is the development of an environmentally friendly, mechanically stable and industrially processable antifouling coating based on a solvent-free polythiourethane.

This thesis is structured as follows: the fundamental theoretical considerations including essential aspects of biofouling and antifouling are outlined in chapter 2. Chapter 3 deals with the methods utilized for the material characteristics as well as its antifouling behavior. Chapter 4 covers the complete mechanical and chemical characterization of the matrix polymer PTU with additional results from immersion-experiments. Chapter 5 deals with the incorporation of ZnO filler particles and their influence on mechanical, chemical and antifouling features. In order to investigate the efficiency of silicone-based fouling-release coatings, chapter 6 focuses on polydimethylsiloxanes (PDMS) which are also reinforced by ZnO micro- and nanostructures. In chapter 8, the findings on PTU and PDMS are combined in order to create a phase-separating polymer composite with fouling-release properties and suitable mechanical stability. Finally, chapter 9 presents the results obtained from long-term field-experiments on a multipurpose vessel.

Chapter 2

2 Fundamentals

This chapter comprises the theoretical fundamentals of the presented work. First, *biofouling* itself as well as its formation will be explained followed by considerations on the principles of attachment by means of the three most significant marine organisms. In order to understand the influence of the surface properties on the growth of micro- and macroorganisms, some information will be given on wetting phenomena as well as on the models used for the determination of e.g. hydrophobicity, hydrophilicity or the surface free energy (SFE).
Second, the history of antifouling technologies is shortly summarized, followed by an overview on the latest developments. Aimed by these considerations, the utilization of polythiourethane (PTU) as basic polymeric matrix as well as the incorporation of tetrapodal-shaped zinc oxide (t-ZnO) as reinforcing filler material will be motivated.

2.1 Biofouling

The formation of biofilms on solid surfaces is a very complex process which was studied extraordinarily extensive during the last century. In general, biofilms contain a huge variety of bacteria and as they are able to produce an extracellular matrix, they can adhere to almost any substrate [38]. In 1989, Wahl introduced a *fouling sequence model* which includes the elementary steps of the attachment process in a simplified and clearly structured manner [39].

2.1.1 Fouling sequence model

It is stated, that the initial colonization steps are usually considered to follow a certain pattern which is nearly independent on the substrate or the environmental

surroundings. The *fouling sequence model* simplifies the complexity of the fouling mechanism to a process consisting of four distinguishable phases which are overlapping in their time sequence (figure 2).

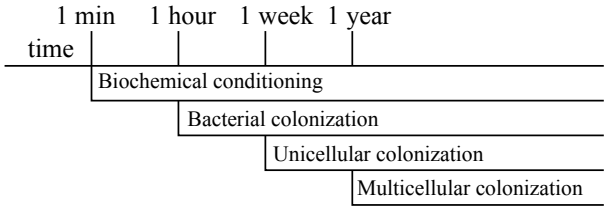

Figure 2: Time-interval of the fouling sequence model as described by Wahl [39].

In the first moments after immersion, the *biochemical conditioning* is initiated which includes the adsorption of chemical compounds [40, 41]. This process is purely physical and as it implicates an entropy reduction, the total free energy of the system has to be reduced in order to provide compensation. It is remarkable to mention, that the initial adsorption is independent of the SFE of the substrate under investigation. The SFE of low-energy surfaces get increased whereas high energy surfaces get reduced. On the other hand, the binding strength of the adsorbed film does depend on the surface properties of the substrate, as it is lowest for films in the medium ranges of surface energies [39]. Like the first phase, also the *bacterial colonization* is a purely physical process as it involves Brownian motion, electrostatic interaction, gravity and Van-der-Waals forces. The colonization starts about one hour after immersion and covers reversible as well as irreversible adsorption. In principle, immersed substrates are surrounded by a layer of water molecules which has to be overcome by approaching bacteria until physical forces start to function. This layer may be surmounted by polysaccharide[1] fibrils[2] which upon shortening pull the bacteria in the direction of the substrate where Van-der-Waals forces accelerate the adsorption process. The bacteria develop covalent bonds to the macromolecular film which implicates the conversion from the adsorption to the adhesion phase. The growing bacterial film is known as *primary film* or *biofilm*. Several days after immersion, the *colonization by unicellular eukaryotes* [3] starts with the accumulation of yeasts and mainly diatoms which cover the substrate and therefore contribute to its chemical and biological development. Several days to weeks after immersion, the *colonization by multicellular eukaryotes* is initiated which comprises the last and longest phase of the fouling process and implicates the growth of larvae and spores [39].

[1] multiple sugar
[2] fine fiber
[3] organisms, whose cells contain a nucleus

However, this fouling sequence model suffers from oversimplification due to the fact that some organisms, e.g. larvae of some barnacles or bryozoans can settle to surfaces before the formation of a biofilm. Callow and Callow stated therefore, that the predicted sequence is not always followed, which implies that the suppression of the initial stages is not necessarily expedient in order to control biofouling [42].

2.2 Bioadhesives

In general, fouling organisms like bacteria, diatoms or macrofoulers attach to surfaces by the aid of adhesive polymers of more or less similar chemical composition [3]. As stated by Callow and Callow [43], these adhesive substances need to fulfill remarkable criteria. Despite the huge variety of possible substrates to attach to, also the different environmental conditions like temperature or salinity must be taken into account. In order to provide effective underwater adhesion, these substances need to be highly viscous in the moment of attraction as a wetting of the surface is unavoidable. On the other hand, surface tension is necessary to avoid dissolution in water. After the wetting process, the adhesive has to bond to the surface and to cure in sufficient short time in order to achieve a bonding strength high enough to withstand the given natural conditions [43].
The review article by Petrone [44] focuses on the attachment strategies utilized by the three major types of fouling organisms, algae, barnacles and mussels. As the prevention of fouling needs to be implemented in the earliest stage of settlement, it is necessary to evaluate the initial adhesion. Therefore, motile single-cell algal zoospores[4] as well as mussel and barnacle larva are considered.

2.2.1 Algae zoospores

The adhesion of zoospores can be exemplary explained by the green alga *Ulva*, as it is frequently used as model for the adhesion processes of soft-foulers. The reproduction of these organisms occurs via microscopic zoospores without a cell wall. Therefore the immediate binding to a surface is required in order to provide the necessary living conditions [43]. Hereinafter, the zoospores release their flagella and get attached to the surface by adhesive polymers. A schematic description of the process-steps involved in the settlement and adhesion process of *Ulva* spores is shown in figure 3.

[4] aquatic spore, movable by flagella

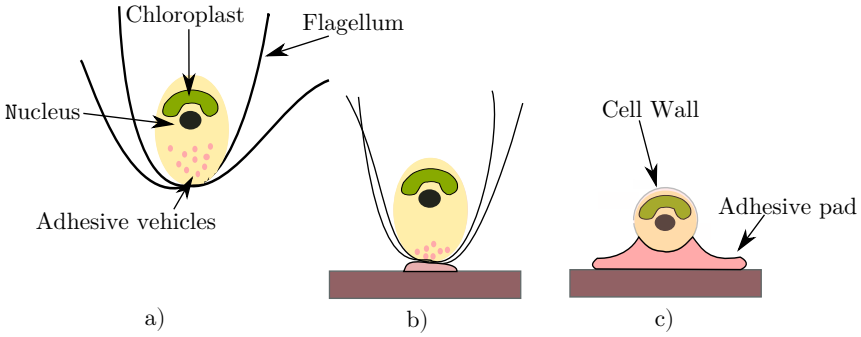

Figure 3: Schematic attachment of the green algea *Ulva* to a substrate, as shown by Callow and Callow [43].

Swimming spores contain characteristic filled vesicles which upon attachment release their contents in order to form the extracellular adhesive. It was shown by different investigations that the filling of these vesicles could contain glycoproteins, but the detailed knowledge of the content is still under research [43].

2.2.2 Mussel larvae

Like many aquatic organisms, mussels are specialized with respect to the adhesion at solid liquid interfaces by utilizing a permanent cement [45]. At the beginning of their life cycle, mussel larvae are able to swim and feed aided by a cilia[5]. The adhesion of mussels is based on mussel silk, also known as byssus, a bundle of threads which is located at the foot organ (figure 4) [44].

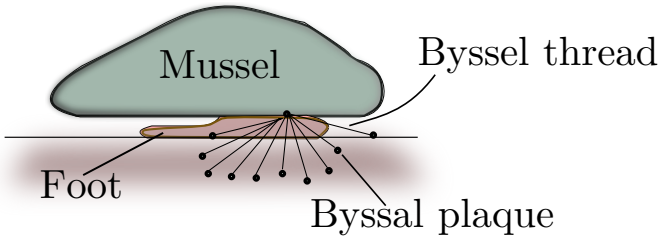

Figure 4: Schematic drawing of a mussel attached to a substrate.

2.2.3 Barnacle larvae

Similar to mussels, also the barnacle, being the only sessile crustacean, can be used as a model in order to explain underwater adhesion by utilizing cement [45]. During the life cycle of a barnacle (see figure 5), a development from temporary adhesion within the period of larval state (cyprid) to permanent adhesion within the adulthood is experienced. The attachment of adult barnacles is based on proteinaceous

[5]cytoplasmic evagination of the plasma membrane

substances with a protein content of more than 90 wt% and after the attachment, barnacles do not move or self-detach. The attachment strength is remarkably high.

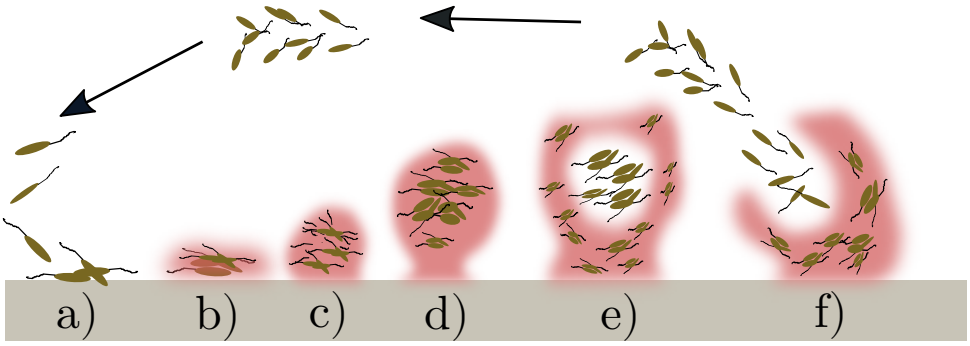

Figure 5: Schematic life cycle of a barnacle. Shown is the initial temporary attachment of the larvae (a) followed by the permanent adhesion phase (b). Hereafter, the primary maturation (c) as well as the secondary maturation (d) is initiated. The last state is characterized by the dispersion of the matured larvae (e and f).

2.3 Role of surface

The attachment of marine organisms is strongly influenced by the surface properties. For that reason, the well known Youngs-equation, which is frequently used for the evaluation of surface wetting, will be introduced. Additionally, the insufficiency of the underlying model will be outlined and complemented by deviating assumptions made by Cassie & Baxter [46] and Wenzel [47]. Subsequently, the concept of surface free energy is shortly described followed by a brief introduction to its frequently used determination method given by Owens, Wendt, Rebel and Kaeble [48].

2.3.1 Wetting

One of the main obstacles in the field of antifouling research is the fact that almost any biomass contains hydrophobic, hydrophilic and charged components. Therefore most proteins are able to adhere to nearly any surface [49]. For that reason, it is essential to explain the driving force for bacteria to accumulate on surfaces. As wettability relates both chemical and physical properties, it is of importance to summarize its theoretical backgrounds.

As described by Thomas Young in the beginning of the 19th century [50], *wetting* can be expressed by the contact angle which is a measure for the force acting on a liquid droplet. The Young equation (1) relates the interfacial energies occurring between the interfaces solid-liquid (γ_{SL}), solid-vapor (γ_{SV}) and liquid-vapor (γ_{LV}).

$$cos(\theta) = \frac{\gamma_{SV} - \gamma_{SL}}{\gamma_{LV}} \tag{1}$$

If values for $\theta < 90°$ appear, the surface is hydrophilic, the reverse case of $\theta > 90°$ leads to hydrophobic surfaces. The extreme cases of these two measures are known as superhydrophilic ($\theta < 5°$) and superhydrophobic ($\theta > 150°$).

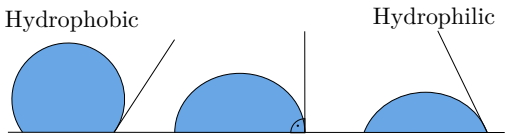

Figure 6: From left to right: hydrophobic case, ($\theta > 90°$), neutral case, ($\theta < 90°$) and hydrophilic case, ($\theta < 90°$).

As this equation only holds for perfect flat surfaces, it has to be extended for real situations where throughout two contact angles are present, the advancing (θ_{ADV}) and the receding (θ_{REC}) contact angle. The difference between these two angles is the contact angle hysteresis which is a representation for the *non ideality* of a surface.

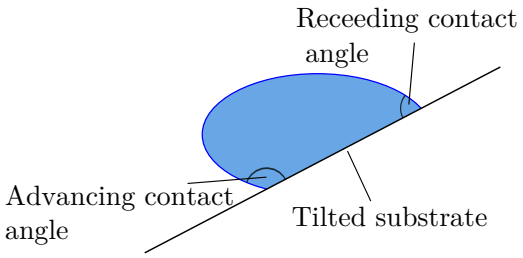

Figure 7: Schematic of contact angle hysteresis with advancing (θ_{ADV}) and receding (θ_{REC}) contact angle.

When considering the roughness of a surface, two different cases need to be distinguished. According to the model of Wenzel [47], the liquid wets the complete surface, but an additional roughness factor R describing the deviation from an ideally smooth surface has to be taken into account in equation (2).

$$cos(\theta_W) = cos(\theta)R = \frac{\gamma_{SV} - \gamma_{SL}}{\gamma_{LV}}R \tag{2}$$

This equation underlines, that an additional roughness R promotes either hydrophobicity or hydrophilicity. As wetting is a property which is predetermined by the chemical nature of the substrate, roughness simply amplifies the contact angle in the direction of the extreme cases.
A different model introduced by Cassie and Baxter [46] assumes that the surface cannot be completely wetted due to outstanding protrusions.

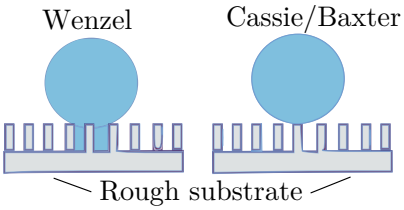

Figure 8: Wetting of rough surfaces after Wenzel [47] and Cassie & Baxter [46].

An incomplete wetting of the surface results which can be expressed as the ratio f of wetted surface to non-wetted surface. The contact angle $\theta_C B$ for the Cassie-Baxter model can be written as equation (3).

$$cos(\theta_C B) = Rf\frac{\gamma_{SV} - \gamma_{SL}}{\gamma_{LV}} + f - 1 \tag{3}$$

As both models suffer from incompleteness, it can be stated, that in nature an overlap of the two assumptions will be found. For this reason, both considerations have to be taken into account for a complete description of the surface.

2.3.2 Surface free energy

Many modern antifouling solutions are based on the assumption that materials with a low surface free energy (like silicone, PTFE) are best suited as low fouling surfaces as the adhesion of microorganisms is too weak to ensure long-lasting attachment (See also section 2.4.2, State of the art) [42, 51]. For that reason, the surface free energy is discussed here and the assumptions necessary for its determination are additionally covered.

As explained by Chawla [52], all surfaces posses deviating characteristics when compared to the bulk as they include the termination of a phase. Inside a material, atoms or molecules are bonded in all directions which causes a reduction of the potential energy. On the other hand, atoms or molecules from a surface are not bonded in every direction which results in unsaturated bonds and therefore higher potential energy. This energy is known as SFE. In that context, also the expression *surface tension* needs to be mentioned as it describes the tendency to minimize the surface energy by minimizing the surface area. In the case of liquids, surface energy and surface tension are equal due to the predominance of molecular mobility which implies that liquids cannot resist shear forces. For that reason, liquids tend to minimize their free energy which results in the formation of spheres. In contrast, surface tension and surface energy are not equal for solids which can resist shear.

The surface energy of solids is usually measured by contact angle experiments which are based on the already described Youngs equation (1). Here, the contact angle of a liquid droplet is measured on a solid surface and the energies γ_{SV} and γ_{LV} can be easily determined. In contrast, γ_{SL} cannot be measured directly for what rea-

son the utilization of mathematical models is required. Here, different approaches were made which are mostly based on the assumption that the SFE is composed of different components which are dependent on the substrate itself as well as on the measurement liquid. The method of Owens, Wendt, Rabel and Kaeble (OWRK) [48] is widely used and was also part of this work, therefore, a description in more detail is given in the next subsection.

2.3.3 Method of Owens, Wendt, and Rabel

The OWKR method is widely used for the estimation of the free surface energy of a solid [48]. A detailed description of this method can be found in the textbook by Schwartzberg and Hartel [53]. Here, a short overview on the mathematical backgrounds will be presented.
The measurement includes the estimation of the contact angle by different liquids whereby it is assumed that the surface energy is split into polar γ^P and dispersive γ^P components. The polar component involves the fraction of the surface energy that is based on polar interactions (Coulomb interactions between permanent dipoles and induced dipoles), while the dispersive component covers the fraction of the surface energy that is based on dispersive interactions (Van-der-Waals interactions).
After OWKR, the surface energy γ is given by cohesive interactions within one phase. The sum of the polar and dispersive components reveals the overall surface energy, equation (4).

$$\gamma = \gamma^P + \gamma^D \tag{4}$$

From the contribution of energy of the liquid phase γ_l and the solid phase γ_s, the interface energy $\gamma_s l$ between the adjacent phases can be written as equation (5):

$$\gamma_{sl} = \gamma_l + \gamma_s - 2(\sqrt{\gamma_l^D * \gamma_s^P} + \sqrt{\gamma_l^P * \gamma_s^P}) \tag{5}$$

Rearranging this expression leads to a linear equation $y = mx + b$, (6):

$$\frac{\gamma_s * (cos(\theta) + 1)}{2\sqrt{\gamma_l^D}} = \sqrt{\gamma_s^P} * \frac{\sqrt{\gamma_l^P}}{\sqrt{\gamma_l^D}} + \sqrt{\gamma_s^D} \tag{6}$$

Here, the measured contact angle θ provides the values for y and x, given in equation (7) and (8):

$$y = \frac{\gamma_s * (cos(\theta) + 1)}{2\sqrt{\gamma_l^D}} \tag{7}$$

$$x = \frac{\sqrt{\gamma_l^P}}{2\sqrt{\gamma_l^D}} \tag{8}$$

The values for the polar and dispersive components of the surface energy of the solid can be calculated by the slope m and the y-intercept b in equations (9) and (10):

$$m = \sqrt{\gamma_s^P} \tag{9}$$

$$b = \sqrt{\gamma_s^D} \tag{10}$$

2.4 Antifouling

Antifouling, the combat of organisms attached to surfaces which are subjected to water, concerns human kind since men sailed the world for what reason effective technologies are under continuous research [7].

2.4.1 History of antifouling technologies

The history of strategies to prevent biofouling dates back to more than 2000 years where the most important developments took place within the 1950s with the application of triorganotins in combination with polymeric matrices as paints.
Since 1977, the most-effective antifouling coatings were based on copper and tributyltin (TBT) which were constantly released from the paints as effective biocide agents and could therefore completely prevent the accumulation of marine organisms. As stated by Abarzua and Jakubowski [3], TBT was used in different ways. Self-polishing copolymers (SPC), where the biocides are chemically bonded to a polymeric matrix and are slowly released over time, were most effective. Due to the possibility to prevent biofouling for up to five years, SPCs found application all over the world and caused environmental pollution on an enormous scale. Earlier research on the extent of pollution and the influence of the released biocides on marine organisms has shown, that especially the embryogenesis of oysters was strongly impacted [54]. Consequently, a global regulation initiated in 2003 was stated which implicated the prohibition of TBT based antifouling paints [16]. Convincing alternatives based on copper combined with organic biocides were an acceptable alternative,but as they also impact strongly the environment, they are pending prohibition within the next years [23].

2.4.2 State of the art

During the last years, a huge variety of alternatives was introduced which underlines the urgent need of an efficient environmentally friendly antifouling solution [55, 56]. Here, only an extract of the findings is presented whereby a categorization in chemical, biological and physical methods is performed [57].

Chemical methods

As already stated, the most efficient chemical antifouling methods were the self-polishing TBT copolymer coatings until their prin 2008. One convincing alternative was provided by tin-free SPCs where metals like copper, zinc or silicon provide the released biocides. One major drawback of self-polishing antifouling paints is the degradation of the coating during the release of biocides as the polymeric completely removed over time. The durability of these coatings is therefore strongly limited. Additionally, also copper-containing coatings are suspected to have a harmful influence on marine organisms for what reason they are pending prohibition within the next years [23].

Biological methods

Instead of environmentally harmful biocides, the biological antifouling strategies are based on benign organisms which secrete enzymes or metabolites in order to prevent the accumulation of fouling species. Regarding the principle of operation of these enzymes, four different mechanisms can be considered. First, they can degrade the adhesive polymers used for attachment which has already proven to inhibit the growth of Ulva zoospores as well as barnacles cyprids [58]. Secondly, the initial biofilm may be destructed leading to a lack of the substantial underground. But as the variety of biofilms is rather complex and adaptable to the environment, this approach is not realizable [57]. The third mechanism is based on the creation of biocides which hinder the fouling process. Several experiments were conducted within this particular field, but up to now no appropriate solution was introduced. Regarding the last mechanism, the enzymes may use quorum sensing (QS), the intracellular chemical communication of cells which are able to sense information on the cell-density of their local population [59]. As shown by Waters and Bassler for some bacteria [60], QS requires $N - Acyl$ homoserine lactones (AHL) which implicates that the elimination of AHL would led to the prevention of biofouling. It is therefore stated, that the inhibition of the biofilm can also lead to reduced settlement of macrofoulers. For the effective implementation of this mechanism, many aspects, e.g. water temperature, salinity or the distribution of the particular enzymes within a suitable matrix need to be taken into account. The fabrication

of a well-performing antifouling solution based on quorum sensing is therefore still under investigation and not yet ready for the market [57].

Physical methods

A very common physical antifouling method is provided by electrolysis of seawater. Here, strong oxidants like e.g. hypochlorous acid or hydrogen peroxide are produced and spread over the ship hull in order to remove fouling organisms. On the other hand, the major disadvantage of this method is an increase in corrosion of the steel-made ship hull caused by a high voltage drop across the surface [7]. A related approach involves the utilization of vibration methods which have proven to reduce the attachment of organisms. However, high power is needed for the implementation of vibration antifouling methods for what reason their establishement is not useful with respect to ecologic aspects.

Besides the utilization of electrolysis or vibration, the influence of surface on biofouling such as topography or roughness was under investigation [57]. One big research field is therefore given by the development of a highly adjusted surface topography where it is aimed to imitate natural antifouling surfaces, e.g. the skin of sharks or dolphins [61]. Some of these bio-inspired surfaces could show reduced growth of marine organisms but as the structuring of such surfaces is highly complex, the transfer from the laboratory scale towards commercial applicability is a rather complicated procedure. Additionally, these artificial skins are usually made from silicones whose mechanical stability is insufficient for mechanically highly stressed areas like ship hulls [7].

Furthermore, non-toxic fouling-release coatings attracted a lot of interest as they are based on the materials properties itself. A combination of low surface energy and low elastic modulus leads to low adhesion forces of settled organisms, therefore hydrodynamic forces of a moving ship are sufficient to simply wash-off or *release* the species [57]. At present, only fluoropolymers and silicone offer these desired material properties but as fluor containing polymers have shown to bring along negative impacts on the environment [62], silicones dominate the FR market. On the other hand, the low elastic modulus brings along the major drawback of these coatings as it includes low mechanical stability. Additionally, the low surface energy provides a disadvantage as it leads to low adhesion to the substrate as well as the difficulty to recoat after damage [7].

2.5 Polymers and additives

In order to develop an ecofriendly, mechanically stable antifouling coating, a suitable polymer matrix needs to be selected and eventually reinforced by inorganic

materials. Polyurethanes (PU) offer a huge variety of products as their main components isocyanate and dialcohol can be combined in many ways. A mechanically stable PU without solvents containing harmful volatile organic compounds (VOC) is needed. Additionally, UV-stability is necessary in order to withstand the harsh environmental conditions. Another aspect may be the ease of application, therefore a two component system which is able to react without additional catalysts would be advantageous.
In this work, a solvent-free two-component polythiourethane was chosen as basic polymer matrix. The utilized isocyanate HDI offers UV-stability as it possesses the desired aliphatic structure, the appropriate dialcohol PETMP contains a highly reactive SH group which makes the use of catalysts unnecessary. In the following sub chapter, the basic chemical considerations on PU and PTU will be discussed.
As already mentioned, silicones are used as foul-release coatings due to their low surface energy and low elastic modulus. One approach to overcome their mechanical weakness is the formation of PTU/silicone phase-separating copolymers for what reason some basics on silicones is provided [63].
To further enhance the polymeric matrices, ZnO was chosen as filler material as it can be fabricated in a huge variety of morphologies and on a large scale. An overview on ZnO and some of its applications, its beneficial shapes as well as its fabrication method will be provided.

2.5.1 Polyurethanes

An extensive overview on polyurethanes, the corresponding chemical reactions as well as the processing techniques is given by Becker and Braun [64]. In this subchapter, only a small extract is presented which is fundamental for the understanding of this thesis.

Polyurethanes (PU) represent a diverse group of materials which are based on polyisocyanates and which appear in a huge variety of applications. Due to the great number of possible component combinations, the diversity in processing and the targeted influencing of the polymerization reaction, the abundance of final products is unique in the field of polymers. Their properties can be modified in that way that they form thermosets, thermoplastics or elastomers wherefore PUs are utilized in e.g. paints, adhesives, electrical encapsulation, foams or fibres as to name only a few [65].
Typically, PUs are formed by the polyaddition of a polyol (-OH) and a diisocyanate (-N=C=O) whereby many applications require the inclusion of additives such as catalysts or chain extenders. The resulting structural unit which is also reponsible for the naming is the urethane group (-NH-CO-O-).

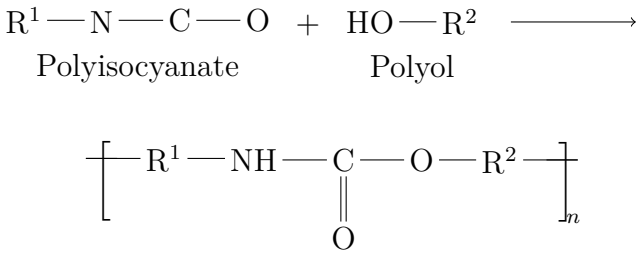

Polyurethane

Isocyanates are particularly interesting because they possess an enormous reactivity which is basically attributed to the positive charge of the C-atom. In the shown polyaddition, R can stand for an aromatic, aliphatic or cycloaliphatic rest, which has a strong influence on the resulting end-product. Aromatic isocyanates show a substantial higher reactivity and are quantitatively more common. Aliphatic isocyanates belong to a different organic group as they do not contain the aromatic benzene ring. This results in their main advantage over aromates, their non-yellowing features, as they do not contain any series of double bonds which would cause the yellowing [29].

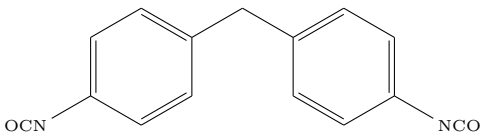

Aromatic polyurethane

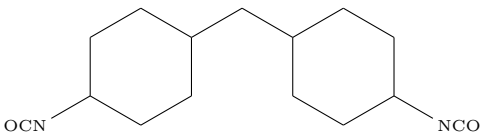

Aliphatic polyurethane

Besides the quality of the isocyanates, the polyols are mainly responsible for the properties as the chain length and the number of interconnections predetermine the mechanical features of the final product. Linear polyols lead to a linear polymer without interconnections. Trifunctional polyols lead to a slightly interconnected network and tetrafunctional polyols lead to a highly interconnected polymer.

The structure of the processed polymer is based on hard segments (HS) provided by the isocyanate as well as on soft segments (SS) provided by the diol. The ratio between HS and SS has a strong influence on the mechanical properties of the polymer as high amounts of HS lead to a hard and rigid product whereby a low amount leads to soft and elastic materials.
During this thesis, a sulfur-containing polyol was used which ends up in a polythiourethane (PTU) upon reaction with an isocyanate. These kind of polymers become more and more attractive due to their convincing features. Besides excellent optical properties and bio compatibility, also the flexibility and the crystallinity may be enhanced [66]. For the majority of the conducted experiments, the solvent free two-component thermoset system based on HDI and PETMP was used. Their

polyaddition reaction is therefore considered in more detail.

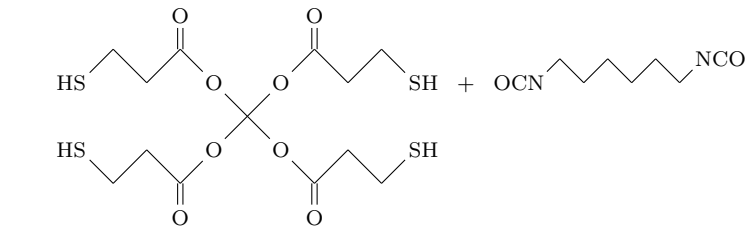

Pentaerythritoltetrakis (3-mercaptopropionat) 1,6 Diisocyanatohexan

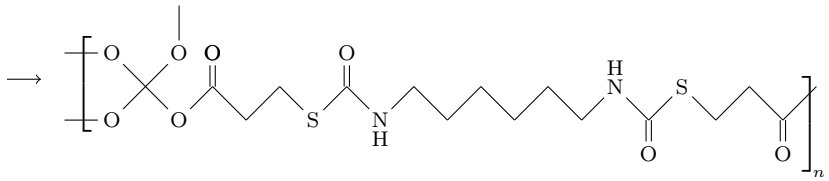

Polythiourethan

HDI is a linear polymer with two functional NCO groups whereby PETMP is a tetrafunctional polymer with four reactive SH groups. The polyaddition reaction of the two components is initiated directly after mixing. The double bonds of PETMP break and provide therefore reactive sites for the HDI component. The reaction of the linear HDI with the tetrafunctional PETMP leads to a strongly interconnected network which provides the necessary mechanical stability.

2.5.2 Silicones

Polysiloxanes or *silicones* as they are usually named, open up a unique class of materials as they combine the characteristics of organic polymers and anorganic silicates [67]. Their repeating unit is known as *siloxane* and it is based on silicon atoms linked to oxygen atoms. The free valences of the silicon are bound to organic rests R wherefore the general structure of a linear silicone can be expressed as [64]:

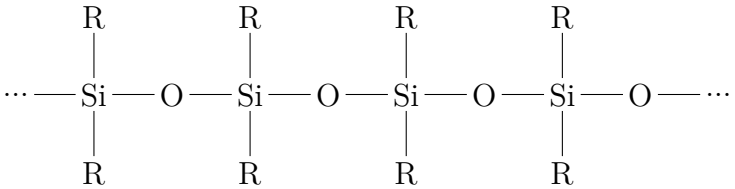

Polyisiloxane

Due to the Si-O backbone, silicones provide a variety of properties which are of special relevance in many technical applications. In high temperature applications, silicones benefit from the Si-O bonding strenght, in fields where low sticking is desirable, its low surface free energy is of major importance.

As the molecular structure of silicones can be varied in a wide range, also their features can differ remarkably. With respect to technical applications, polydimethylsiloxane (PDMS) where R = CH_3, is most relevant and was also used in this work [68]:

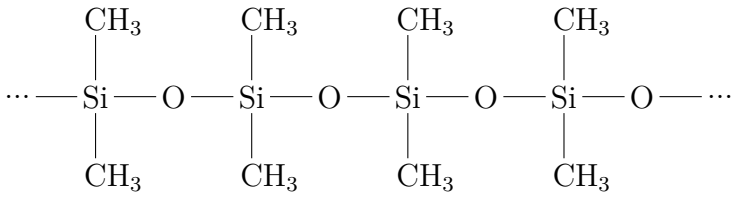

Polydimethylsiloxane

Another aspect within the field of polymers is the possibility to reinforce the matrix mechanically by incorporation of suitable inorganic nano- and microstructures [31]. ZnO tetrapods (t-ZnO) are of particular potential due to their unique three-dimensional morphology provided by their four arms pointing in different directions [32, 33, 69]. In addition, ZnO tetrapods are biocompatible for what reason they are best suited as reinforcing filler material for non-toxic antifouling paints [36]. The recently developed flame-transport synthesis [Mishra et.al, 2013] enables large-scale fabrication of t-ZnO particles which makes them suitable for industrial utilization. The following subchapter focuses on the special properties of t-ZnO structures and points out their diverse fields of applications.

2.5.3 Zinc oxide and its morphologies

Since ages, Zinc oxide (ZnO) and especially ZnO micro- and nanostructures are attracting extensive interest due to their diverse fields of application [70]. Advantageous characteristics of ZnO are its direct bandgap at 3.37 eV, its non-centrosymmetric crystal-structure resulting in piezoelectric and pyroelectric properties and its biocompatibility. Therefore it is a useful material for e.g. optoelectronics, piezolelectric sensors or antiviral products [71, 72, 73]. Additionally, ZnO offers the possibility to be fabricated in a huge variety of morphologies like needles, wires or belts as to name only a few [74, 75]. Of special interest are tetra-needle shaped particles as they provide a three-dimensional microstructure which is a promising additive for compound materials. Besides other interesting features, it has already proven to increase the mechanical strength of polymers when being incorporated into the matrix [76, 31, 77, 78, 79]. In figure 11, a SEM micrograph of tetrapodal-shaped ZnO (t-ZnO) microstructures fabricated by the already patented flame transport synthesis [80, 33] is shown.
The detailed growth mechanism of ZnO tetrapods is still under discussion and different growth models are described. The foundation of all growth models is the assumption that t-ZnO starts growing from a seed nucleus, different theories about

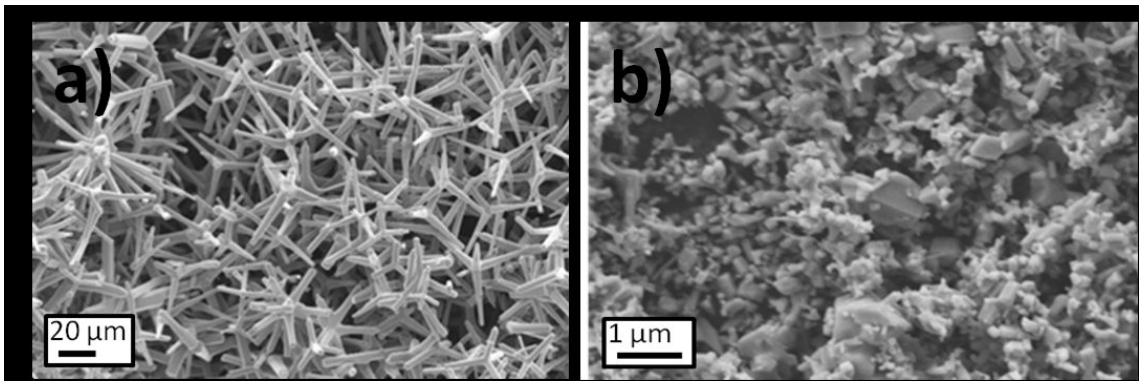

Figure 9: a) Typical tetrapodal-shaped ZnO nano- and microstructures synthesized by flame-transport approach [33]. b) Spherical ZnO micro- and nanoparticles.

the subsequent growing steps can be found in literature [74, 81, 82, 83].

In addition, ZnO tetrapods offer the possibility to fabricate tetrapodal structures from other materials which can be used as fillers, too. Furthermore, the subsequent removal of t-ZnO after deposition of the respective material would lead to hollow nano- and microstructures. Such particles could be very beneficial for reinforcement as the polymer could penetrate inside the hollow arms leading to superior interlocking at very low particle concentration.
One approach for the utilization of t-ZnO as template for the fabrication of hollow three dimensional microstructures was presented by Mecklenburg et al. in 2012 [80]. The synthesis of Aerographite, one of the most lightweight materials in the world (99.999 % porosity), was presented in detail [80]. This template correlated fabrication of hollow structures can be easily implemented for other materials, the deposition of silicon thin films on t-ZnO and the subsequent template removal will therefore be exemplary presented here. Detailed information on the deposition process and material characteristics were found by Hölken et al. [84].

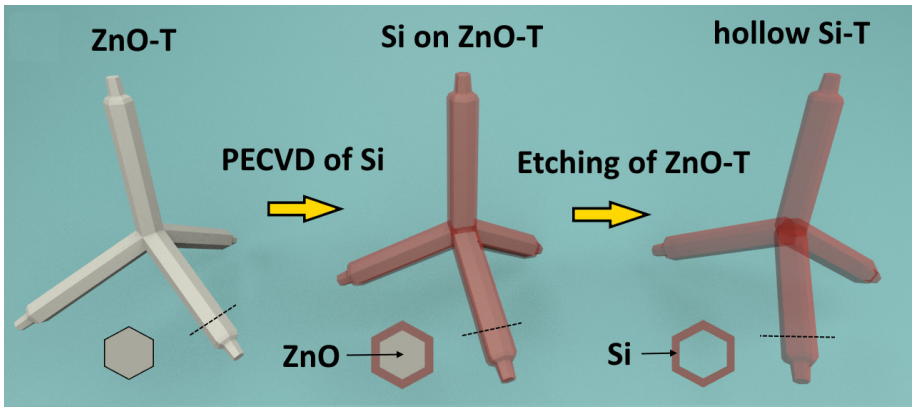

Figure 10: Schematic process of the fabrication of hollow Si structures based on t-ZnO templates.

In order to obtain hollow silicon microstructures, t-ZnO templates were homogeneously distributed on silicon wafers and a silicon thin film was deposited by plasma enhanced chemical vapor deposition (PECVD) utilizing the process gases argon and silane, respectively. Hereinafter, the t-ZnO templates were removed wet-chemically by an aqueous solution of hydrochloric acid. The formation-process of hollow Si-structures based on ZnO templates is schematically shown in figure 10.
Besides the possibility to obtain homogeneous films at comparatively low deposition temperatures, in PECVD the thin films characteristics can be tuned in a broad range by varying process parameters. In the following figure 11 a Si coated tetrapod arm is shown, the columnar morphology of the film is demonstrated. The hollow structure after etching can be seen in figure. The threedimensional structure is not affected by the etching procedure and hollow Si structures could successfully be produced.

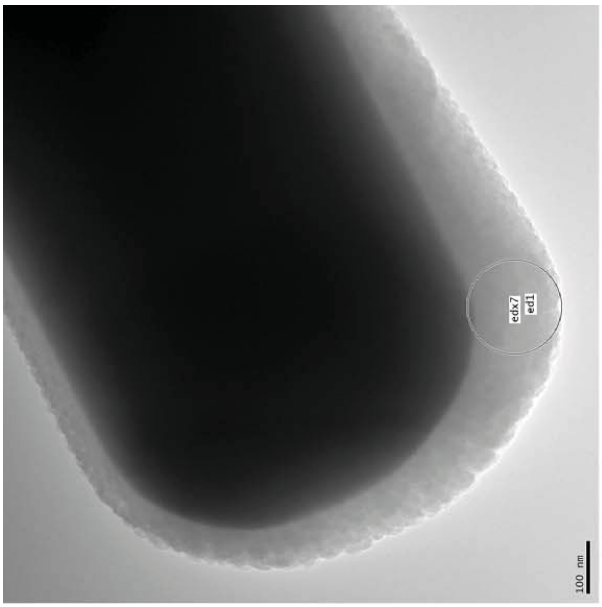

Figure 11: TEM image of hollow tetrapodal-shaped silicon microstructures.

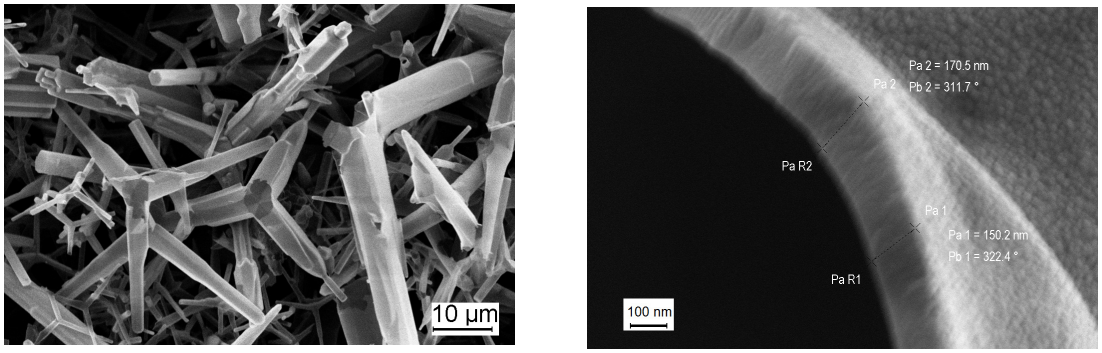

Figure 12: SEM image of hollow Si structures, morphology of the template is maintained.
(a) Overwiew. (b) Close-up view on wall.

Chapter 3

3 Materials and methods

3.1 Materials

The two-component polythiourethane was purchased from Fluid- & Prozesstechnik GmbH (Waltershausen, Germany), whereby detailed information about the characteristics of the components hexamethylene diisocyanate (HDI) and pentaerythritol tetrakis(3-mercaptopropionat) (PETMP) were already published by Strzlec and Baczek [27]. The acetic interlacing ethyltriacetoxysilane (ETAS) one component system was purchased from Wacker Chemie AG (Munich, Germany), methyltriacetoxysilane (MTAS) from Probau, Germany. A two component polydimethylsiloxane (PDMS) system Sylgard 184 was purchased from Sigma Aldrich (Taufkirchen, Germany). Tetrapodal shape ZnO micro- and nanoparticles were fabricated at the faculty of engineering (Kiel, Germany), spherical-shaped ZnO-particles were purchased from Sigma Aldrich (Taufkirchen, Germany).

3.2 FT-IR

In analytical chemistry, infrared spectroscopy (IR) is of major importance as it provides an enormous range of information and allows statements on structural molecular elements which are hardly to achieve with other methods. As the location and intensity of the absorption bands are very specific for individual substances, the IR-spectra are comparable to a fingerprint and can be used as identification instrument. The textbook by Guenzler and Heise [85] provides a detailed description on the underlying theory as well as on practical application aspects.

In infrared-spectroscopy, an electromagnetic beam with wavelengths in the infrared region (800 nm to 1 mm) is passed through the material under investigation. As

the energy of IR-radiation is in the order of rotational levels of small molecules as well as in the order of vibrational levels of molecular bonds, its absorption leads to excitations. In general, only the transmission $\tau = \frac{I}{I_0}$ is recorded as function of the wavenumber $\tilde{\nu}$ (reciprocal wavelength and therefore proportional to the frequency ν of the electromagnetic field due to the relation $\tilde{\nu} = \frac{\nu}{c}$, with c = velocity of light), whereby I is the irradiation intensity in front of the sample and I_0 is the intensity after transmission. For the description of the intensity loss caused by the transmission of light through a material, the Lambert-Beer Law is applied as it provides a correlation to the concentration of the substance c and its thickness d.

$$I = I_0^{-\epsilon_\lambda * c * d} \tag{11}$$

Here, the extinction coefficient ϵ_λ is a constant of proportionality which depends on the specific material.

As the irradiation with an electromagnetic beam in the frequency region of infrared light leads to characteristic vibration excitations of molecular bonds, IR-spectra provide information on the molecular structure.
Possible molecular vibrations as a result of interactions between the electromagnetic irradiation and the molecule are shown in figure 13 for the asymmetric and symmetric stretching of the CO_2 molecule. In general, a molecular vibration can be detected by IR-spectroscopy if it involves changes in its dipole moment (movable electric charges are necessary). During the asymmetric stretching of the CO_2 molecule, the negative charge of the O-atoms and the positive charge of the C-atom move apart whereby during the symmetric stretching they fall together.

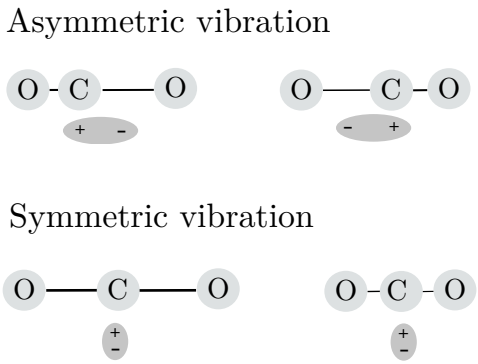

Figure 13: Molecular vibrations of the CO_2 molecule. a) The asymmetric stretching of the CO_2 molecule involves a change of the dipole moment and is therefore IR-active. b) The symmetric stretching of the CO_2 molecule does not causes a change in the dipole moment and is therefore IR-inactive.

For complete evaluation, the raw data is transformed to a spectrum by Fourier transformation, the technique is therefore widely known as Fourier-transformed

infrared-spectroscopy (FT-IR).

Polyurethanes show two characteristic bands in the IR-spectra which are located at 1530 cm^{-1} and 1220 cm^{-1}. Additionally, IR spectroscopy allows the identification of unreacted functional groups which is extremely important in order to prove the accuracy of the handling. The -NCO rest is allocated at 2270 cm^{-1} and is nearly unaffected by the absorption of other molecules [64]. The S-H vibration of the sulfur containing diol used in this thesis can be found at 2545 cm^{-1} [86].
For the evaluation of the quantitative polyaddition of HDI and PETMP, FT-IR was performed with a Bruker Tensor 29 system (Bruker, Bremen, Germany).

3.3 Raman spectroscopy

Like IR-spectroscopy, also Raman-spectroscopy is a method for the detection of molecular vibrations. The spectra are often comparable but as different physical principles are responsible for the results, many cases require the simultaneous usage of both methods for a complete analytical inspection.

In 1923, the Raman effect was predicted by Adolf Smekal and only five years later the name giver Chandrasekhrara Raman was able to prove the theoretical considerations. Raman spectroscopy is used to investigate molecular vibrations and the underlying considerations are well described by Demtroeder [87].
Compared to IR-spectroscopy where radiation is passed through the sample, the Raman signal results from inelastic scattering events at vibrating molecules caused by a monochromatic laser beam. The irradiation causes a transition to a deviating energetic level of the molecule under investigation. Such a transition is only possible if the polarisability of the molecule undergoes a change within the vibration. Figure 14 visualizes the influence of the asymmetric and the symmetric stretching of the CO_2 molecule on the change of the polarisability.
If light of the energy $\hbar\omega$ impinges on a molecule, the majority is scattered elastically as Rayleigh-scattering and only a small amount is scattered inelastically. During this inelastic scattering, the molecule is transferred from its original energy state E_i to a higher state E_f whereas the photon with frequency ω_s looses energy (figure 14, inelastic photon-scattering).

$$\Delta E = E_f - E_i = \hbar(\omega_i - \omega_s) \tag{12}$$

The energy difference ΔE can be transferred to rotational, vibrational or electronic energy and is characteristic for the molecule under investigation. During scattering,

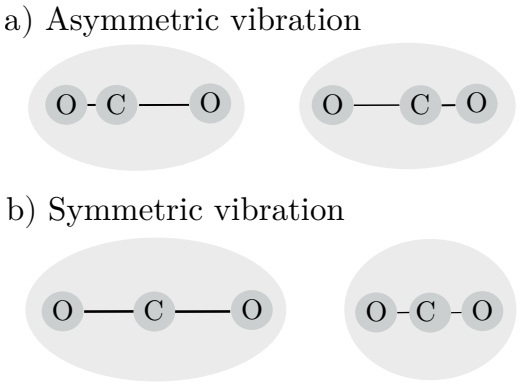

Figure 14: Molecular Raman vibrations a) The asymmetric stretching of the CO2 does not involves a change in polarisability. b) In contrast, the symmetric stretching of the CO2 molecule causes a change in polarisability as it is bigger in the stretched state when compared to the clinched state.

the system consisting of molecule and photon is located in the formally known *virtual state* of the energy:

$$E_v = E_i + \hbar\omega_i \tag{13}$$

In the special case of resonant-scattering, this *virtual state* coincides with a real energy state of the molecule (figure 14, Stokes Raman scattering).
Three different mechanisms occur during the scattering, namely Stokes-scattering, Anti-Stokes scattering and Rayleigh scattering. These states and the corresponding energy transfers are schematically shown in the following figure 15.

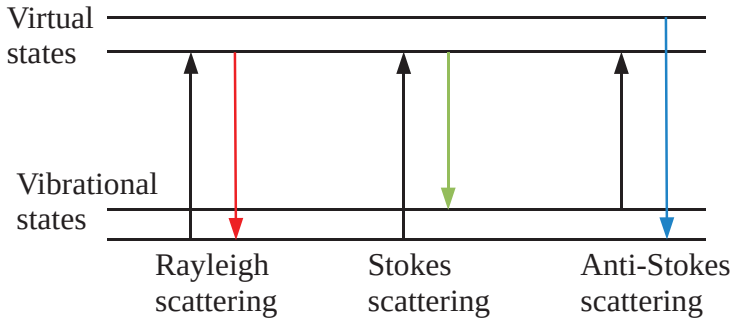

Figure 15: Energy levels of the different possible Raman interactions.

During the Stokes-scattering, the molecule transfers from its ground state to a virtual level. After energy release, it falls back to an energy level higher than the ground state so the photon absorbs energy. As the ground state is mostly occupied at room temperature, the Stokes-Raman scattering gives the highest intensity and

is therefore most often recorded. The Anti-Stokes scattering appears less intense as the molecule transfers from an excited state (not preferential at room temperature and therefore less possible) to the virtual level, falls back to the ground state and releases energy. During the Rayleigh-scattering, the photon is scattered elastically. Therefore it does not loose energy and falls back to the ground state. These energy differences are specific for each individual molecule and can particularly be used to characterize non-polar or slightly polar bonds [87, 88].

For polyurethanes, the conversion of the endgroups is usually of interest as it provides information on the completeness of the chemical reaction. In the case of polythiourethanes, Raman spectroscopy offers the possibility to qualify the presence of unreacted SH-endgroups resulting from incomplete reactions of the sulfur containing component PETMP. The SH peak is located at a wavenumber of $2575\,\mathrm{cm}^{-1}$ and as its intensity depends on the amount of free endgroups, a more or less qualitative statement is possible within one system.
Within this work, a confocal Witec Alpha 300RA Raman spectrometer with an Ar laser of 532 nm wavelength was used.

3.4 TGA

In thermogravimetric analysis (TGA), the weight loss of a sample is measured as a function of temperature or time. The article by Chattopadhyay and Webster [89] provides a detailed description of the thermal degradation of polyurethanes. Parts of it will be shortly summarized in the following subchapter.
During a TGA experiment, the thermal stability as well as the amount of residual material of a sample can be determined. In order to ensure an inert atmosphere, the measurements are usually conducted under a constant flow of nitrogen, helium or argon. For isothermal measurements, the sample is heated more or less instantaneously to the desired value and than hold at that temperature for a defined time, whereby during non-isothermal measurements the sample temperature is linearly increased with time. A TGA setup usually consist of a high precision balance with a small sample pan. During the measurements, the pan is completely enclosed by a heated furnace which has to posses a thermocouple in order to measure the temperature. The results are usually depicted in thermograms which contain the percentage weight loss as a function of temperature or time. On the other hand, the differentiation of the thermogram is often calculated in order to get detailed information on the beginning temperature and the end temperature of the decomposition, the temperatures which belong to the maximum weight loss or the steps

involved in the decomposition [89].

In order to investigate the thermal decomposition of PTU and PTU/t-ZnO composites, a TGA7 Thermogravimetric Analyzer (Perkin Elmer, Massachusetts, USA) was used. The sample mass was set to 2 mg. The heating was performed from 50 °C to 650 °C at a constant heating rate of 10 °C/min and a constant nitrogen flow of 20 ml/min.

3.5 SEM

Scanning electron microscopy (SEM) in general is used to investigate the surface of conductive specimens by scanning an electron beam across the sample surface where electrons from different depths are emitted and collected. When compared to optical microscopy, SEM provides the advantage of high spacial resolution (1 μm) as well as topographical imaging. For detailed information on electron microscopy, the reader is referred to the textbook by Goodhew et al. [90].
For imaging, electrons from an electron source (e.g. thermionic emission tungsten filaments or field emission gun) are accelerated towards the sample surface. Before reaching the sample, the electron beam is unmagnified by a system of condenser and than scanned across the surface. In SEM, radiation can be used for signaling and each interaction can be used to get different information on the sample. The radiations which occur upon electron irradiation include secondary electrons (SE), backscattered electrons (BE), Auger electrons and X-rays and the scattering events are schematically shown in figure 16.

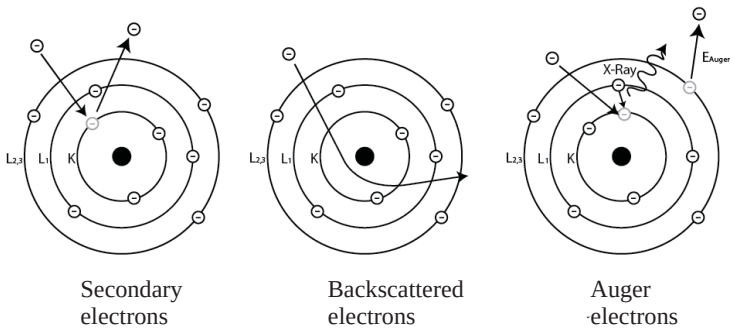

Figure 16: Schematic overview on the radiations which occur in SEM during electron irradiation.

SE are inelastically scattered, BE are elastically scattered and Auger and X-rays are

generated by the release of inner electrons which are compensated by an electron from an outer shell. The correlation of electron-beam and scanned sample surface is known as interaction volume and a schematic depiction of a typical example is shown in figure 17.

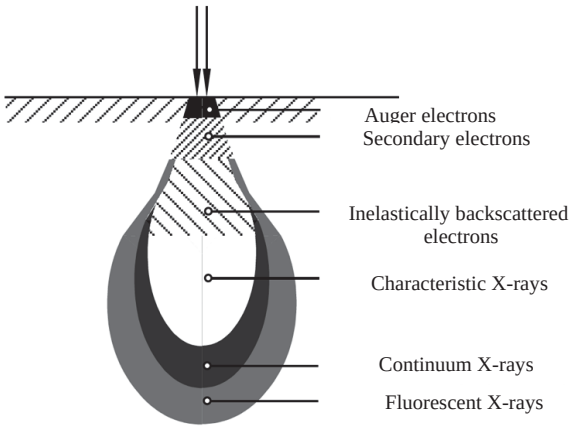

Figure 17: Schematic overview of the interaction volume generated by an accelerated electron beam.

Commonly, SE and BE are used for imaging in SEM as X-rays are mostly used for chemical analysis and Auger electrons require ultra high vacuum systems combined with specialized detectors due to their low energy. The numbers of SE and BE are known as *secondary electron coefficient* (δ) and *backscattered electron coefficient* (ν) whereby the latter strongly depends on the atomic number of the sample whereas (δ) does not.
For the detection of the most widely used SE, a scintillator-photomultiplier system is used which is commonly known as Everhart-Thornley detector whereas BE can be detected by three different types, namely scintillator detectors, solid-state detectors or through-the-lens detectors.
As mentioned, the irradiation of a sample with accelerated electrons also leads to the release of characteristic X-rays whose wavelength depends on the atoms present in the sample. The related analytical method is known as energy dispersive X-ray spectroscopy (EDX) where generated X-rays are recorded by an energy-dispersive detector. Such a detector is usually based on silicon where incoming X-rays excite electrons in the conduction band as well as the same number of holes in the valence band. As the energy required for one excitation amounts to 3.8 eV, the number of generated electron-hole pairs is proportional to the X-ray for a specific element.

In this work, SEM was performed in order to investigate the distribution of particles inside a polymeric matrix, the integrity of e.g. tetrapods after immersion into

a polymeric solution or the investigation of sample surfaces after immersion into aquatic surroundings. For these investigations, the samples needed to be conductively coated wherefore a 20 nm layer of gold was sputtered onto the surfaces of interest. A Zeiss ULTRA PLUS microscope with GEMINI column was employed and an Everhart-Thornley-Detector was used for detection of secondary electrons.

3.6 Tensile test

Tensile testing belongs to the destructive examination methods as it measures the force which is necessary in order to elongate a material until fracture. Commonly, the force is recorded as a function of constant deformation rate and for comparability, stress-strain characteristics are calculated from the measured datasets. The stress σ is obtained by dividing the force F by the sample area A, the strain ϵ is obtained by dividing the initial sample lenght l_0 by the lenghts change ΔL.

$$\sigma = \frac{F}{A} \tag{14}$$

$$\epsilon = \frac{L_0}{\Delta L} \tag{15}$$

The stress is usually denoted in MPa whereas the strain is given in %. Additional parameters that can be derived from tensile testing are the yield stress, the tensile strenght and the stress at failure. Another frequently considered material constant is the Youngs modulus which can be calculated from the slope of the elastic region of the stress-strain diagram. For polymers, the considered slope has to be calculated between 0.25 % and 0.05 % strain in order to consider defined standards.

$$E_0 = \frac{\sigma_{0.25} - \sigma_{0.05}}{\epsilon_{0.25} - \epsilon_{0.05}} \tag{16}$$

It has to be taken into account that under tensile force, also the cross-sectional area of the sample would undergo a change due to thinning. The actual stress in the material would therefore be greater than the calculated one wherefore the commonly shown stress-strain diagrams are widely known as *engineering stress-strain diagrams* [91].

For the tensile tests performed in this work, dog-bone shaped samples with a diameter of 1 mm, a width of 5 mm and a measuring lenght of 20 mm were casted into silicone molds following the described sample-preparation procedure. The measurements were performed with a Zwick 1445 universal testing machine with an initial load of 5 N and an applied constant strain rate of 1 mm/min whereby mean values and corresponding standard deviations were calculated from ten specimen datasets.

3.7 Pull off test

Aimed by pull off testing, the adhesiveness between a coating and a substrate can be determined by measuring the minimum force that is necessary in order to subtract the coating vertically.
The experiments conducted during this thesis were based on DIN EN ISO 4624, which is generally used for the investigation of lacquer systems on metal substrates.

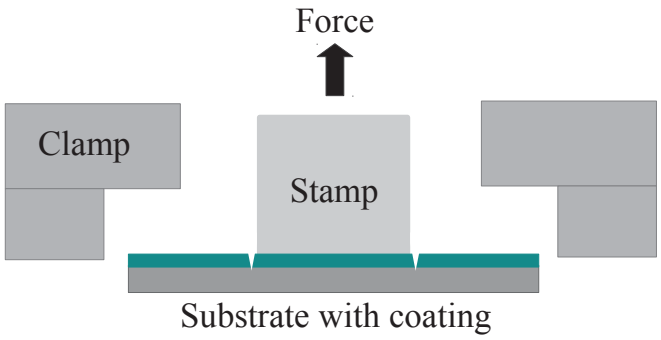

Figure 18: Schematic setup for the pull off test according to DIN EN ISO 4624.

For the adhesion testing, rectangular AlMg3 substrates of the dimensions 80 mm * 80 mm were coated with the material to be analyzed. A cylindrical AlMg3 rod with a radius of 10 mm was positioned in the middle of the sample, glued to it with UHU enfest 300 and dried at ambient temperature for 24 h. The adhesion test was performed with a Zwick universal testing machine (Zwick GmbH und Co. KG, Ulm) with a pre-load of 30 N and a constant test speed of 1 mm/min. Mean values and standard deviations were calculated from 5 data records.

3.8 Shore-D Hardness

In general, the term *hardness* describes the resistance of a material to a penetrating force which can be expressed as modulus. Detailed information on the different hardness test used for polymeric materials can be found in the textbook by Brown [91]. In this chapter, only the most common scale, the Shore durometer hardness, will be summarized.
The two main variants of the Shore durometer are Shore A and Shore D whereby both modifications are standardized according to DIN EN ISO 868. Basically, an indentor of specified geometry is pressed into the sample surface with a normalized spring force. The penetration depth of the indentor is a measure of the Shore hardness which is directly related to a suitable scale reaching from 0 (2.5 mm penetration

depth) to 100 (0 mm penetration depth) in hardness degree. The specifications of the samples require a minimum thickness of 6 mm and the measurement time is set to 3 s.

The Shore A scale is used for soft plastics and the corresponding indentor consists of a conic section with an aperture of 35 ° and a diameter of 0.79 mm at the tip. The applied contact force amounts to (12.5 +/- 0.5) N. The Shore D scale is suitable for hard plastics and the indentor is similar to a needlepoint with an aperture of 30 ° and a tip of 0.1 mm radius. For this variant, an applied contact force of (50 +/- 0.5) N is committed [91]. For the hardness testing in accordance to Shore-D, rectangular samples of 20 mm edge lenght and 8 mm thickness were casted into teflon molds and milled on both sides in order to provide planar surfaces. The measurements were performed with a Zwick/Roell device with a contact force of 50 N. Mean values and corresponding standard deviations were calculated from ten readings.

3.9 Sessile drop-technique

The sessile drop-technique is a widely used method for the determination of the contact angle of surfaces. In general, two variants of this method are established, the static sessile drop-method as well as the dynamic sessile-drop method. During the static method, a liquid droplet of defined volume is vertically placed onto the sample surface and the contact angle is measured optically by a camera. During the dynamic sessile drop-method, the volume of the droplet is changed by adding/decreasing its volume without affecting the solid/liquid interface between droplet and surface. Therefore, the advancing contact angle represents the largest possible contact angle whereby the receding contact angle represents the smallest possible contact angle. The difference between the advancing and receding contact angle is known as contact hysteresis and it is an important method for the characterization of real surfaces [92].
Details on the related well-established Young equation and the considerations regarding wetting phenomena were already shown in chapter 2.2.2.

The wetting behavior as well as the surface free energy (SFE) and ist polar and dispersive components were estimated according to the method of Owens, Wendt, Kaeble and Rebel (OWKR) and Adamson [93] in accordance with Gorb and Gorb [94]. An optical contact angle measuring device OCAH 200 (DataPhysics Instruments GmbH, Filderstadt, Germany) was utilized, three defined liquids (water, diiodomethane, ethylene glycol with densities of 1,000 kg/m^3, 3,325 kg/m^3 and 1,113 kg/m^3, respectively) were used. The drop volume was set to 2 μl.

3.10 Immersion-experiments

Preliminary Immersion-experiments were conducted at Aquarium Geomar, Kiel, Germany. In order to investigate the influence of the aquatic surroundings on the fouling behavior of the samples, they were immersed into two different habitats (Pacific tank and the Baltic-Sea tank). The growth of fouling species was investigated and recorded weekly by photographs.

Regarding the subsequent filed experiments, samples were glued to PVC plates by silicone-sealant (see figure 19) and were immersed into two different habitats, the river Schwentine ($54°19‘39.2“N; 10°11‘15.0“E$), Kiel, Germany and Laboe Harbor ($54°24‘10.2“N; 10°12‘56.9“E$), Germany. The growth of fouling species was investigated and recorded weekly by photographs.

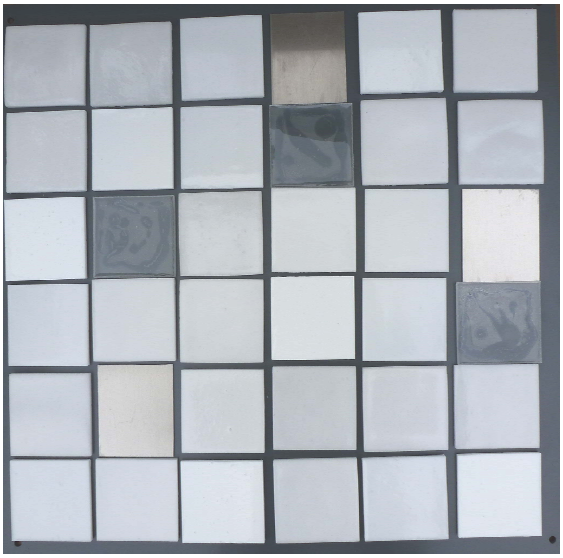

Figure 19: Exemplary assembly of samples glued to a PVC plate. 3 samples of the different compositions are randomly distributed over the surface, respectively. The sample size amounts to 80 mm * 80 mm.

3.11 Cleaning-experiment

In the general case, ships or other fouled surfaces are cleaned by high-pressure water-blasters to remove attached species. For this reason, in this work a Kaercher Professional HD 6/12-4C high-pressure water-blaster with a power of 2.800 W and possible pressures between 30 - 130 bar was used in order to evaluate the ease of cleaning of the immersed samples (figure 20).
To ensure reproducibility of the conducted experiments, a PVC-mask of 40 mm * 40 mm was designed in order to define the dimension of the tested area. The distance between nozzle and sample surface was set to 50 cm. The pressure was set to the maximum of 130 bar and the duration of water exposure amounted to 10 s.

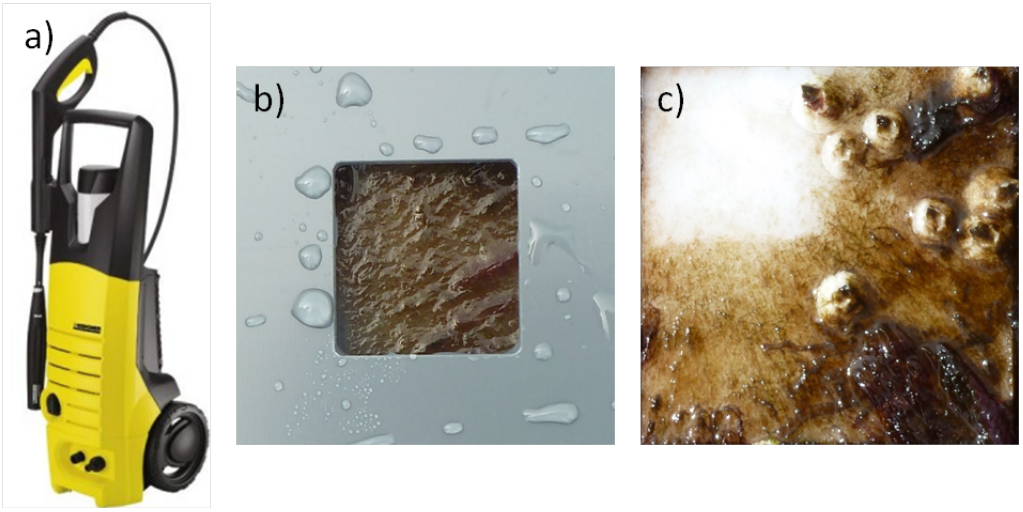

Figure 20: Cleaning setup. a) High-pressure water-blaster. b) Pattern for sample cleaning with the dimension 40 mm * 40 mm on an overgrown sample. c) Exemplary view of a sample surface partially cleaned by high-pressure water-blaster.

Chapter 4

Influence of hardener variations on the structural properties of polythiourethane

4 PTU

In the following subchapter, the mechanical and chemical characteristics of polythiourethane were investigated. Additionally, varying ratios of the two components HDI and PETMP were fabricated and analyzed. The initial ratio was predetermined to 58 wt.% HDI : 42 wt.% PETMP and it was varied in the range of excess HDI (up to 75 wt.%) as well as in the range of shortage HDI (down to 30 wt.% HDI). Immersion experiments were implemented with selected samples. As it is well known, that a low elastic modulus is favorable in order to reduce biofouling [25], HDI/PETMP ratios with decreasing elastic modulus were chosen.

4.1 Preparation of PTU

The two component PTU used in this work was purchased from Fluid-und Prozesstechnik (Waltershausen, Germany), whereby the components HDI and PETMP were delivered separately. The preparation of the different samples basically followed the same pattern, slight deviations will be announced in the appropriate subchapters.

Initially, PETMP was weighted, the appropriate proportion of HDI was added and the blending was hand-stirred. A complete degassing in a desiccator followed. Than the mixture was casted into molds or spread onto substrates whereupon a curing step at 84 ℃ for 24 h in an atmospheric furnace was performed.

4.2 Mechanical properties

4.2.1 Tensile response

For the evaluation of the mechanical properties of PTU with the initial ratio of HDI:PETMP, tensile tests were performed with five specimens, the corresponding stress-strain diagrams are shown in figure 21.

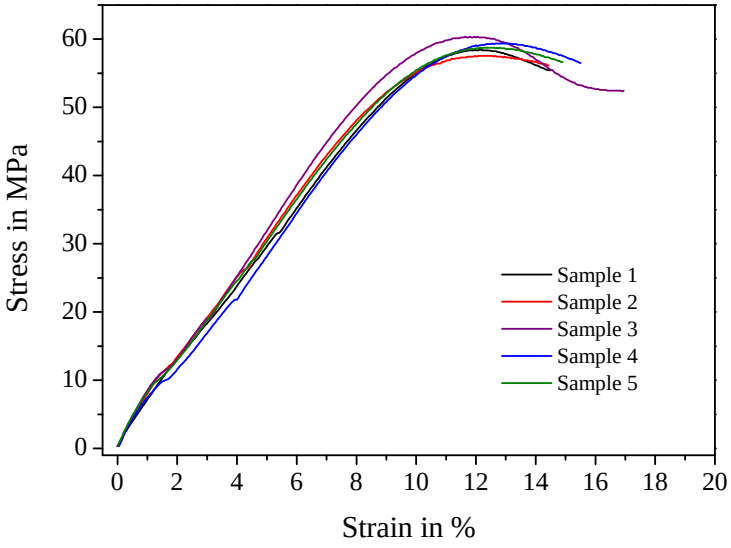

Figure 21: Comparision of five Stress-strain diagrams of PTU to show the reproducibility of the samples. A mean tensile strenght of around 60 MPa was reached, the mean elongation at fracture amounted to more than 15 % and the mean elastic modulus was calculated to nearly 1000 MPa.

The tensile strength reached almost 60 MPa with a corresponding elongation at fracture of about 15 wt.%. The five stress-strain diagrams show comparable courses which resulted in relatively low deviations. The maximum elongation at fracture was recorded to 16.95 wt.% for sample 3, the minimum value accounted to 13.15 wt.% for sample 1. Regarding the tensile strength, the maximum value was reached by sample 3 with 58.39 MPa, the minimum value was 55.63 MPa for sample 2. The elastic modulus was calculated according to equation 16, the maximum value of 1052.6 MPa was reached for sample 5, the minimum value of 923.7 MPa belonged to

sample 4. Mean values and corresponding standard deviations from tensile strength, elongation at fracture and elastic modulus are listed in table 1.

Table 1: Mean values and standard deviations for tensile strength, elongation at fracture and elastic modulus for PTU.

	Tensile strenght (MPa)	Elongation at fracture (%)	E-modulus (MPa)
PTU	57.1 ± 0.4	15.4 ± 0.9	981.5 ± 74.7

The influence of the stoichiometric HDI:PETMP variations on the stress-strain behavior was examined. Figure 22 shows exemplary stress-strain diagrams with decreasing amount of HDI.

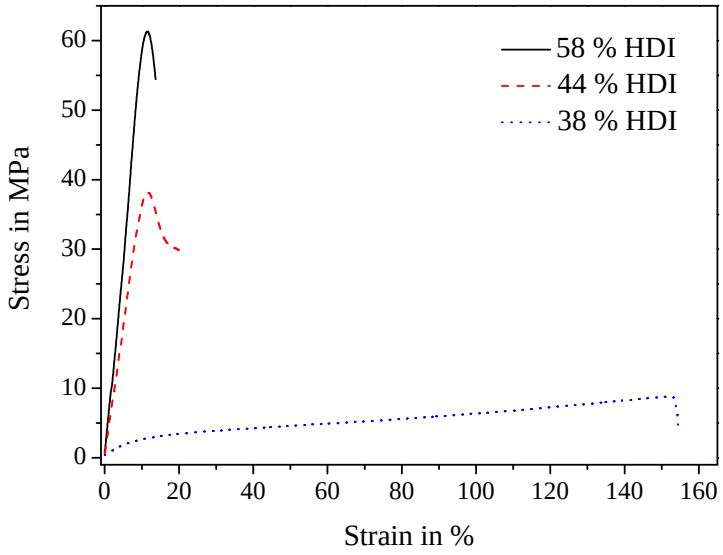

Figure 22: Stress-strain diagrams of PTU with decreasing amount of HDI. The tensile initial strength of aabove 60 MPa was strongly decreased when reaching values below 58 wt.%, HDI whereas the initial elongation at fracture of 15 % was strongly increased.

As stated, the initial amount of 58 wt.% HDI led to a high tensile strength of above 60 MPa with an elongation at break of around 15 %. A decreased amount of 44 wt.% HDI slightly increased the elongation at fracture whereby the tensile strength was slightly reduced. At 38 wt.% HDI, strong deviations occurred as the elongation at fracture was increased to above 150 % whereby the tensile strength was significantly reduced to below 10 MPa. Regarding the elastic modulus (see 1), the mean value of around 1000 MPa for the initial composition was decreased to around 350 MPa for the samples containing 44 wt.% HDI, and again strongly decreased down to around

60 MPa for the samples with 38 wt.% HDI.

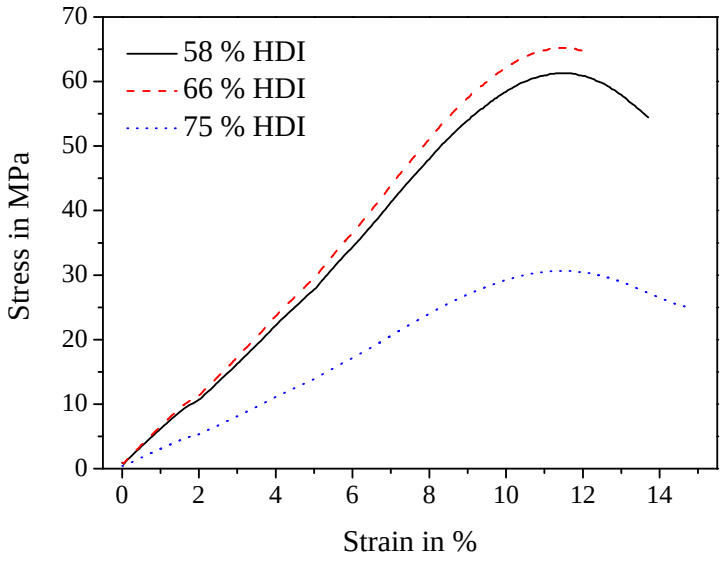

Figure 23: Stress-strain diagrams of PTU with increasing amount of HDI. The initial tensile strength of around 60 MPa was decreased when reaching values above 58 wt.%, whereas the initial elongation at fracture of 15 % was slightly increased.

On the other hand, the influence of excess HDI was evaluated and corresponding stress-strain diagrams are shown in figure 23. At a small surplus of HDI (e.g. 66 wt.% as shown in the figure), only small deviations occurred and the tensile strength of around 60 MPa was nearly not affected whereas the elongation at fracture was slightly decreased from 14 % to 12 %. Higher amounts (75 wt.% HDI) led to a decreased tensile strength down to 30 MPa together with a slightly increased elongation at fracture of above 15 %. The elastic modulus was not affected for the sample containig 66 wt.% HDI. A decreased mean value of around 680 MPa was recorded for the sample with 75 wt.% HDI.

For a comparative overview, mean values and standard deviations of tensile strength and elongation at fracture were compared (figure 24). The tensile strength was highest for the initial composition of 58 wt.% HDI : 42 wt.% PETMP, however, only slight deviations appeared in the range between 45 wt.% HDI and 68 wt.% HDI. Below and above these values, the tensile strength decreased strongly and reached a minimum of below 10 MPa. Regarding the elongation at frature, a more or less constant value of 18 % was observable from 45 wt.% HDI to 75 wt.% HDI, a strong increase up to nearly 160 % occured at amounts below 45 wt.%.

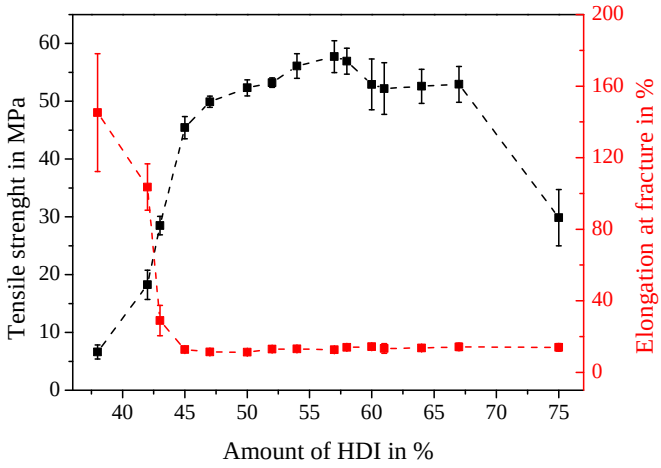

Figure 24: Influence of the HDI-content on the tensile strength as well as the elongation at fracture of PTU. The datapoints depict mean values and corresponding standard deviations, the line connecting the points is a guide for the eye.

4.3 Chemical properties

4.3.1 Raman-spectroscopy

In order to identify the characteristic Raman vibrations of PTU, figure 25 shows the complete Raman spectra for the initial HDI:PETMP composition.

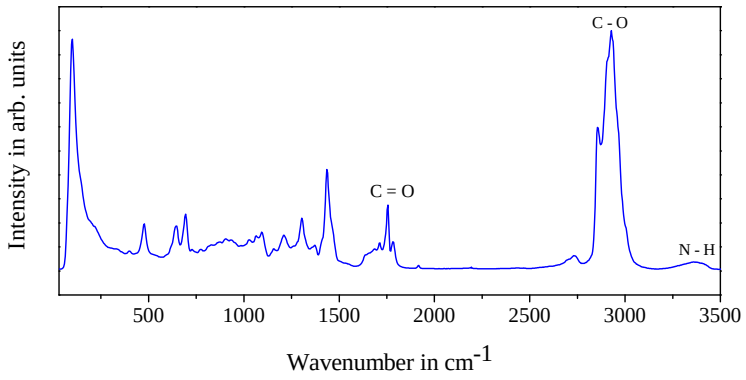

Figure 25: Characteristic Raman spectrum of PTU with the initial HDI:PETMP composition. The fingerprint region is located below 1500 cm^{-1}. Peaks: 1750 cm^{-1} from C=O, 2918 cm^{-1} from C-H, 3350 cm^{-1} from NH-.

The fingerprint region, which is a characteristic for the complete molecule, can be found in the range below 1500 cm^{-1}. The moderate peak at around 1750 cm^{-1} can be attributed to C=O, the strong vibration at 2918 cm^{-1} is caused by C-H and the

moderate peak at 3350 cm^{-1} results from NH-groups [95].

The conversion of the SH-functional groups with varying amounts of HDI was analyzed by Raman-spectroscopy. The reduced Raman-spectra (2520 cm^{-1} - 2625 cm^{-1}) are shown in figure 26 (a). The course of the increase of the SH-peak is visualized in figure 26 (b) where mean values and standard deviations of the Raman-intensity as function of the HDI:PETMP amount are depicted.

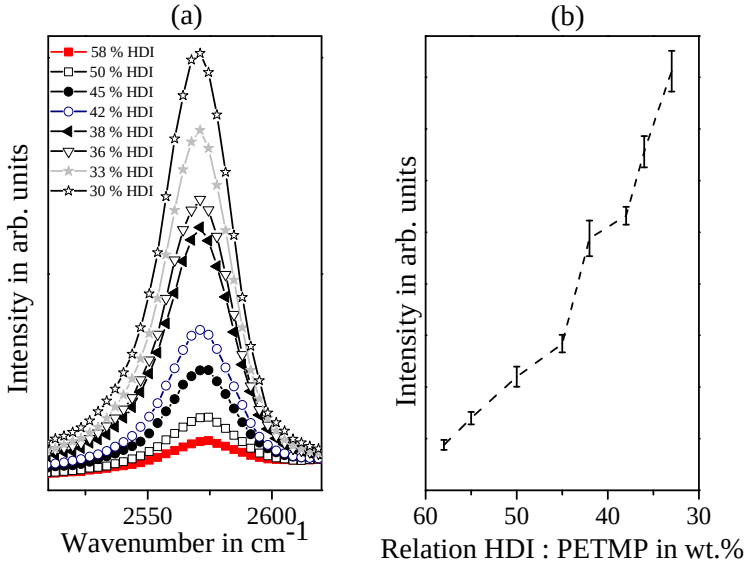

Figure 26: Raman-spectroscopy of HDI:PETMP ratio. a) The SH- vibration is shown in order to visualize its dependency on the amount of HDI. b) Shows the mean intensity of the SH-vibration as a function of the HDI:PETMP ratio. Lines connecting the datapoints are a guide for the eye.

At the initial amount of 58 wt.% HDI, only a very small SH-peak was observable which strongly increased with decreasing amounts of HDI.

4.3.2 FT-IR spectroscopy

In order obtain a complete overwiev on the effect of the HDI:PETMP ratio on the chemical structure of the cured polymer, IR-spectroscopy was performed on three samples with different amounts of HDI (initial amount of 58 wt.%, high amount of 75 wt.% and low amount of 40 wt.%.
The characteristic peaks above the fingerprint region below 1500 cm^{-1} obtained for the initial HDI:PETMP composition can be attributed to: 3340 cm^{-1}: NH; 2918 cm^{-1}: C-H; 2848 cm^{-1}: C-H. At an HDI-excess, the characteristic -NCO peak

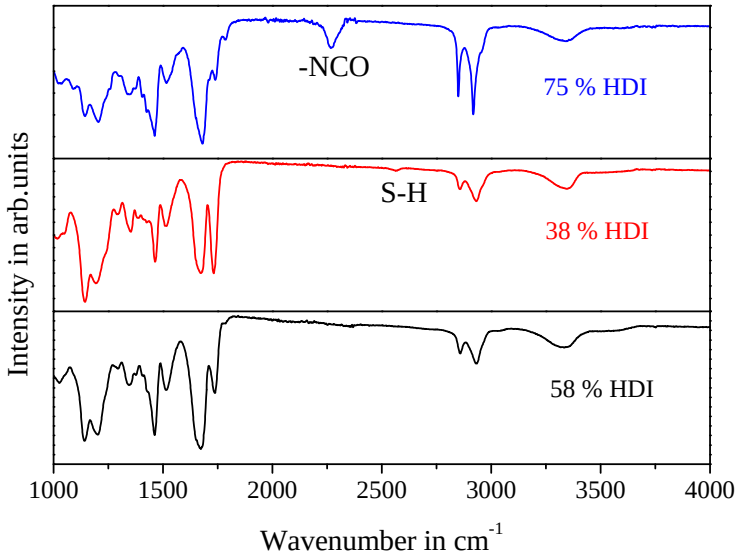

Figure 27: IR spectroscopy of HDI:PETMP ratio. a) The SH- vibration is shown in order to visualize its dependency on the amount of HDI. b) Shows the mean intensity of the SH-vibration as a function of the HDI:PETMP ratio.

appeared distinctly at 2300 cm^{-1}. On the other hand, a small SH-peak at 2550 cm^{-1} was observable at an excess of PETMP.

4.3.3 Thermal stability

In order to investigate the influence of HDI:PETMP variations on the thermal degradation behavior of the samples, thermogravimetric analysis was performed (figure 28 a) and differential thermograms (DT) were calculated from the measured data (figure 28 b).
As all samples revealed a multistage mass loss without a stage of constant mass in between, DT are taken for further analysis and the resulting mean values and corresponding standard deviations are shown in table 2.

Table 2: Thermogravimetric analysis of the PTU/t-ZnO composites. Shown are the three degradation steps obtained by differential thermal analysis.

Sample	1st degr. (C°)	2nd degr. (C°)	3rd degr. (C°)
PTU	261 ± 1.5	330 ± 1.5	453 ± 1.2
PTU, 38 wt.% HDI	269 ± 1.2	347 ± 1.0	472 ± 1.5
PTU, 75 wt.% HDI	288 ± 1.8	350 ± 1.1	500 ± 1.3

The DT revealed a first degradation step of PTU of around 260 °C, a similar value

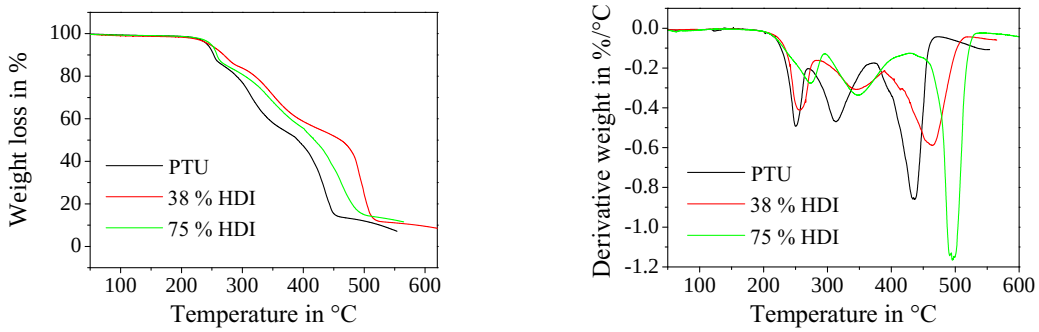

Figure 28: Thermogravimetric analysis of PTU with varying ratios of HDI:PETMP.
(a) Influence of the HDI:PETMP ratio on the thermal degradation behavior of PTU. (b) Differential thermal analysis of the HDI:PETMP variations.

was obtained for the sample with 38 wt.% HDI, PTU with 75 wt.% HDI showed a slightly increased value of around 290 °C. The second degradation step was accounted to around 330 °C for PTU, both component variations showed similar and slightly increased values of around 350 °C. The third degradation step was different for all variations, as PTU had a value of 453 °C, the sample with 38 wt.% showed a step at around 470 °C and the highest temperature was found for the sample containing 75 wt.% HDI at 500 °C.

4.4 Immersion results

The immersion experiment was conducted at three different locations (Aquarium Geomar, Kiel; Laboe harbor; Schwentinemuendung, Wellingdorf) and time periods of 12 months.

4.4.1 Evaluation of fouling process in Aquarium

In general, it has to be mentioned that the water inside the aquarium tanks are filtered in order to prevent strong growth of algae and therefore time-consuming cleaning work. For this reason, the fouling process proceeded very slow and also the diversity of fouling organisms was strongly reduced. Figure 29 shows the fouling process of PTU with varying ratios of HDI:PETMP in time lags of four months in the "'Pacific tank"' of Geomar.

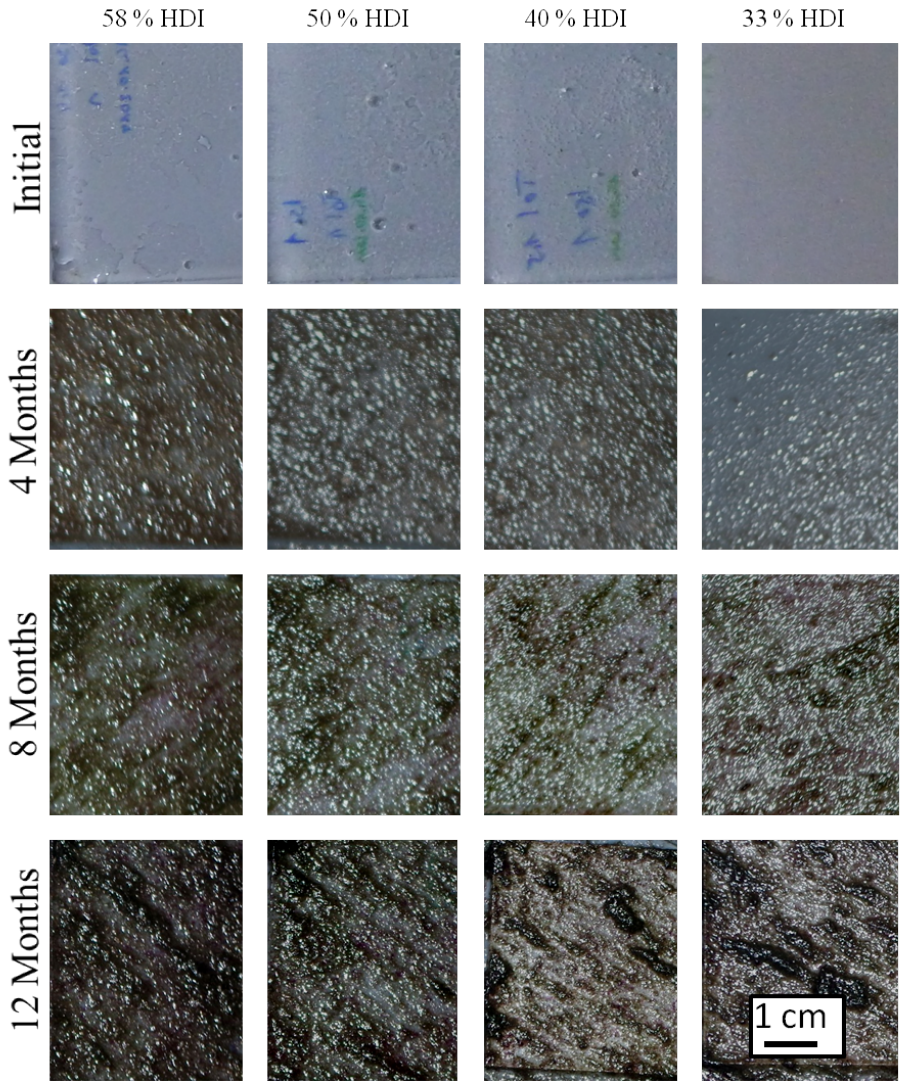

Figure 29: Immersion experiment of HDI:PETMP variation over time (overall 12 months) in the "'Pacific"' tank of the Aquarium Geomar. After four months, a thin film of algae were found, fouling proceeded slightly reduced with increasing HDI. After 8 and 12 months, fouling proceeded and no differences were found anymore on the respective samples.

After four months, only a thin film of algae was present on the samples, whereby a slightly reduced growth was observable with increasing amount of PETMP. After 8 and 12 months, the fouling film was increased but still not very distinct. The deviations regarding the growth on the different HDI:PETMP variations were no longer observable, a nearly uniform coverage with algae was found on every sample.

4.5 Evaluation of fouling process in Baltic Sea

In order to investigate the fouling characteristics of the HDI:PETMP variations, samples with different ratios of HDI:PETMP (58 wt.% HDI, 50 wt.% HDI, 45 wt.% HDI, 533 wt.% HDI) were immersed into the Baltic Sea at Laboe harbor. Figure 30

shows exemplary the fouling process on three different samples. Similar results were obtained for the s-ZnO containing coatings.
Compared to the aquarium, the growth proceeded much faster and also the variety of fouling organisms was much more pronounced.
After two months, a uniform thin film of algae was found on every sample, no deviations could be observed regarding the HDI:PETMP variation. Four months later, this film was developed to a thick coverage consisting of mainly algae. Again two months later, the growth was slightly reduced. After 10 months, the growth of sessile ascidiae was initiated and after 12 months, the whole sample areas were covered by this species.

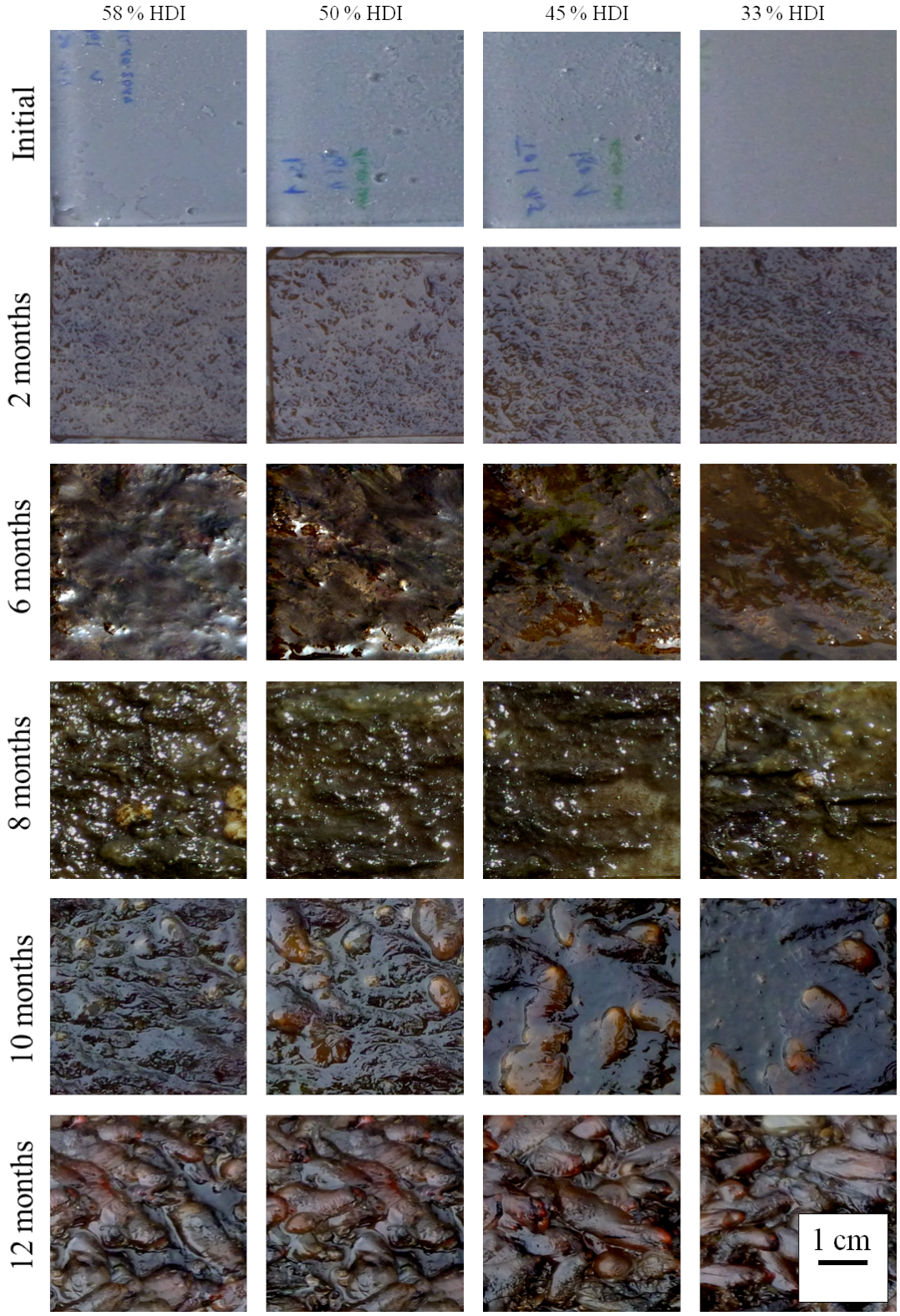

Figure 30: Immersion experiment of HDI:PETMP variation over time (overall 12 months) in Laboe harbor. 2 months after immersion, all samples were covered uniformly by algae. After 10 months, the growth of sessile ascidiae sarted and proceeded to cover the whole sample surfaces after 12 months of immersion.

4.6 Cleaning ability

Cleaning experiments were performed after an immersion time of eight months where the samples were already strongly fouled. To visualize the effect of cleaning onto a high-fouling surface, figure 31 shows a PVC sample before and after cleaning. For the evaluation of the residues, SEM images were taken and EDX-measurements were performed for the determination of the existing elements.

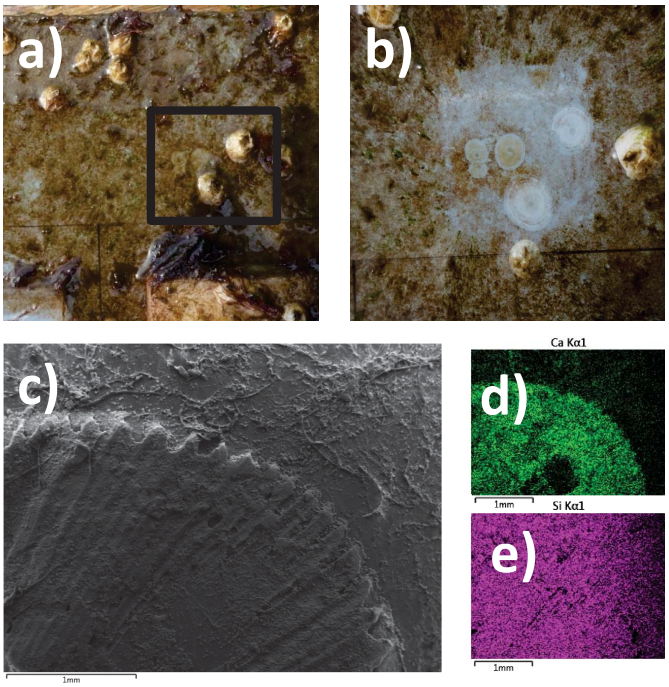

Figure 31: Cleaning experiment on PVC surfaces. a) barnacles attached to the PVC surfaces after eight months of immersion chosen for cleaning. b) Selected area after cleaning, the remaining parts of the barnacles are clearly visible. c) remaining barnacle cement, visualized by SEM. d) and e) corresponding EDX measurements showing, that the barnacle residue is composed of mainly calcium, other residues consist of mainly silicon.

It was demonstrated, that the PVC sample surfaces revealed a high amount of residues after cleaning which could also not be removed by additional water-pressure exposure time (see figure 31 a) and b)). Additionally, it can be deduced from the optical investigations that the PVC itself was degraded by biocorrosion.
Investigations by SEM demonstrated, that the majority of residues were caused by barnacles (see figure 31 c)) which are mainly composed of calcium (see figure 31 d)). The whole sample surface was additionally covered by a layer of mainly silica (see figure 31 e)).

In contrast, the cleaning experiment was much more successful on the PTU surfaces. Figure 32 shows exemplary two samples with different ratios of HDI:PETMP,

whereby a) and b) show the initial ratio of 58 wt.% HDI and c) and d) show the sample with lacking HDI (38 wt.%) both before and after cleaning. Again, SEM and EDX investigations were performed onto the cleaned surfaces to evaluate the composition of possible existing residues (see figure 32 e) and f)).

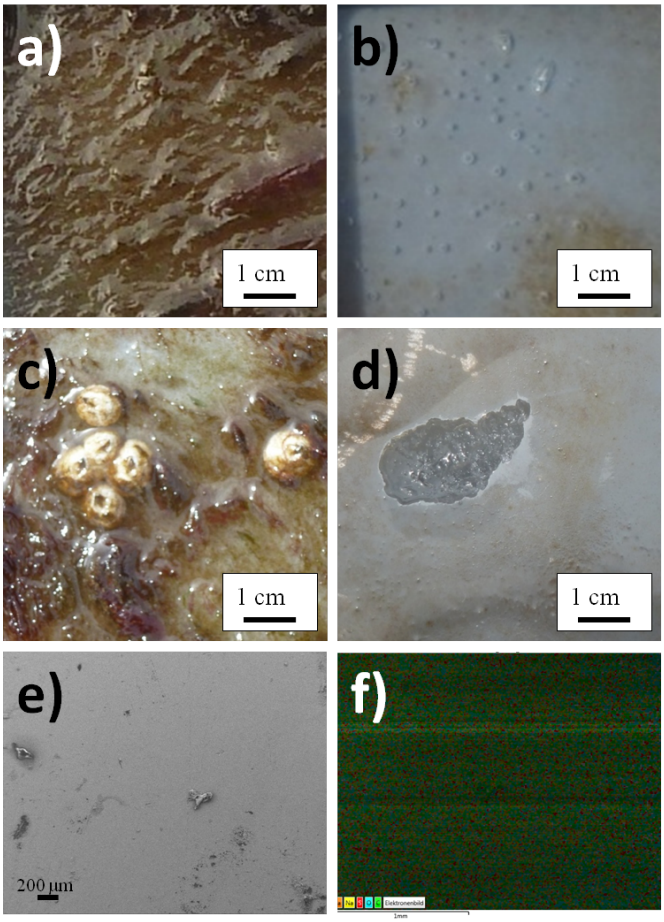

Figure 32: Cleaning experiment on PTU. a) fouled PTU surface with initial HDI:PETMP composition after eight months of immersion. b) PTU surface with initial HDI:PETMP composition after cleaning, no residues of sessile organisms visible. c) fouled PTU surface with lacking HDI (38 wt.%HDI) after eight months of immersion, a high amount of barnacles is present. d) PTU surface with lacking HDI after cleaning. The barnacles were completely removed, no residues were present. On the other hand, the surface was damaged due to the high water pressure. e) SEM-micrograph of a cleaned PTU surface, nearly no residues were obtainable. f) EDX measurements underlined, that the cleaning experiment was successful for PTU.

It was shown, that both samples were nearly completely cleaned by the Kaercher system and nearly no residues were visible. Additionally, it can be stated that the material was not at all degraded within the time of immersion.
However, the sample with lacking HDI could not withstand the strong water pressure for what reason damages within the sample surface appeared.

Regarding the SEM images, it could be underlined that the cleaned surface showed a nearly residue-free surface. These results were underlined by EDX investigations where only small and evenly distributed residues of mainly calcium and magnesium appeared.

4.7 Discussion

The mechanical and chemical properties as well as the fouling behavior of the utilized polythiourethane (PTU) were evaluated in the first chapter. Additionally, the ratio of the two components 1,6 Diisocyanatohexan (HDI) and Pentaerythritoltetrakis (3-mercaptopropionat) (PETMP) was varied.

Tensile testing has shown that PTU has a high tensile strength of nearly 60 MPa and a high elastic modulus of around 1000 MPa combined with a comparably high elongation at fracture of around 15 %. As PTU is a thermoset with a tetrafunctional polyol, the presence of cross-linking provides additional tensile strength when compared to thermoplastic polyurethane (PU) [96]. Furthermore, a ratio of hard segments (HS) and soft segments (SS) is present which ends up in a hard but not completely rigid polymer. As shown by Chattopadhyay and Raju [96], the ratio between HS and SS has a strong influence on the mechanical properties of polyurethanes for what reason their ratio is usually predetermined by the manufacturer in order to provide the stoichiometric ratio necessary for the required material properties [95].

It was demonstrated, that deviations from the initial ratio (58 wt.% HDI) have a strong influence on the mechanical and chemical properties. Tensile tests revealed, that decreasing HDI led to increased elasticity combined with decreased tensile strength. The increased elasticity as a result of lacking HDI can at first be attributed to lower cross-linking. These findings are again in accordance to the study by Chattopadhyay and Raju [96] where it is stated that the height of the tensile strength is dependent on the degree of cross-linking. As cross-linking occurs via the reactive SH and NCO bonds, a lack of available NCO bonds causes unreacted SH bonds and therefore less points of interconnection.
Another factor is the lower amount of hard segments within the polymeric structure for what reason the long, flexible soft segments provided by PETMP predominate. As already mentioned, Chattopadhyay and Raju [96] stated that the ratio between HS and SS is crucial for the mechanical properties of the final polymer.
On the other hand, a surplus of HDI did not influence tensile strength and elongation at fracture up to a certain limit were the tensile strength decreased drastically

[64]. In the case of surplus HDI, nearly no unreacted functional groups will be found because the highly reactive NCO bonds will react with themselves. Additionally, the increased amount of hard segments results in the formation of a mainly hard and rigid polymer structure which again is in accordance to Chattopadhyay and Raju [96] and Chattopadhyay and Webster [89].
Summarizing, tensile testing revealed a strong dependency of the mechanical features on the ratio between HDI and PETMP. Increasing HDI did not led to strong deviations within a certain range (up to nearly 70 wt.% HDI), whereas decreasing HDI caused significantly higher elasticity and reduced tensile strength.

Raman-spectroscopy revealed an increased SH-peak for a decreasing amount of HDI. The peak at 2551 cm^{-1} can be attributed to SH, so an increase in the peak intensity indicates a surplus of PETMP which coincides with the conducted component variations. The NCO-peak cannot be detected by Raman-spectroscopy. Therefore, additional Fourier-transformed-infrared-spectroscopy measurements were performed on the component-variations. Despite the SH-peak already investigated by Raman, an increased -NCO peak at 2300 cm^{-1} caused by an excess of HDI was shown which indicates that a small amount of unreacted NCO groups were still present within the samples. Similar results were obtained by Papaj et al. [95] who investigated the effect of hardener variations on the properties of a polyurethane. It was shown, that component variations deviating from the recommended ratio led to additional IR-peaks indicating the presence of unreacted functional groups. These findings are in accordance to the results obtained by tensile testing where deviations from the stoichiometric ratio led to changes within the mechanical properties. It was shown, that PTU with a low amount of HDI caused an elasticity comparable to that one of silicone. This is beneficial for the application as antifouling coating as it was stated by Callow and Callow that a low elastic modulus is beneficial for the prevention of marine fouling [42]. However, a low elastic modulus is in general accompanied by low overall mechanical stability which is unfavorable for mechanically stressed areas like ship hulls. Additionally, the high elasticity is a result of unreacted functional SH-groups which are known to be toxic and are therefore unsuited as antifouling paints.

Regarding the thermal stability of PTU, thermogravimetric analysis showed that the decomposition is a multistage process with three partial decomposition reactions. Additionally, it was shown that the decomposition steps depend on the HDI:PETMP ratio.
In general, the degradation of PU involves the release of volatile compounds which explains the slight weight loss before the first degradation step. Differential thermo-

grams revealed a first degradation step at around 260 °C for PTU and the sample with reduced HDI, whereas PTU with excess HDI showed a value of around 290 °C. This first decomposition step can be attributed to the degradation of the hard segments accompanied by the breakage of weak side chains and the formation of gaseous byproducts [89]. The increased degradation temperature for the sample with excess HDI may be caused by the higher rigidity of the polymer which may cause stronger side chains. This effect does not occur for samples with less HDI. The first degradation is therefore not affected.
The second degradation step of 330 °C for pure PTU was slightly increased to around 350 °C for both samples with deviating HDI content. In principle, the second and third degradation steps are attributed to the degradation of the soft segments [89]. The increase in degradation temperature for decreased HDI amount may be caused by the raised number of SS which may cause a delayed degradation. On the other hand, the lack of soft segments caused by additional HDI may cause a higher degree of cross-linking which again results in higher thermal stability. The last degradation temperature-step was increased for both samples with deviating HDI contents. This step can be again attributed to the presence of SS, the explanation for the increased degradation temperature is similar to the second degradation.

In order to evaluate the influence of the HDI:PETMP variation on the fouling properties, samples with decreasing HDI and therefore increasing elasticity were immersed into three different habitats. Preliminary experiments were conducted in the aquarium Geomar, field experiments took place in saltwater (Baltic Sea, Laboe harbor, Germany) on the one hand and in freshwater (river Schwentine, Wellingdorf, Germany) on the other hand.
A small influence of the fouling properties on HDI:PETMP ratio was determined within the course of the preliminary experiments conducted in the aquarium Geomar. It was shown, that the growth was slightly reduced on samples with reduced HDI within the first four months. After eight and 12 months, this difference with respect to fouling was no longer found because all surfaces were completely overgrown by a relatively thin layer of green algae. The decrease in fouling during the first months may be a result of the reduced elastic modulus present for the samples with reduced HDI. A low elastic modulus combined with low surface free energy is beneficial with to combat biofouling [42]. On the other hand, the surface free energy of PTU with around 40 mN/m is relatively high when compared to silicone with around 22 mN/m [42]. The reduced growth on samples with reduced HDI in the beginning of the experiments may be a result of toxic unreacted SH groups were the settlement of fouling organisms is unfavored. With process in time, these

groups may also react for what reason the toxic effect is diminished.

Regarding the field experiments within the Baltic Sea, in general it can be stated that the growth was much more pronounced and proceeded much faster compared to the aquatic environment. This is a result of the much higher diversity of fouling organisms within the natural surroundings as the water within the tanks is filtered. In contrast to the aquarium, the samples immersed into the Baltic Sea did not show any differences with respect to the HDI content. This fact may again be attributed to the great diversity of present fouling species, which implies the constant presence of different organisms being able to cope with the special conditions on these samples [7].

The adhesion of fouling organisms on PTU and PVC was tested by high-pressure water blaster experiments. Those have shown superior cleaning results for PTU with no residues and complete intact polymer surface after cleaning. These results were underlined by SEM and EDX measurements where only a small and evenly distributed amount of calcium and silicon was found. Different results were found for the PVC surfaces treated in the same way. Those surfaces showed residues of the fouling organisms as well as degraded polymer surfaces as a result of biocorrosion. These findings were underlined by SEM and EDX measurements showing up the calcinated residues of barnacles. Furthermore, it was shown that the PVC surfaces were degraded within the time of immersion. This degradation is caused by the aggressive constituents used by aquatic organisms to attach to surfaces. These organisms try to decompose their underground in order to obtain increased adherence .

Regarding the materials stability towards degradation by aquatic organisms, it can be stated that the PTU surfaces remained completely unaffected. Therefore, it can be assumed that PTU offers high stability towards the aquatic environment for what reason it is best suited as matrix polymer for long-lasting applications in natural seawater surroundings.
However, it was shown that reduced HDI led to surface damages after high-pressure cleaning. This can be attributed to the lower mechanical stability of the polymer. As shown by tensile testing, decreased HDI led to lower mechanical strength combined with increased elasticity for what reason the applied water pressure was too high and caused damage within the polymeric structure.

Chapter 5

Complex shaped ZnO nano- and microstructure based polymer composites: Mechanically stable and environmentally friendly coatings for potential antifouling applications

5 PTU/ZnO composites

In the following chapter, the influence of ZnO particles on the chemical, mechanical and antifouling characteristics of PTU is summarized. Despite the different filler amounts (0 wt.%, 1 wt.%, 5 wt.%, 10 wt.%), also the particle morphology was varied (t-ZnO and s-ZnO) in order to investigate the influence of the particle shape onto the material properties.

5.1 Preparation of PTU/ZnO composites

Initially, PETMP was weighted and if required, the necessary amount of additives was stirred in by hand. The appropriate proportion of HDI was added, whereby

the mixture ratio accounted 58 wt.% HDI : 42 wt.% PETMP. The mixture was completely degassed in a desiccator and casted into molds or spread on substrates whereupon a curing step at 84 °C for 24 h in an atmospheric furnace was performed.

5.2 Mechanical properties

5.2.1 Tensile response

The influence of the particle amount and the particle shape on the mechanical properties was at first investigated by tensile testing. In order to illustrate the different courses of the stress-strain curves, figure 33 shows exemplary pure PTU as well as PTU with 5 wt.% t-ZnO and 5 wt.% s-ZnO, respectively.

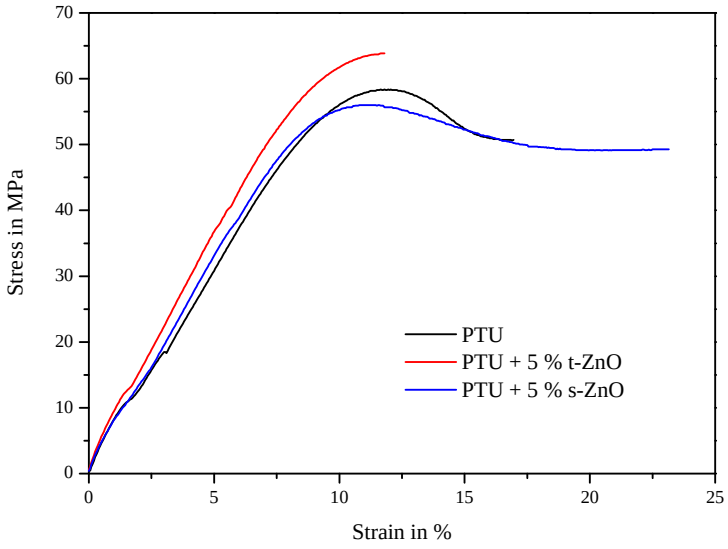

Figure 33: Influence of differently shaped ZnO particles onto the stress-strain behavior of PTU. Shown is pure PTU in comparison to two exemplary samples with 5 wt.% filler amount and different ZnO particle morphologies (t-ZnO and s-ZnO). 5 wt.% t-ZnO caused an increase in tensile strength accompanied by a decrease in elongation at fracture. On the other hand, 5 wt.% s-ZnO led to decreased tensile strength and increased elongation at fracture.

Within the chosen graphs is shown, that t-ZnO led to a slightly increased tensile strength from initially below 60 MPa to nearly 65 MPa combined with a slight reduction in elongation at fracture from more than 15 % down to around 12 %. In contrast, s-ZnO decreased the tensile strength down to below 55 MPa and caused an increased elongation at fracture to more than 22 %.
For an overview in more detail, figure 34 a), figure 34 b) and figure 35 show mean val-

ues and corresponding standard deviations of tensile strength, elongation at fracture and elastic modulus as function of the particle amount.

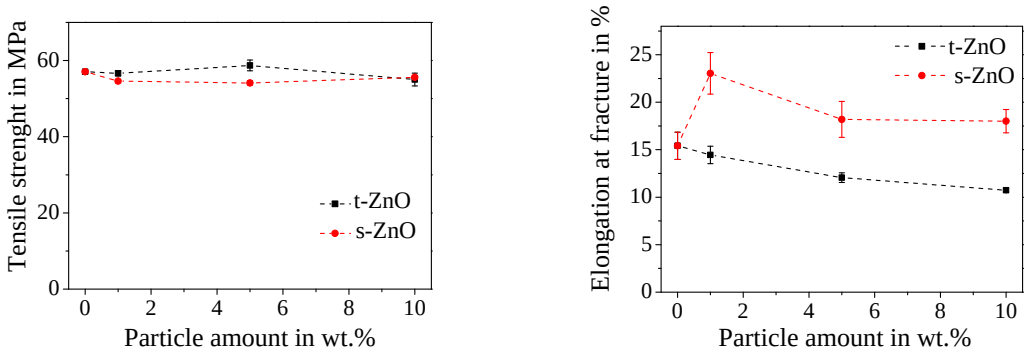

Figure 34: Tensile test of PTU/t-ZnO composites.
(a) Fracture toughness as a function of particle amount. An increase in elongation at fracture was obtained for 5 wt.% t-ZnO, other filler amounts and the spherical morphology could not enhance the tensile strength. (b) Elongation at fracture as a function of particle amount. A strong influence of the s-ZnO addition was observable as the elongation at fracture increased significantly at 1 wt.% s-ZnO. t-ZnO led to slightly decreased values with increasing filler amount. Lines connecting the points are a guide for the eye.

Pure PTU reached a mean tensile strength of 57 MPa and a mean elongation at fracture of 15.5 wt.%. No effect on the tensile strength was observable for 1 wt.% t-ZnO whereas 1 wt.% s-ZnO caused a slight decrease to below 55 MPa. On the other hand, the elongation at fracture was strongly affected by the particle shape as 1 wt.% s-ZnO caused an increase up to 23 wt.% whereby t-ZnO had nearly no effect. At 5 wt.% filler amount, the tensile strength as well as the elongation at fracture differed significantly for t-ZnO (59 MPa and 12 wt.%) and s-ZnO (54 MPa and 18 wt.%). Regarding the filler amount of 10 wt.%, the tensile strength was not affected whereas the elongation at fracture was significantly higher for s-ZnO (18 wt.%) compared to t-ZnO (11 wt.%).
Regarding the elastic modulus, pure PTU reached a mean value of nearly 1000 MPa which was not affected by the addition of 1 wt.% t-ZnO and 5 wt.% t-ZnO. On the other hand, 1 wt.% s-ZnO caused a slight reduction to a mean value of below 900 MPa which stayed unaffected for 5 wt.% s-ZnO. At a filler amount of 10 wt.%, the elastic modulus was again slightly affected as a small increase was observable for s-ZnO (mean value of around 1000 MPa) whereby t-ZnO led to a slight decrease (mean value of around 950 MPa).

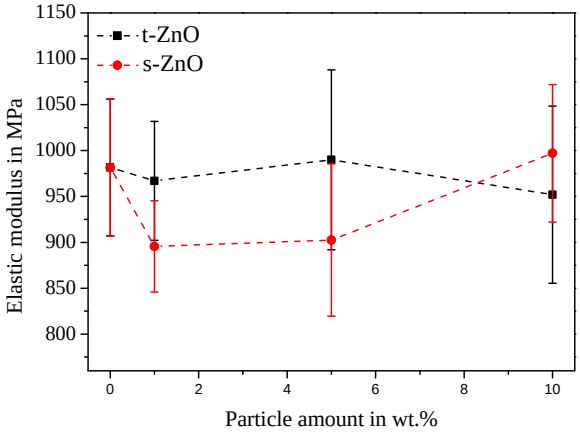

Figure 35: Elastic modulus of PTU as a function of particle amount. 1 wt.% and 5 wt.% t-ZnO addition did not cause a change, 1 wt.% s-ZnO caused a reduction. No effect was observable for 5 wt.% s-ZnO. 10 wt.%. S-ZnO caused an increase whereas 10 wt.% t-ZnO caused a slight decrease.

5.2.2 Shore-D hardness

The influence of the particle amount and the particle morphology on the Shore-D hardness was evaluated and mean values as well as corresponding standard deviations are depicted in figure 36.

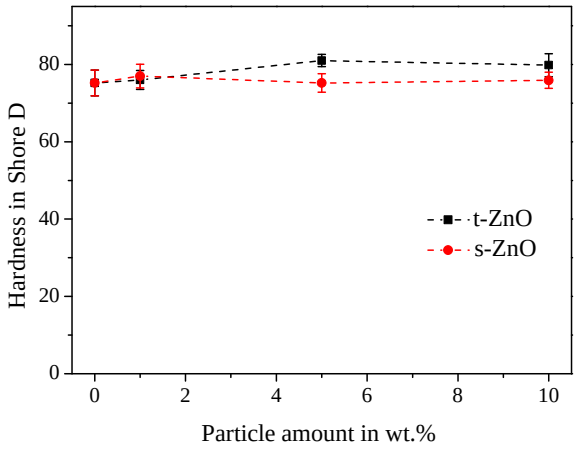

Figure 36: Shore-D Hardness of PTU as a function of particle amount. The initial value of 75 Shore-D could be increased to 81 Shore-D for 5 wt.% addition of t-ZnO, s-ZnO did not cause a increase.

Pure PTU showed a mean hardness of 75 Shore-D which was not significantly changed by the addition of 1 wt.% t-ZnO or s-ZnO particles. An increase up to around 81 Shore-D was determined for samples with 5 wt.% t-ZnO which was not

observable for those containing 5 wt.% s-ZnO. The addition of 10 wt.% t-ZnO showed no significant deviations to the values obtained for 5 wt.% t-ZnO.

5.2.3 Adhesive properties

The influence of the ZnO particle amount and morphology on the adhesion to AlMg3 substrates was investigated by pull-off testing (figure 37).

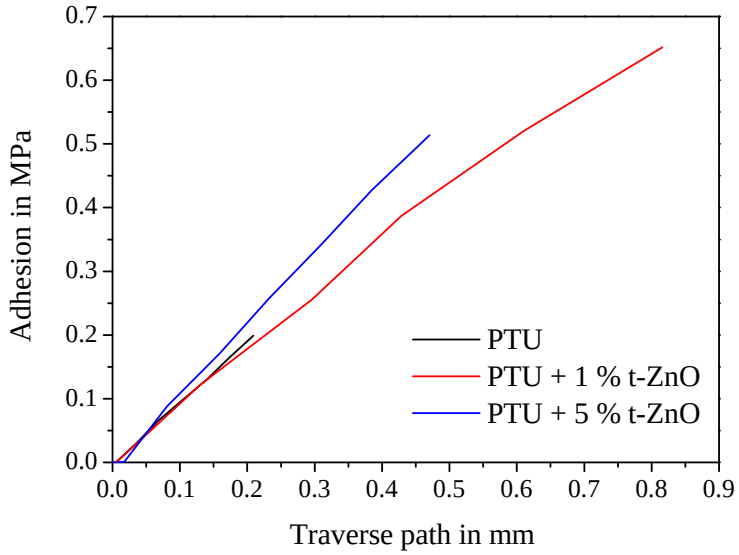

Figure 37: Adhesion of PTU to AlMg3 with different amounts of t-ZnO filler particles. The adhesion was strongly increased with increasing filler amount.

In figure 37, exemplary results are shown for three samples with different t-ZnO filling (0 wt.%, 1 wt.%, 5 wt.%,), whereby the most remarkable changes are shown for illistration. The corresponding mean values and standard deviations are depicted in figure 38. It was demonstrated, that the adhesion was strongly enhanced by increased t-ZnO filling. Pure PTU reached an adhesion strength of around 0.2 MPa which was already increased to more than 0.5 MPa. For 5 wt.% t-ZnO a further increase to nearly 0.7 MPa was reached. Further t-ZnO addition of 10 wt.% did not led to higher adhesion strength.

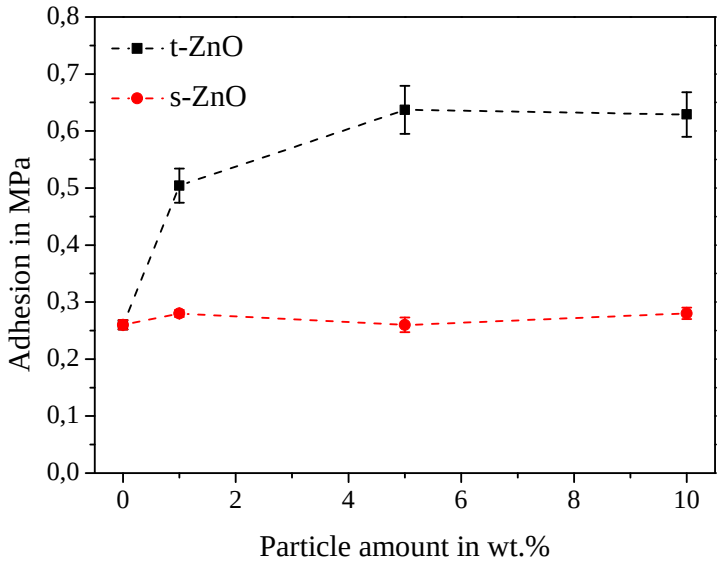

Figure 38: Adhesion of PTU to AlMg3 as a function of particle amount. A strong increase with increasing ZnO amount is visible for tetrapods whereas spherical particles led the composite unaffected. Lines connecting the points are a guide for the eye.

Figure 38 underlines, that the addition of spherical ZnO could not enhance the adhesion strength as the mean values for all particle concentrations lay in the region of the initial 0.25 MPa for pure PTU.

5.3 Chemical properties

5.3.1 Raman-spectroscopy

In order to investigate weather the addition of ZnO particles has an influence on the polyaddition of HDI and PETMP, Raman-spectroscopy was performed and the full spectra are depicted in figure 39.

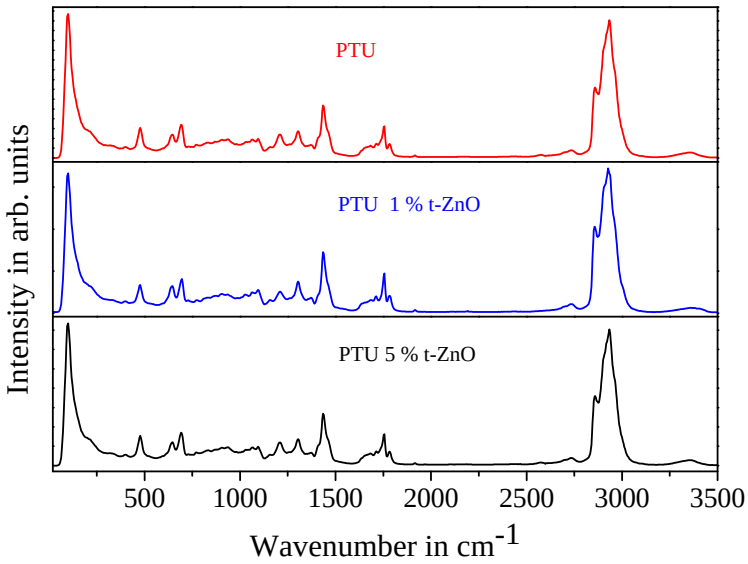

Figure 39: Raman spectrographs of PTU with different amounts of t-ZnO. It can be derived that the addition of ZnO has no effect on the quantitative polyaddition of PETMP and HDI as no additional peaks appeared.

Regarding the fingerprint region which is located below 1500 cm^{-1}, all spectra appear similar, the ZnO particles did not led to additional or missing peaks. Also the moderate peak at around 1750 cm^{-1} from C=O, the strong vibration at 2918 cm^{-1} caused by C-H and the moderate peak at 3350 cm^{-1} caused by NH-groups did not show any differences.

5.3.2 FT-IR spectroscopy

Aimed by FT-IR, the influence of the particles on the chemical structure was evaluated. The spectra obtained for 0 wt.%, 1 wt.% and 5 wt.% t-ZnO are compared in figure 40.

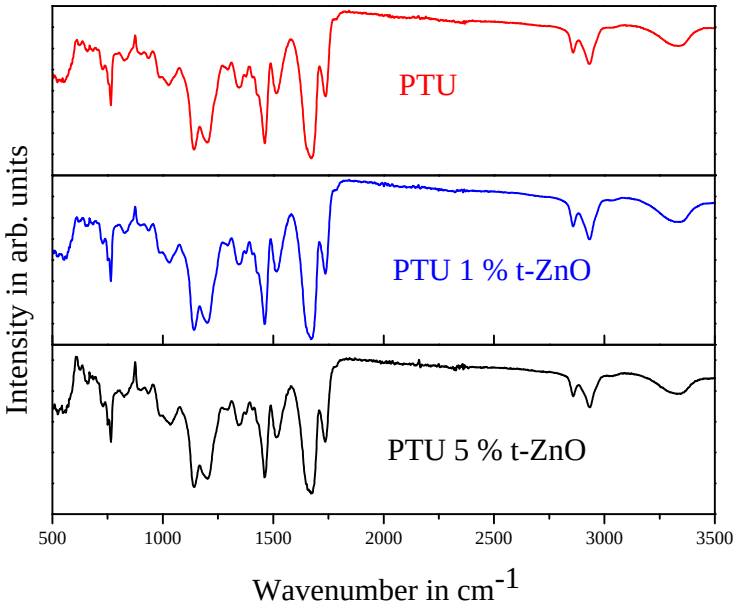

Figure 40: Infrared spectrographs of PTU with different amounts of t-ZnO. It can be derived that the addition of ZnO has no effect on the quantitative polyaddition of PETMP and HDI.

The FT-IR spectra underline the results obtained by Raman-spectroscopy as they show similar results, the fingeprint region below 1500 cm^{-1} was not influenced. The characteristic peaks above the fingerprint region attributed to NH (3340 cm^{-1}), C-H (2918 cm^{-1}) and C-H (2848 cm^{-1}) appear for all investigated samples.

5.3.3 Thermal stability

The influence of the particles on the thermal degradation behavior was investigated by thermogravimetric analysis as well as by differential thermal analysis. Figure 41 shows exemplary three graphs. The values for the different degradation stages evaluated from three measurements as well as the corresponding mean values are schown in table 3.

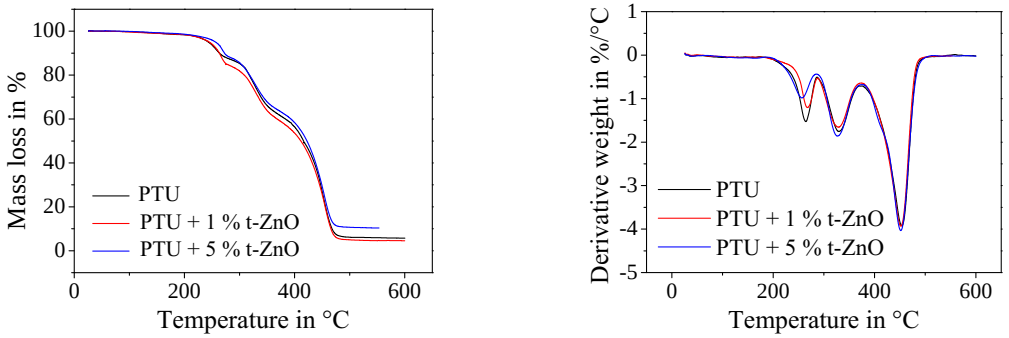

Figure 41: Thermogravimetric analysis of PTU.
(a) TGA Thermogram, shown in the percentage mass loss over time of different PTU/t-ZnO composites. (b) Differential thermal analysis of different PTU/t-ZnO composites.

Table 3: Thermogravimetric analysis of the PTU/t-ZnO composites. Shown are the three degradation steps obtained by differential thermal analysis.

Sample	1st degr. (C°)	2nd degr. (C°)	3rd degr. (C°)
PTU	261 ± 1.5	330 ± 1.5	453 ± 1.2
PTU, 1 wt.% t-ZnO	264 ± 1.0	330 ± 1.5	454 ± 1.0
PTU, 5 wt.% t-ZnO	262 ± 1.5	327 ± 1.5	453 ± 1.5

In general, it can be stated that the addition of t-ZnO particles had no significant effect on the thermal properties of PTU. All samples were thermally stable up to around 260 °C and showed three degradation steps. The beginning decomposition temperature was found at around 260 °C whereas the end decomposition temperature amounted to around 450 °C. A third degradation step appeared at 330 °C.

5.4 Wettability

5.4.1 Contact angle measurements

Contact angle measurements on PTU were conducted at three different amounts of t-ZnO (0 wt.%, 1 wt.%, 5 wt.%,). The surface free energy was calculated according to the OWKR method with its polar and dispersive parts and the obtained mean values and standard deviations are shown in table 4.

Table 4: Contact angle measurements of different PTU/-t-ZnO composites. Shown are the values for the contact angles CA, the surface energy SE and the polar and dispersive proportions, respectively.

Sample	CA (°)	SFE (mN/m)	Pol. (mN/m)	Disp. (mN/m)
PTU	67.4 ± 3.4	40.7 ± 0.5	12.4 ± 1.7	28.4 ± 1.2
PTU, 1 wt.% t-ZnO	70.4 ± 3.7	39.9 ± 0.8	10.0 ± 2.3	29.8 ± 1.7
PTU, 5 wt.% t-ZnO	72.8 ± 3.4	37.4 ± 1.6	9.2 ± 1.0	28.2 ± 1.3

The increased amount of t-ZnO was accompanied by a slight increase in the contact angle from around 67° for pure PTU up to nearly 73° for PTU with 5 wt.% t-ZnO. Simultaneously, the total SFE showed a slight decrease from around 41 mN/m down to 37 mN/m. However, remarkable changes occurred regarding the polar and dispersive parts of the SFE. While the dispersive proportion stayed nearly unaffected at around 28 mN/m, the polar proportion strongly decreased from around 12 mN/m for pure PTU to nearly 9 mN/m at 5 wt.% t-ZnO.

5.5 Immersion results

5.5.1 Evaluation of fouling process in aquarium

A preliminary experiment was performed in the aquarium Geomar and the results after 20 weeks (Pacific tank) and 30 weeks (Baltic Sea tank) of immersion into the Pacific and Baltic Sea tank are shown in figure 42. Compared are the differently filled samples (0 wt.% t-ZnO, 1 wt.% t-ZnO, 5 wt.% t-ZnO) and the high SFE PVC surface as reference [97, 98].

Strong differences regarding the growth appeared for the different investigated samples in both aquatic environments. When compared to pure PTU, a remarkable reduction of fouling organisms was observable for the samples containing 1 wt.% t-ZnO in the pacific tank which was not as pronounced in the Baltic Sea tank. At a filler amount of 5 wt.% t-ZnO, nearly no growth of organisms could be found on the samples. Regarding the PVC surface, it can be stated that the growth within

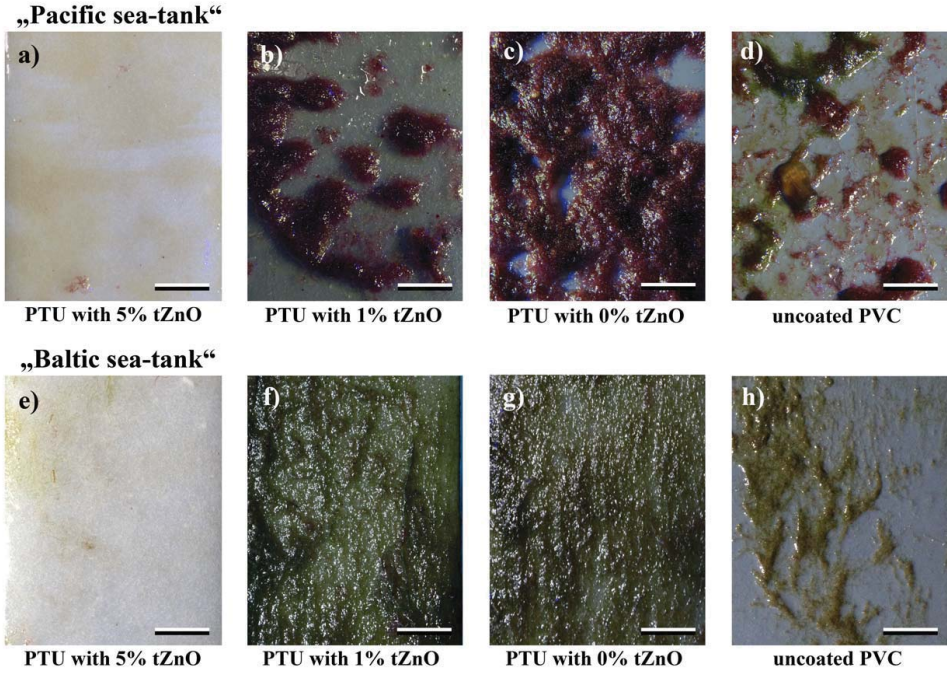

Figure 42: Preliminary experimental study on the fouling characteristics of three PTU/particle variations (0 wt.%t-ZnO, 1 wt.%t-ZnO, 5 wt.%t-ZnO) compared to a PVC reference. The dwell time for the samples immersed in the pacific tank was 20 weeks whereas the samples in the Baltic Sea tank stayed for 30 weeks.

the pacific tank was comparable to the sample containing 1 wt.% t-ZnO but the diversity of fouler species differed. Deviating growth phenomena were present in the Baltic Sea tank as the growth species on PVC did not differ from those observed on pure PTU and the sample containing 1 wt.% t-ZnO, only the density of growth was slightly reduced.

In order to visualize the process of time of the preliminary experiments, figure 43 shows an overview on the growth of the polymer/particle -composites and the PVC reference. Until approximately week 7, a continuous growth was observable on all samples whereby the highest amount was found on the PVC surface followed by the pure PTU sample. Decreased fouling appeared on the composite containing 1 wt.% t-ZnO and nearly nothing was found on the 5 wt.%t-ZnO surface. For the two latter named samples, the maximum presence of fouling organisms was found during week 8 and 9 followed by decreased growth and constant state of low growth until the remaining time of the experiment. Regarding the PVC reference and the pure PTU sample, a different process of time proceeded as an almost continuous growth of organisms showed up. Slight deviations occurred on the PVC sample were the growth also decreased slightly from week 8 to week 9. Additionally, the variety of organisms was increased compared to the polymer/particle composites.

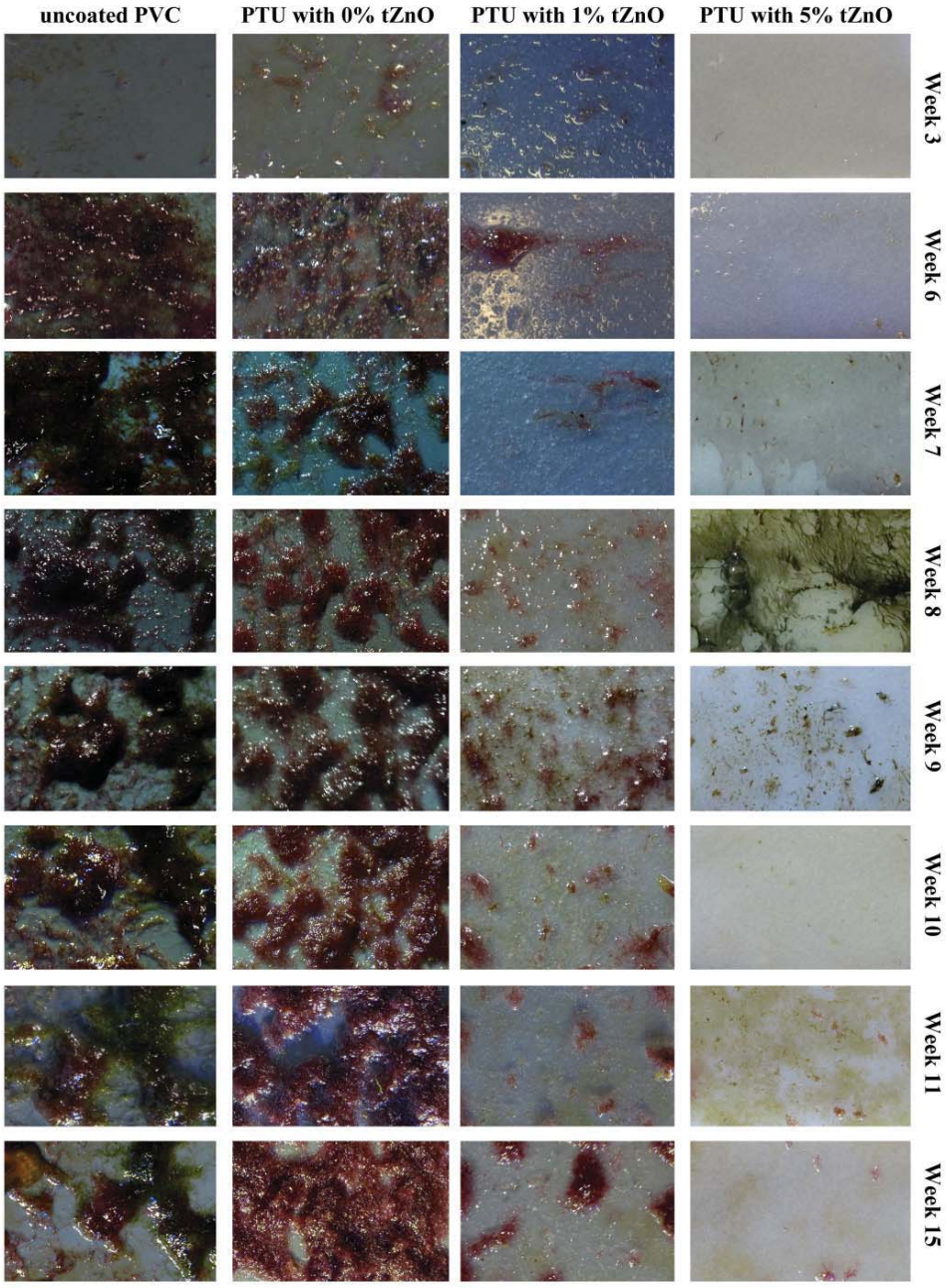

Figure 43: Exemplary time sections from the preliminary immersion test of three PTU/particle variations (0 wt.% t-ZnO, 1 wt.% t-ZnO, 5 wt.% t-ZnO) compared to a PVC reference exposed to the Pacific sea tank at the Aquarium Geomar. After three weeks slight biofouling is occured. Continuous growth appeared until week six on all samples but with varying degrees of severity. Between week six to eleven fouling proceeded differently on the samples. From week eleven until the end of the experiment (20 weeks), the amount of marine organisms was almost constant on the respective samples.

5.5.2 Evaluation of fouling process in Baltic Sea

The field experiment conducted in Laboe harbor revealed a strongly deviating fouling characteristic when compared to the results of the aquarium tanks. Figure 44 shows, that the growth on the samples under investigation (PTU, PTU + 1 wt.% t-ZnO, PTU + 5 wt.% t-ZnO) did not depend on the respective addition of t-ZnO. A homogeneous fouling was observable within the first three months. After six months of immersion, the samples were covered by mainly algae. No differences were found between the surfaces. After nine months, the attachment of sessile microorganisms like barnacles and ascidiae occurred whereby again no differences were discoverable when comparing the different samples. 12 months after the first immersion, all PTU samples showed a complete fouled surface with small amounts of sessile barnacles and ascidiae, the growth on the PVC surface was slightly increased.

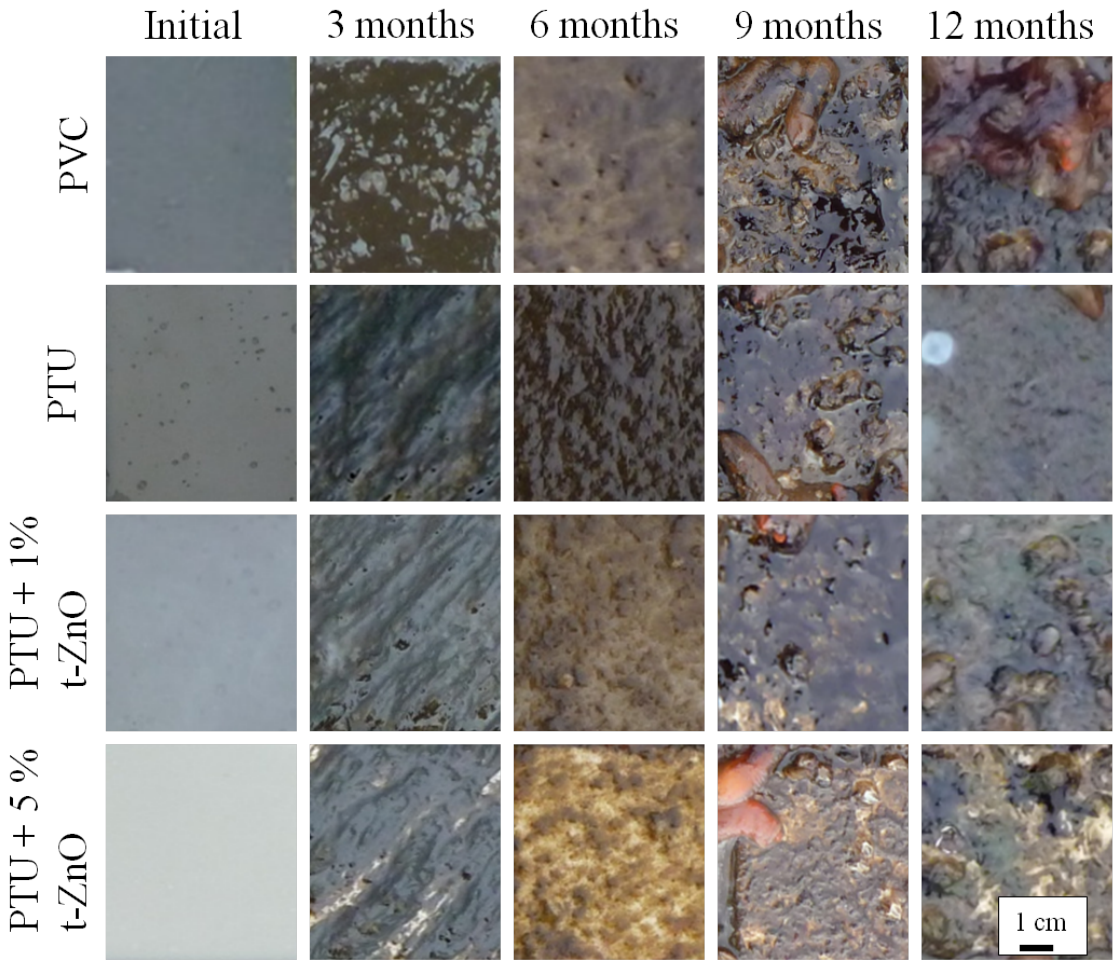

Figure 44: Process of fouling of time of the preliminary immersion test of three PTU/particle variations (0 wt.%t-ZnO, 1 wt.%t-ZnO, 5 wt.%t-ZnO) exposed to the river Schwentine

5.5.3 Evaluation of growth process in freshwater surroundings

For the comparison of the local conditions, the fouling process over time of the PTU/t-ZnO composites immersed into the Schwentinemuendung are schown in figure 45. Compared to the degree of fouling determined in Laboe harbor, the growths was comparable within the first six months as a homogeneous overgrow by algea could also be found in the freshwater surrounding. Comparing the last six months, it could be clearly seen that the degree of fouling is strongly reduced in the Schwentine, additionally, no sessile mocroorganisms were obtained. Regarding the different polymer-particle composites (PTU, PTU + 1 wt.% t-ZnO, PTU + 5 wt.% t-ZnO) as well as the PVC surface, the results were comparable to Laboe harbor as no significant differences in the degree of fouling were found within the samples.

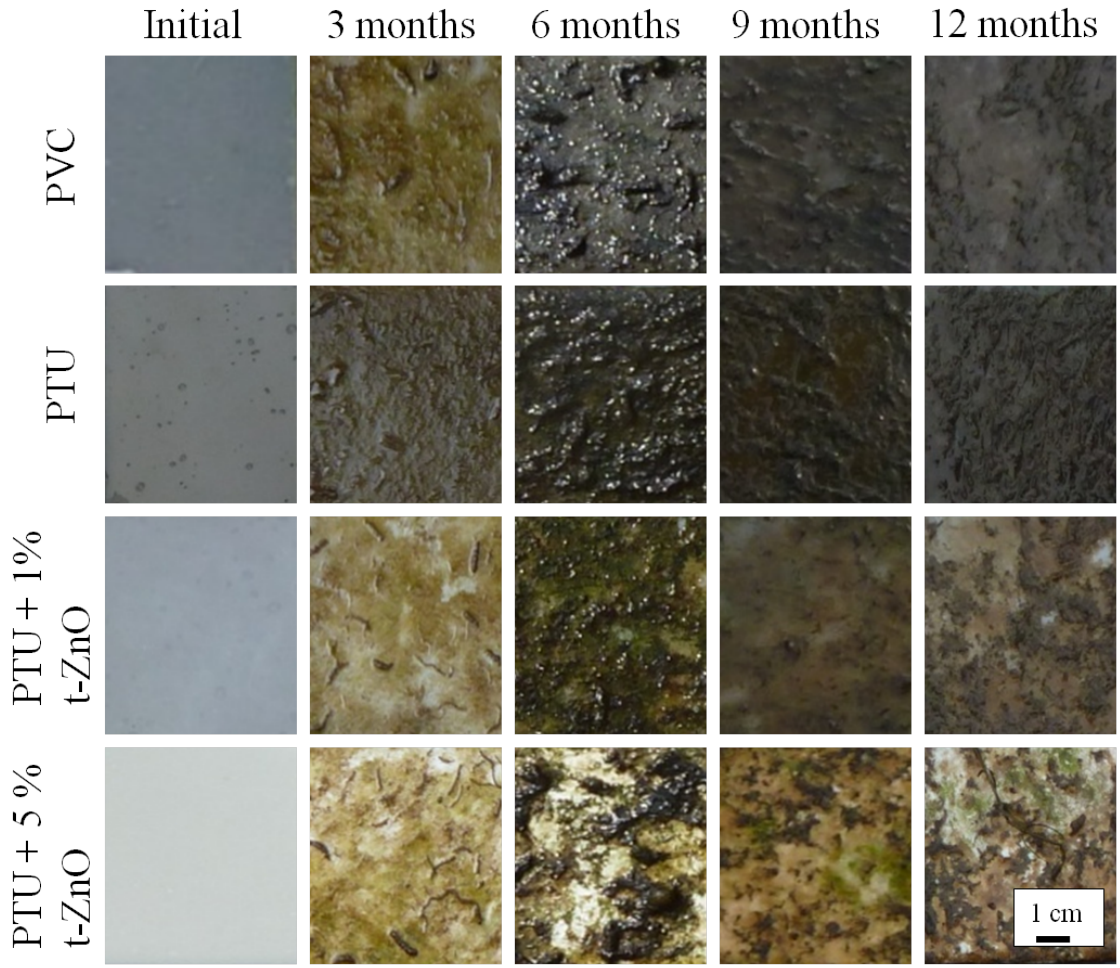

Figure 45: Fouling process of time of the preliminary immersion test of three PTU/particle variations (0 wt.%t-ZnO, 1 wt.%t-ZnO, 5 wt.%t-ZnO) exposed to the Schwentinemündung.

5.6 Cleaning results

Again, cleaning experiments were performed after an immersion time of eight months were the samples were already strongly fouled. Figure 46 shows a PTU sample with 5 wt.% t-ZnO before (a)) and after (b)) cleaning. For the evaluation of the residues, SEM images were taken and EDX-measurements were performed for the determination of the existing elements (figure 46 c) and d)). Similar SEM and EDX results were obtained for all PTU/ZnO composites for what reason the cleaning experiment is evaluated exemplary at this point.

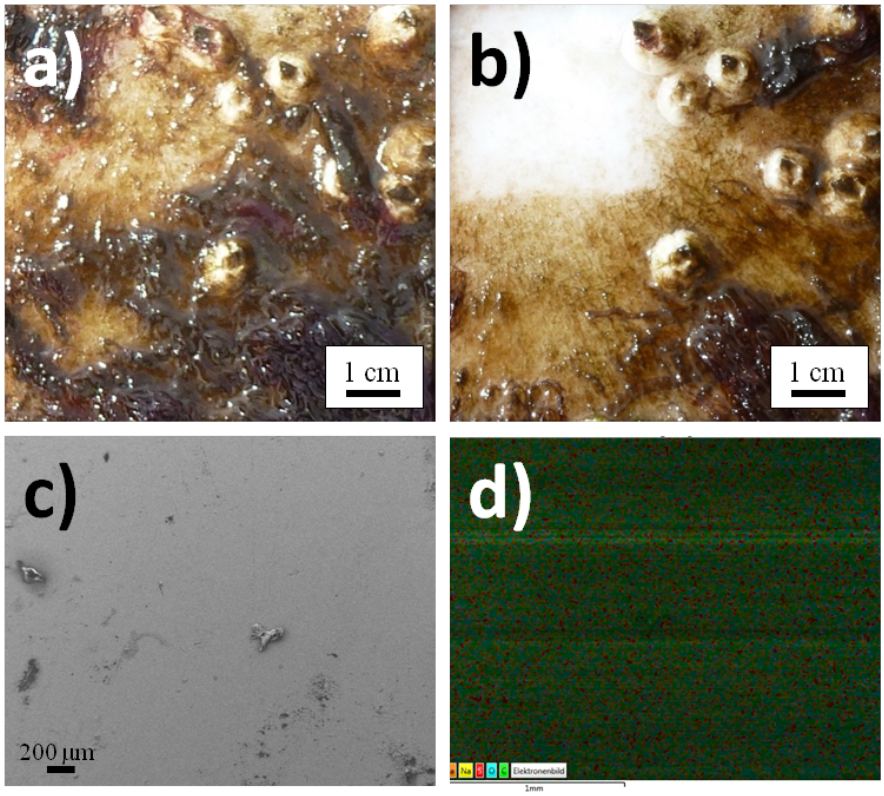

Figure 46: Results of pressure cleaning on PTU/ZnO composites immersed into Laboe harbor. a) Exemplarly fouled sample surface with hard foulers (barnacles) attached to the surface. b) Partially cleaned sample, no residues remained on the surface, no biocorrosion appeared. C) SEM micrograph of the cleaned sample surface underlines the lack of residues and biocorrosion. d) EDX-measueremnts showed the absence of marine residues.

Figure 46 depicts, that the PTU surface was completely cleaned and the SEM and EDX-measurements revealed a very low concentration of an evenly distributed film consisting mainly of silicon and calcium. As shown in the previous chapter, these observations differ strongly from those obtained for the reference PVC surface where a high amount of residues was found. Additionally, it was shown that the easy-to-

clean characteristics appear for all PTU/ZnO composites which were additionally all unaffected from degradation by marine organisms.
Figure 47 shows three different PTU/ZnO samples (0 wt.%, 1 wt.%, 5 wt.%) before and after cleaning. A PVC surface is added as reference.

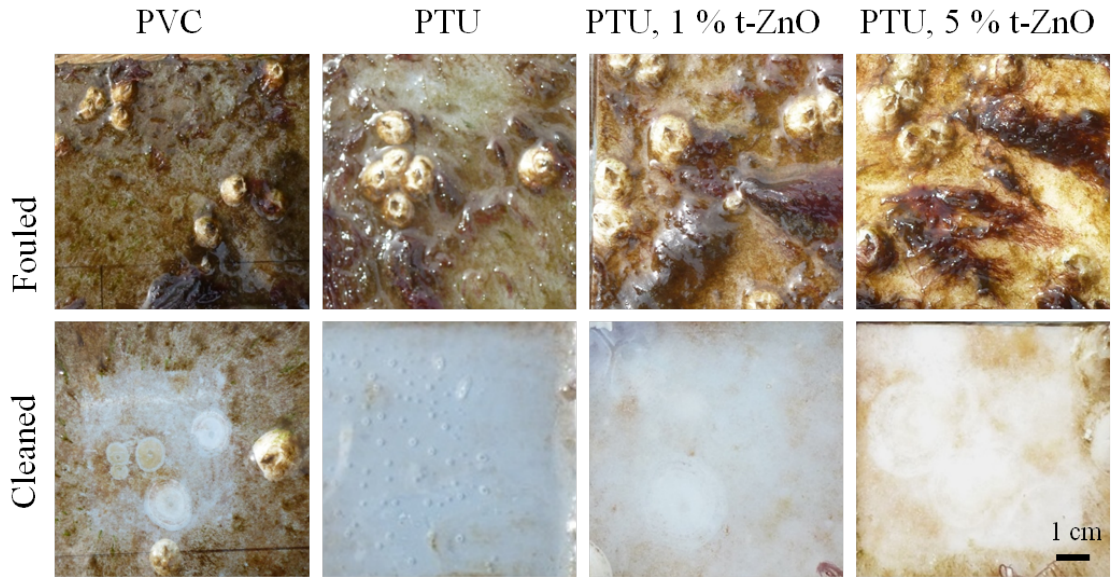

Figure 47: PTU/ZnO samples and the PVC reference after immersion of 12 months and after subsequent cleaning. The PVC sample showed a remarkable amount of abrnacle cement accompanied by material degradation due to biocorrosion. the PTU surfaces were nearly completely cleaned, no residues of hard foulers and no effect of biocorrosion was obtained.

Like already shown, the PVC surface was not completely cleaned, a remarkable amount of barnacle residues was found and the surface was affected by the fouling procedure. In contrast, pure PTU as well as the PTU with 1 wt.% and 5 wt.% t-ZnO could be nearly completely cleaned, no residues of barnacle cement was found and the surfaces were not degraded within the time of immersion.

5.7 Discussion

The mechanical properties of PTU/ZnO composites were determined by tensile testing, hardness measurements and pull-off tests. It was shown, that the tensile strength of pure PTU (57 MPa) was increased to nearly 60 MPa at a filler amount of 5 wt.% t-ZnO whereby lower or higher amounts did not led to any improvement in tensile strength. For spherical particles, the most relevant changes appeared for 1 wt.%, t-ZnO. Higher amounts did not show remarkable deviations. The tensile strength was slightly decreased down to 54 MPa accompanied by an increased elongation at fracture of nearly 50 % more.
The reinforcement of polymers by the incorporation of tetrapodal-shaped ZnO

particles was already shown in earlier reports. Xu et al. [76] ascribed the effect to the prevention of crack propagation as a result of the particles geometry reinforcing the matrix material in four different directions. The obtained result that filler amounts of more than five percent could not evoke an additional strengthening is in good accordance with the results presented by Niu et al. [31].
Regarding the elastic modulus, no significant deviations were found within the PTU/ZnO composites. When making the assumption of polymer reinforcement as a result of hindered crack propagation, it can be assumed that the effect is much more pronounced within the region of plastic deformation. The elastic deformation from which the elastic modulus is calculated is attributed to reversible changes within the polymer chains where no cracks appear.

The shore D hardness of PTU experienced a slight increase for an addition of 5 wt.% t-ZnO and 10 wt.% t-ZnO which was not observable for s-ZnO. The hardness of a material is defined as the resistance against a penetrating force, a compressive load. In 2010, Cao et al. [7] investigated the influence of tetrapodal-shaped ZnO nanowhiskers on the compressive behavior of a fiber composite. It was shown, that the embedding of ZnO nanowhiskers could increase the mechanical strength of fiber-reinforced polymers significantly. The proposed model explaining the mechanism of reinforcement can be transferred to the PTU/ZnO-composites investigated in this work. Under compressive load, one tetrapod arm will bear the normal stress as well as the shear stress of the interface. The remaining three arms can bear the remaining stress. For that reason, stress is transferred from one arm to another which results in overall stress relaxation and therefore strengthening of the composite [57].

The adhesion of PTU to an AlMg3 substrate could was with the addition of only 1 wt.% t-ZnO and a nearly threefold increase was obtained for 5 wt.% t-ZnO particles. On the other hand, spherical ZnO could not enhance the adhesion, the value stayed constant for all investigated particle concentrations. The increase can be attributed to the tetrapodal shape of the ZnO particles. As shown by Jin et al. [34], t-ZnO can be used for the joining of the two well known low surface energy polymers teflon and silicone which is known to be highly unfavorable. Within the work it was shown, that the joining was a result of pure mechanical interlocking mechanisms by the four armed tetrapods building up a three dimensional framework. A similar effect is conceivable for the increased adhesion encountered in this work. As the AlMg3 substrates were sandblasted before coating, a roughness was provided which would led to a locking of the tetrapod-arms at the metallic surface. As these locked tetrapods may be similarly connected to the PTU matrix, an increased adhesion can

be achieved. As spherical particles are not able to create an interlocking between metal surface and polymeric matrix, an increased adhesion was not expected.

Using Raman-spectroscopy and infrared spectroscopy, it was investigated, whether the addition of ZnO particles has an influence on the quantitative polyaddition of the two components HDI and PETMP. No additional molecular vibration at 2545 cm-1 (would be caused as a result of unreacted S-H groups from PETMP) or 2272 cm-1 (would be caused as a result of unreacted -NCO groups from HDI) appeared, it can therefore be assumed that ZnO has no effect on the completeness of the reaction.

In order to evaluate the thermal degradation behavior of PTU and PTU/ZnO composites, thermogravimetric analysis was performed. It could be shown, that PTU has a high first degradation temperature of around 260 °C which was not affected by the addition of ZnO particles. Also the second and the third degradation step was not affected which is why it can be stated that the thermal degradation is not influenced by ZnO particle incorporation.

Regarding the surface characterization, contact angle measurements were performed and the surface free energy as well as its polar and dispersive components were calculated by the method of Owens, Wendt, Rabel and Kaelble [48]. It was shown, that the SFE was slightly increased from 40.7 mN/m for pure PTU down to 37.4 mN/m for 1 wt.% t-ZnO. On the other hand, the contact angle was slightly increased from 67.4° for pure PTU to 72.8° for 5 wt.% t-ZnO. As the corresponding values for the surface roughness did not change by the addition of t-ZnO, this effect cannot be ascribed to increased surface roughness. Although it was shown that the polyaddition as well as the thermal degradation were not affected by t-ZnO incorporation, it has to be assumed that the polymer structure is changed with increasing amount of t-ZnO and that this change brings along the differences in surface energy and contact angle characteristics. Regarding the lack of additional Raman-peaks, it has to be clarified that unreacted NCO groups do not appear in the spectra. They can therefore not be identified by this method. On the other hand, IR-spectroscopy, which allows the appearance of NCO vibrations, is not surface sensitive as radiation is passed through the complete sample and gives therefore information about the whole material under investigation.

A remarkable influence of the ZnO particle addition was noticed regarding the polar and dispersive components as the polar component was reduced from around 12 mN/m for pure PTU down to around 9 mN/m for PTU with 5 wt.% t-ZnO. On the other hand, the dispersive component stayed nearly unaffected at a value of

around 29 mN/m.
The antifouling properties of the polymer-particle composites (PTU, PTU + 1 wt.% t-ZnO, PTU + 5 wt.% t-ZnO for these experiments) were initially evaluated by immersion tests in the aquarium Geomar where it was shown, that the lowest fouling appeared onto the sample containing 5 wt.% t-ZnO and that the adhesion of the organic film was strongly reduced. These results are in good accordance with the reduced free surface energy of the sample containing 5 wt.% t-ZnO as it was shown by Chen et al. (2008) [99] and Holland et al. (2004) [100] that reduced free surface energy is opportunistic to decreased biofouling on silicone surfaces or to facilitate cleaning due to reduced adhesion of the biofilm.

In order to test the samples under natural conditions, they were reproduced and immersed into the Baltic Sea at Laboe harbor and the river Schwentine. For investigations on the influence of the particles morphology, additional samples with spherical particles of the same concentration were fabricated. The samples were analyzed weekly by photographs. It was recognized that all surfaces overgrow similarly independent on the ZnO content or morphology. Despite the initial soft foulers like algae, after some months the surfaces were occasionally colonized by barnacles followed by a complete coverage of ascidiae.

After eight months of immersion, a cleaning experiment was conducted where PVC surfaces served as reference. Besides optical investigations by photograph, SEM and EDX measurements were conducted to identify possible residues. For the PVC surface it was shown, that the barnacle cement could not be removed by the water-pressure. This was underlined by SEM and EDX measurements which clearly demonstrated calcinated barnacle residues on the cleaned surfaces. Additionally, the material was degraded by the fouling organisms showing up that PVC cannot withstand the harmful organics. On the other hand, all PTU/particle composites were completely cleaned by the water-blaster leaving nearly no residues. The conducted SEM and EDX investigations underlined the easy-to-clean behavior of PTU by showing nearly no rests on the surfaces. Regarding the material itself, it can be furthermore stated that it is very robust against materials degradation by aquatic organisms as the surface stayed completely unimpaired.

Chapter 6

tetrapodal-shaped ZnO nano- and microstructures as reinforcement for mechanically stable PDMS-based fouling-release coatings

6 PDMS/ZnO-composites

In the following chapter, the influence of ZnO particles on the chemical, mechanical and antifouling characteristics of polydimethylsiloxane (PDMS) is summarized. Similar to the experiments conducted within the characterization of PTU/ZnO-composites, the filler amounts (0 wt.%, 1 wt.%, 5 wt.%, 10 wt.%) as well as the particle morphology (t-ZnO and s-ZnO) were varied in order to investigate the influence of the shape onto the materials properties.

6.1 Preparation of PDMS/ZnO-composites

For the preparation of PDMS/ZnO-composite samples, the silicone elastomer Sylgard 184 consisting of a pre-polymer base and a crosslinking curing agent was purchased from Sigma Aldrich (Germany). The crosslinking agent was stirred in with an amount of 10 wt.%, additives were possibly blended in and the mixture was completely degassed in a desiccator. Similar to the preparation of PTU, the samples were casted into molds or spread onto substrates and finally cured at 84 °C for 24 h.

6.2 Mechanical characterization

6.2.1 Tensile test

In order to investigate the influence of the particles on the mechanical properties of Sylgard 184, tensile tests were performed. Exemplary stress-strain diagrams of with varying amounts of ZnO at both morphologies (t-ZnO, s-ZnO) are shown for each composition in figure 48. Corresponding mean values and standard deviations of tensile strength, elongation at fracture and elastic modulus are shown in the figures 49 and 50.

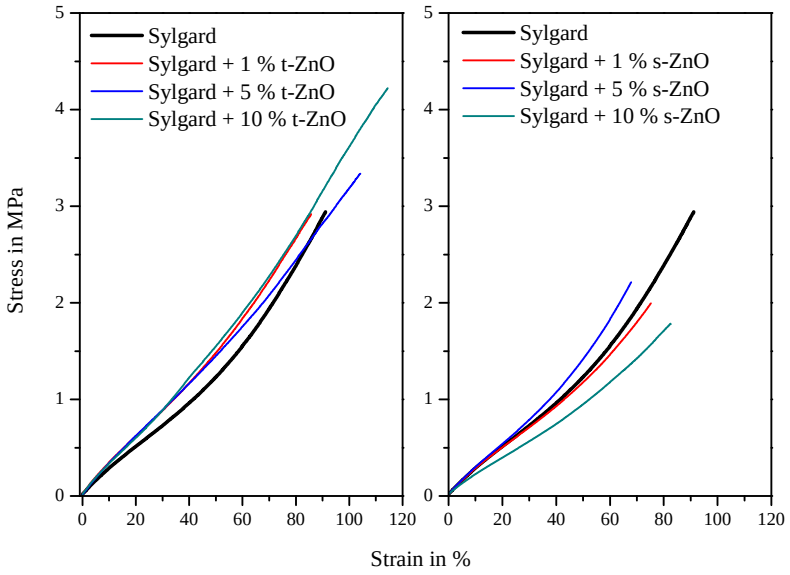

Figure 48: Stress-strain diagrams of Sylgard and Sylgard with different amounts of ZnO fillers. The left graph shows the results of t-ZnO fillers, the right graph shows the results for s-ZnO fillers.

The tensile strenght amounted to 2.8 MPa and stayed nearly unaffected for the addition of 1 wt.% t-ZnO and 5 wt.% t-ZnO, respectively. At 10 wt.% filling of t-ZnO, the mean tensile strength was increased to nearly 3.5 MPa. A deviating behavior was obtained for the addition of spherical particles. A decrease to nearly 2 MPa at 1 wt.% was followed by a slight increase back to the initial value for 5 wt.% s-ZnO. At 10 wt.% s-ZnO, a strong decrease down to below 2 MPa occured. Similar results were obtained for the elongation at fracture were the initial value of around 85 % could be raised constantly until more than 100 % for 10 wt.% t-ZnO. In contrast, the addition of s-ZnO led to decreased values, the lowest elongation at fracture of nearly 70 % was obtained for 5 wt.% s-ZnO. Additionally, also the elastic modulus was increased from initially 3.5 MPa to more than 4 MPa for 10 wt.% t-ZnO whereas

the addition of s-ZnO led to a remarkable decrease down to around 2.5 MPa for 10 wt.% s-ZnO filler amount.

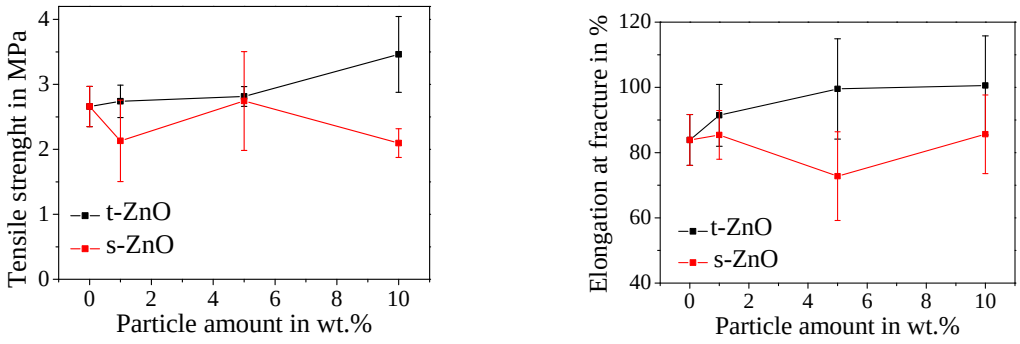

Figure 49: Tensile test of PDMS/ZnO composites.
(a) Tensile strength as a function of particle amount. A strong increase was obtained for 10 wt.% filling of t-ZnO, s-ZnO caused decreased values. (b) Elongation at fracture as a function of particle amount. Again, an increase was observable for t-ZnO addition while s-ZnO caused a decrease. Lines connecting the points are a guide for the eye.

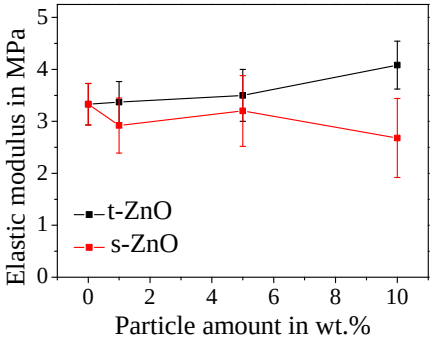

Figure 50: Elastic modulus of PDMS as a function of the particle amount (t-ZnO and s-ZnO). An increase from initially 3.5 MPa to more than 4 MPa was obtained for 10 wt.% t-ZnO whereas the addition of s-ZnO caused remarkable decreases. Lines connecting the points are a guide for the eye.

6.3 Chemical characterization

6.3.1 Raman-spectroscopy

In order to obtain information on the influence of the ZnO addition on the chemical structure of PDMS, Raman-spectroscopy was performed on the different PDMS/ZnO composites. Exemplary spectra for pure PDMS as well as 1 wt.% t-ZnO and 5 wt.% t-ZnO are shown in figure 51. Comparable results were obtained for all other specimens.

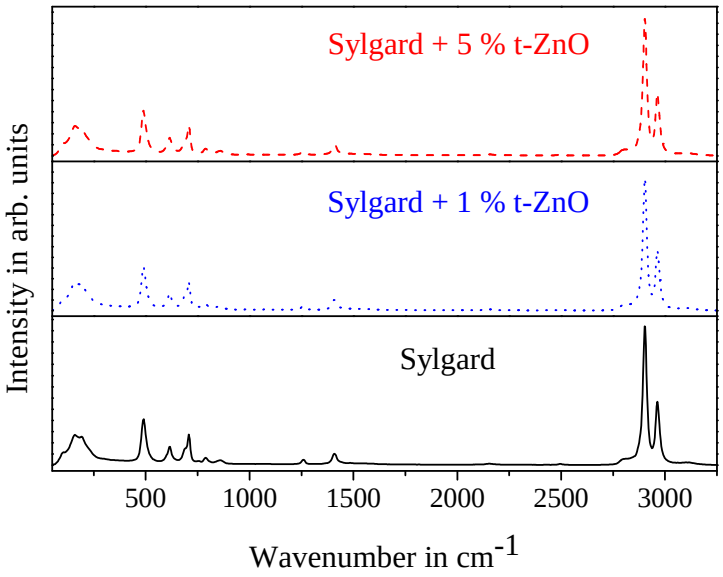

Figure 51: Raman-spectra of PDMS/ZnO composites. No influence of the polymerization reaction was found for any filler amount or morphology.

Similar to the results obtained for PTU/ZnO-composites, the obtained Raman-spectra did not differ from each other.

6.4 Surface characterization

6.4.1 Contact angle experiment

Contact angle experiments were conducted in order to investigate whether the surface energy of the PDMS/ZnO-composites is influenced by the addition of particles. Figure 52 illustrates the dependency of the contact angle on the particle amount whereby mean values and corresponding standard deviations were calculated from ten measured datasets.

The addition of ZnO particles had a slight influence on the contact angle as the initial mean value of around 108 ° was increased to roughly 114 ° at a filler amount

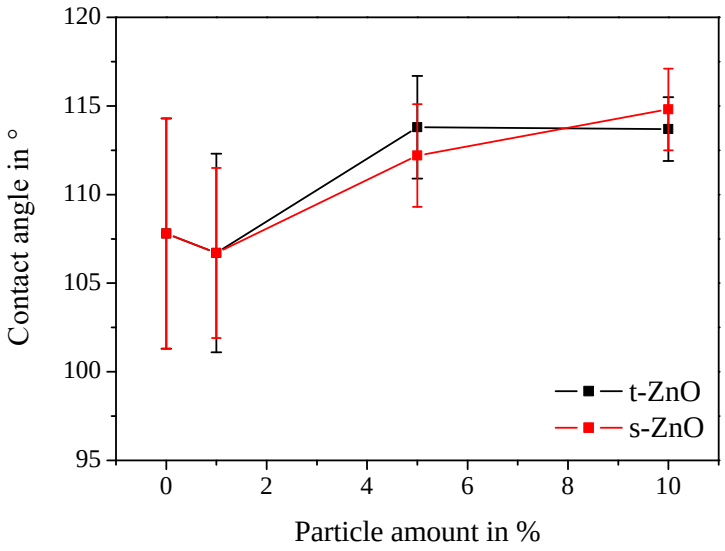

Figure 52: Influence of the particle amount on the contact angle of PDMS. An influence of ZnO particle addition was observed as increased contact angles resulted for filling factors above 1 wt.%. The morphology did not cause significant differences with respect to the values. Lines connecting the points are a guide for the eye.

of 5 wt.% and 10 wt.%. At lower filling amounts (1 wt.%), no significant deviation was observable. Regarding the influence of the particle morphology, it can be stated that the shape did not influence the results as comparable values were received for both spherical and tetrapodal-shaped ZnO.

6.5 Immersion experiment

6.5.1 Evaluation of fouling process in Baltic Sea

In order to investigate the fouling process on PDMS and PDMS/ZnO-composites under natural conditions, the samples were immersed into the Baltic Sea at Laboe harbor. To get a comparative overview on the growths not only for the PDMS/ZnO-composites, the time sequence shown in figure 53 provides PTU as reference.
It can be stated, that the fouling process on PDMS as well as PDMS/ZnO-composites proceeded much slower compared to PTU already within the first three months. Regarding PTU, the surface was completely fouled within short time whereas the PDMS samples showed only slight accumulation of algae. On the other hand, the PDMS and PDMS/ZnO-composites did not show differences in growths for the whole experimental time.
After six months of continuous immersion, the accumulation of sessile marine organ-

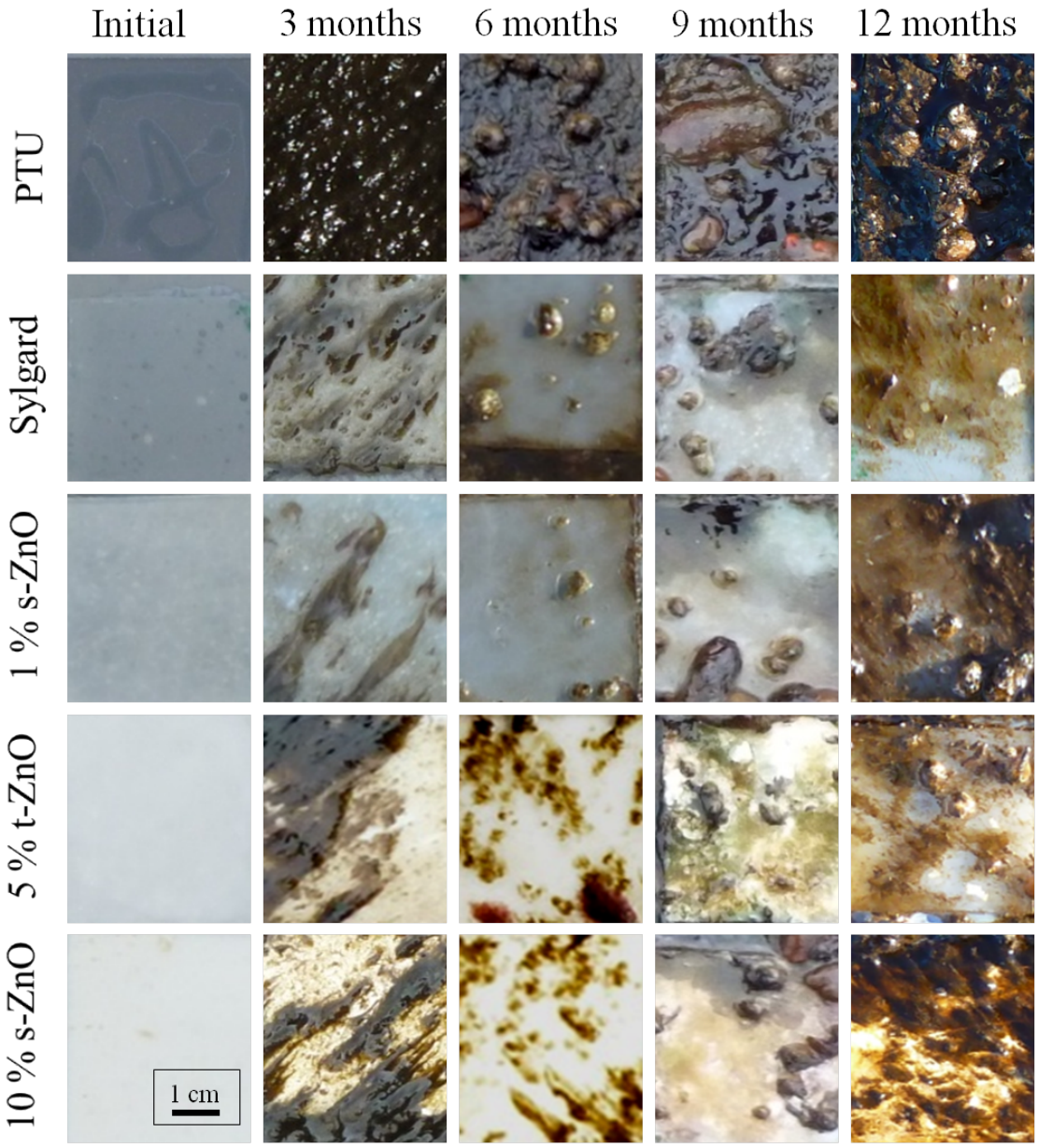

Figure 53: Fouling process over time on PDMS and PDMS/ZnO-composites in Laboe harbor. PTU is shown as reference. After three months, all samples showed a homogeneous layer of fouling organisms whereby the degree of fouling was significantly higher on PTU. After six months, a small amount of hard foulers (barnacles) was found on PDMS, PTU was homogeneously covered by hard and soft foulers. Three months later, the sample surfaces remained similar. After 12 months of immersion, also the PDMS samples were covered by hard and soft foulers, but the degree of fouling was strongly increased on PTU.

isms was initiated. The PDMS samples showed little amounts of attached barnacles combined with reduced algae growth, whereas the PTU surface was completely covered by algae and a comparable high amount of barnacles.
After nine months of immersion, the PDMS surfaces did not show remarkable changes. On the other hand, PTU was covered by ascidiae, another sessile species.
At the end of the experimental time, the PDMS surfaces showed again a slightly increased amount of accumulated algae. On the other hand, self-detachment of the barnacles was observable which did not occur for the PTU sample.
In general, the fouling process on the PDMS and PDMS/ZnO samples showed a fluctuating behavior not only for algae but also for sessile organisms like barnacles. Additionally, ascidiae were nearly not found on the surfaces. In contrast, PTU showed a continuously overgrow of all samples accompanied by an increased number of attached sessile organisms. Here, not only the amount of barnacles was increased, but also a nearly complete coverage with ascidiae was observed leading to a thick layer of accumulated fouling species.

6.5.2 Evaluation of fouling process in freshwater surroundings

To compare the fouling behavior of PDMS and PDMS/ZnO-composites within different natural surroundings, samples were immersed into freshwater in the Schwentine river at Kiel-Wellingdorf. Again, the time sequence shown in figure 54 provides PTU as reference.

After six months of immersion the growth onto the PDMS surfaces was nearly completely vanished including all ZnO-composites while the PTU surface was completely covered by a homogeneous layer of mainly algae.
After nine months, the PDMS surfaces appeared all completely clean like in the beginning of the experiment whereas the PTU surface was completely fouled.
At the end of the experiment, the PDMS-samples showed a slight accumulation of algae. The PTU surface remained covered until that time.
Comparing the fouling behavior to that one observed within the Baltic Sea, the overall amount of fouling was strongly reduced in the Schwentine river. Additionally, no hard-foulers were observed, the surfaces were only covered by algae. Regarding the differences between PTU and PDMS, the fouling process differed much stronger in the Schwentine. Additionally, it was found that the growth on the PDMS surfaces was alternating as the growth was nearly vanished after nine months.

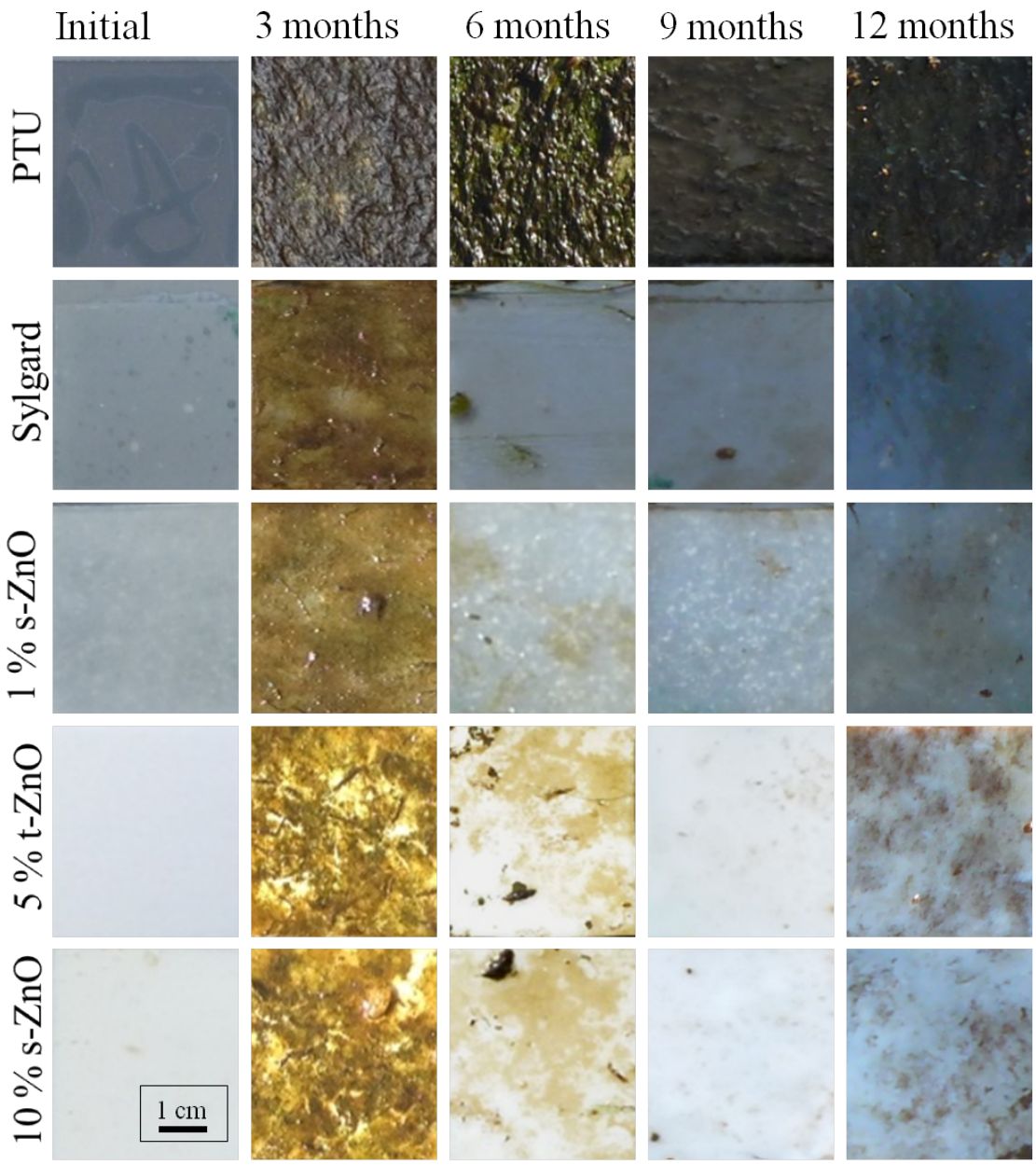

Figure 54: Fouling process over time on PDMS-composites in the Schwentine river. After three months, all samples showed a homogeneous layer of fouling organisms whereby the degree of fouling was silghtly higher on PTU. After six months, the degree of fouling was strongly reduced on PDMS whereas a continuous growth occurred on the PTU sample. From months six to the end of the experiment after 12 months, the PDMS samples were still nearly free of foulers whereas the PTU surface remained completely covered.

6.6 Cleaning experiment

After 12 months of immersion, high-pressure water blaster cleaning experiments were conducted with all PDMS/ZnO composites. The surfaces before and after cleaning are shown in figure 66, PVC and PTU are shown as references.

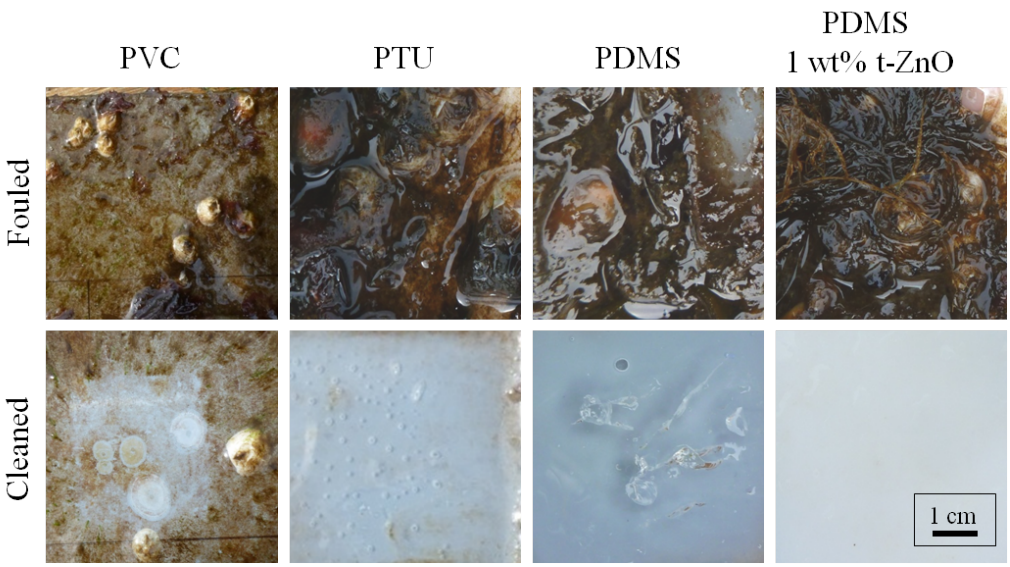

Figure 55: PDMS/ZnO samples and the PVC and PTU references after immersion of 12 months and after subsequent cleaning. The PVC sample showed a remarkable amount of barnacle cement accompanied by material degradation due to biocorrosion.The PTU surfaces were nearly completely cleaned, no residues of hard foulers and no effect of biocorrosion was obtained. All PDMS samples showed convincing cleaning properties as no residues were found on any sample. On the other hand, the PDMS surfaces were destroyed as a result of high-pressure water blaster cleaning.

While PVC showed a remarkable amount of barnacle residues as well as biocorrosion of the material, the PTU surface appeared residue-free after cleaning and the surface did not show failure due to biocorrosion. Regarding the PDMS/ZnO composites, the cleaning ability was convincing for all samples as no residues were found and no signs of biocorrosion were detected. On the other hand, all PDMS surfaces were damaged by the water-jet cleaning underlining the mechanical instability of the material.

6.7 Discussion

Silicones are well-known foul-release surfaces for what reason the fouling properties of the silicone elastomer Sylgard 184 were investigated at the already named locations. As the low mechanical stability depicts the silicones major drawback, ZnO particles of different morphology (spherical, tetrapodal) were incorporated into the polymeric matrix at different filing amounts (0 wt.%, 1 wt.%, 5 wt.%, 10 wt.%,) for

reinforcement.

The mechanical properties of the PDMS/ZnO composites were evaluated by tensile testing. It was shown, that the tensile strength could be increased from 2.8 MPa for PDMS without particles to nearly 3.5 MPa for PDMS with 10 wt.% t-ZnO. Furthermore, the initial elongation at fracture of around 85 wt.% was increased to more than 100 wt.%, again for PDMS with 10 wt.% t-ZnO. A similar increase for the 10 wt.% t-ZnO composite was obtained for the elastic modulus, as the initial amount of around 3.5 MPa was increased to more than 4 MPa. In contrast, the addition of s-ZnO led to decreased values for tensile strength as well as elongation at fracture and elastic modulus.
It was therefore again demonstrated, that the addition of tetrapodal-shaped ZnO particles to a polymeric matrix can be a suitable method for the reinforcement of polymeric matrices. These result are in accordance to the publication by Jin et. al [101] where the influence of tetrapodal-shaped ZnO on stiffness and hydrophobicity of polydimethylsiloxane was investigated and compared to other particle shapes. It was shown, that t-ZnO led to a significant increase in tensile strength and elastic modulus which was not achievable for spherical particles as well as microfibers and whiskers.

Aimed by Raman-spectroscopy, the influence of the ZnO particles on the chemical characteristics of PDMS were evaluated. It was demonstrated, that ZnO particles did not cause changes within the Raman-spectra for what reason it can be assumed, that no reactions between the inorganic filler material and the silicone matrix occured.
Regarding the surface characterization, contact angle measurements revealed a dependency of the contact angle on the particle amount. An initial mean value of around 107 ° was increased to nearly 115 ° for 5 wt.% ZnO whereby no difference was found between the two particle morphologies. This increase in contact angle may be attributed to an increased roughness caused by the addition of particles. As known from the Youngs equation, an increased roughness will enhance the contact angle with respect to its original behavior. For the current hydrophobic PDMS this implies an increase in hydrophobicity as it was shown. Again, these results are in accordance to Jin et. al [101] where an increased hydrophobicity for PDMS filled with ZnO of either tetrapodal or spherical morphology was reported.

The immersion experiment was conducted at two different locations. For the seawater surroundings, Laboe harbor at the Baltic Sea was chosen, freshwater conditions were provided by the river Schwentine in Kiel-Wellingdorf. Besides different con-

centrations of spherical and tetrapodal ZnO, PTU was immersed as reference in order to provide a reliable comparison.
Considering the fouling process itself it has to be stated, that the amount of accumulated species was much more pronounced within the Baltic Sea. Additionally, it was shown that PTU got completely overgrown already in the first months whereas the PDMS samples showed an alternating fouling behavior with increasing and decreasing amounts of fouling species.
Regarding the attachment of sessile organisms, barnacle adhesion was observed within the Baltic Sea on all PDMS/ZnO composites. However, the amount was reduced when compared to PTU and no other sessile species were found which again was the case for PTU. Additionally, a remarkable amount of barnacles self-detached from the PDMS surfaces without leaving residues.
Within the river Schwentine, no sessile organisms were observed. The main foulers were provided by red and green algae. Furthermore, the samples appeared nearly completely clean after nine months of immersion although the surfaces were completely overgrown before.
Summarizing, it can be stated that the fouling process on PDMS proceeded much slower and showed fluctuations with respect to the amount of accumulated organisms when compared to PTU. Additionally, the amount and diversity of sessile organisms was significantly reduced and partially self-detached from the samples. Furthermore, no residues of e.g. barnacle basements were observed and the sample surfaces stayed unaffected from the natural surroundings throughout the time of immersion.

High-pressure water-blaster cleaning showed a convincing cleaning ability for the PDMS/ZnO composites as no residues were found and no signs of biocorrosion were detected. On the other hand, all PDMS surfaces were damaged by the water-blaster cleaning. This failure can be attributed to the low elastic modulus of the material which makes it unsuitable for cleaning with high pressure equipment.
These results are in good accordance to many publications (e.g. [42, 102]) where it is stated that silicone provides a low fouling surface due to its low elastic modulus and low surface energy. On the other hand, silicone is well known to possess weak mechanical stability for what reason it is unsuitable for highly affected surfaces like e.g. ship hulls [28].
However, in this work it was shown, that PDMS can be significantly reinforced by the incorporation of tetrapodal-shaped ZnO particles as the tensile strength was increased about 25 % accompanied by an increase in the elastic modulus of at least 15 % for a particle content of 10 wt.%.

Chapter 7

Ecofriendly Polyurethane/silicone/ZnO-composites as mechanically durable fouling-release coatings

7 PTU/Silicone-composites

One aspect within the development of ecofriendly paints for the challenge to prevent marine fouling is represented by silicone based fouling-release (FR) coatings. Silicone is a well known low-fouling material as its low surface energy and low elastic modulus impedes the attachment of sessile organisms [103]. On the other hand, its mechanical instability and its low adhesion to any surface makes it unsuitable for applications on highly stressed surfaces like e.g. ship hulls [42]. As PTU has already proven to possess suitable mechanical features [104, 105], the incorporation of silicone microdomains into a PTU matrix would combine the anti-fouling characteristics of silicone with the required mechanical stability.
The following chapter reports the fabrication of a biocide-free fouling-release coating with superior mechanical stability. For this purpose, a PTU matrix was combined with two different one-component systems, ehyltriacetoxysilane (ETAS) and methyltriacetoxysilane (MTAS), in order to consolidate the preferable fouling-release properties of silicone and the mechanical stability of PTU. In addition, tetrapodal-shaped

ZnO (t-ZnO) particles were incorporated into the PTU matrix to provide further robustness and to enhance the antifouling features. The PTU/silicone composite systems with different amounts of t-ZnO were investigated with respect to surface characteristics, mechanical stability and antifouling properties in the Baltic Sea and in freshwater.

7.1 Sample Preparation

PTU/silicone-composites were fabricated by the assembling of PTU and silicone elastomers, whereby the one-component acetic interlacing silicones Methyltriacetoxysilane (MTAS, Probau, Germany) and Ethyltriacetoxysilane (ETAS, Wacker, Germany) were compared. Initially, PTU was mixed by the ratio 58 HDI : 42 PETMP whereupon an amount of 10 wt.% silicone was stirred in mechanically. The mixture was magnetically stirred and the stirring time was varied in order to investigate its influence on the dispersion of silicone as well as on the mechanical and surface properties.

7.2 Silicones

In order to find a suitable silicone component for the preparation of PTU/PDMS composites, different PDMS systems were investigated. Their main difference was the number of constituents as one-component-systems were compared to two-component ones. Additionally, silicones from different suppliers were chosen and all utilized systems are listed in table 5.

Table 5: Silicone systems used for the preparation of PTU/PDMS-composites.

Silicone	componenets	cross-linking	provider
ETAS	1	acid	Wacker Chemie
MTAS	1	acid	R &G
B & F	2	cross-linker	Buenger & frese
Raumedic	2	cross-linker	Raumedic
Sylgard	2	cross-linker	Sigma Aldrich

The main goal of these experiments was the tailoring of the PTU surface towards hydrophobic behavior and therefore higher contact angles. Despite the different PDMS systems, also the stirring time was varied (0 h, 0.5 h, 1 h, 1.5 h) and its influence on the contact angle on the composite was evaluated.
With respect to processability, the utilization of one-component silicones is much simpler when compared to two-component systems. Additionally, for most of the two component systems a thin liquid layer was formed onto the sample surface

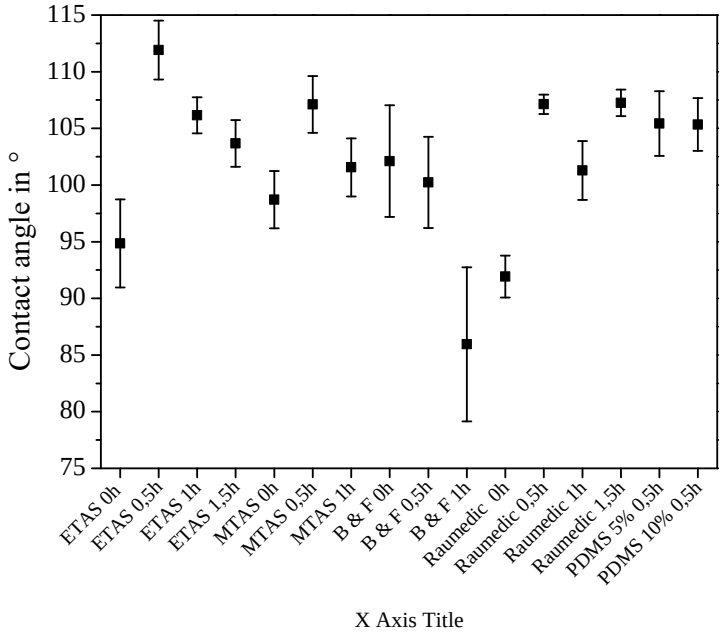

Figure 56: Contact angles of PTU/PDMS composites with different PDMS systems. Highest contact angles were obtained for 30 min of stirring and for the two one-componenet systems MTAS and ETAS.

which is not preferable for application.

Regarding the stirring time, a strong influence on the contact angle was observable. Without stirring, PTU/ETAS-blends showed a contact angle of around 95° which was significantly increased to nearly 115 ° for a stirring time of 1/2 h. With longer stirring times of 1 h and 1/2 h, the contact angle again decreased for what reason the stirring time was set to 1/2 h for future experiments. Similar results were obtained for PTU/MTAS blends were the initial value of around 98 ° could be increased to nearly 110 ° with a stirring time of 1/2 h. The two-component system B & F showed deviating values as the stirring time led to a decrease from around 100 ° down to below 90 ° for 1 h. The other two component systems Raumedic and sylgard showed again a highest contact angle for 1/2 h of stirring.

The highest contact angles were obtained for the one-component systems ETAS and MTAS. The processability was best for these two systems. They were therefore chosen for subsequent experiments.

7.3 Mechanical properties

7.3.1 Tensile response

In order to investigate the influence of the particle amount on the mechanical properties of the PTU/Silicone composites, tensile test were performed and the calculation of the tensile strength, the elongation at fracture and the Youngs modulus are shown in the following figures 57 and 58.

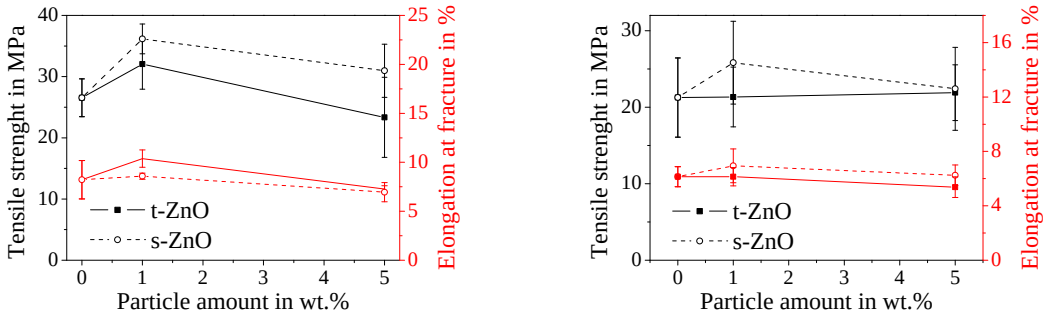

Figure 57: Tensile strenght and elongation at fracture of PTU/PDMS composites. (a) ETAS: tensile strength and elongation at fracture were slightly increased with 1 wt.% t-ZnO whereas 5 wt.% t-ZnO caused slightly decreased values. 1 wt.% s-ZnO as caused an increased tensile strength, no further increase for 5 wt.% s-ZnO. (b) MTAS: no significant effect of particle incorporation on tensile strength and elongation at fracture.

In case of ETAS, tensile strength as well as elongation at fracture were slightly increased with the addition of 1 wt.% t-ZnO whereas 5 wt.% t-ZnO led to slightly decreased values. A more distinct effect was observable for s-ZnO as 1 wt.% led to a remarkable increased tensile strength. Regarding MTAS, the particles had nearly no effect on both tensile strength and elongation at fracture.

Regarding the influence of the particle amount on the elastic modulus of ETAS, it was shown that the initial value of around 700 MPa could be increased to more than 850 MPa for 1 wt.% s-ZnO. The increase for 1 wt.% t-ZnO to nearly 800 MPa was not as pronounced. For 5 wt.% ZnO addition, the value obtained for s-ZnO showed a slight decrease down to around 800 MPa when compared to 1 wt.% while t-ZnO reached the same value and showed therefore an increase.
A different behavior was observed for the elastic modulus of the PTU/MTAS-composites. While the initial value was similar to the one obtained for PTU/ETAS (slightly above 700 MPa), the addition of 1 wt.% s-ZnO did not cause an increase. In contrast, 1 wt.% t-Zno led to a decrease to below 700 MPa. On the other hand, a slight increase to around 800 MPa was achieved by 5 wt.% t-ZnO whereas 5 wt.% s-ZnO caused a decrease to below 700 MPa.

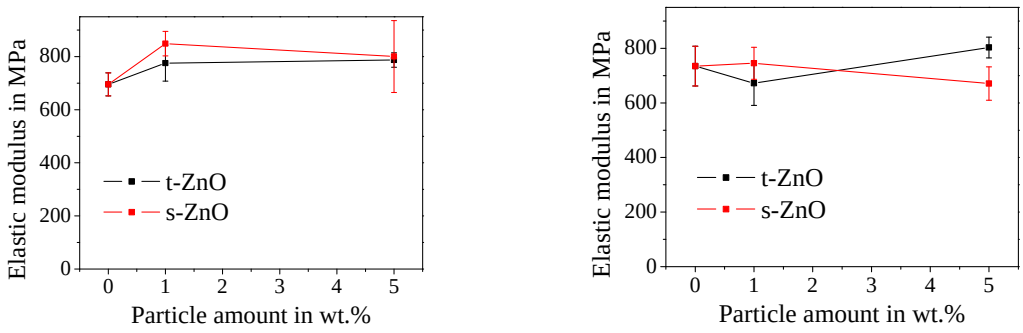

Figure 58: Elastic modulus in dependency of particle amount. A decrease was found for 1 wt.% t-ZnO, 5 wt.% t-ZnO caused increased values. 5 wt.% s-ZnO caused a decrease.
(a) ETAS. (b) MTAS.

To visualize the difference within the stress-strain diagrams of pure PTU, silicone and its composite, figure 59 shows the individual stress-strain diagrams. It can be seen, that the mechanical properties of the PTU/ETAS-composites tend strongly towards those of PTU. Regarding the tensile strength, PTU reaches more than 60 MPa whereas ETAS hardly reaches 5 MPa. With nearly 30 MPa, the tensile strength of PTU/ETAS is comparably high. On the other hand, the elongation at fracture of ETAS amounted to nearly 100 % whereas PTU reached 15 %. Here, the value of PTU/ETAS reaches almost the same as PTU.

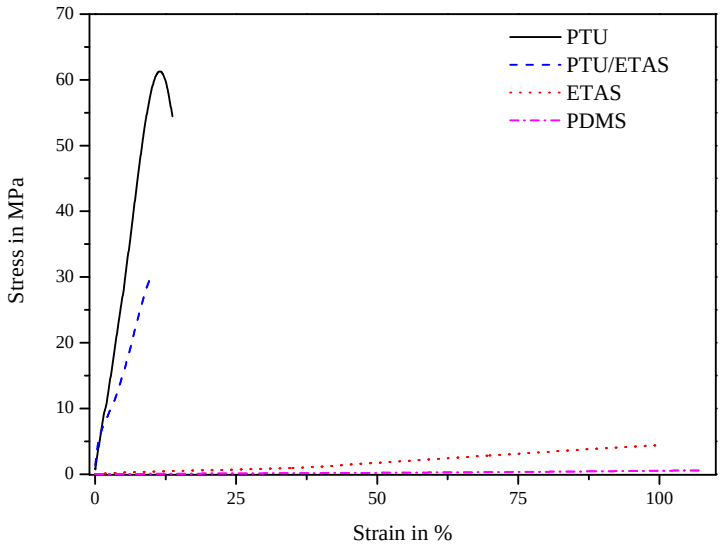

Figure 59: Stress-strain diagrams of PTU, PTU/ETAS, ETAS and Sylgard. The mechanical properties of the PTU/ETAS-composites tend strongly towards those of PTU.

7.4 Chemical and morphological properties

In order to evaluate whether the two polymers PTU and ETAS formed a phase separated structure, the chemical composition of the PTU/ETAS-composites was characterized. As Raman-spectroscopy allows the depiction of defined areas, the visualization of possible silicone microdomains within a PTU matrix was preferred.

7.4.1 Raman-spectroscopy

In order to visualize the phase separation of the two polymer components, each polymer system was initially measured separately to provide the appropriate characteristics (figure 60). The PTU/PDMS components were measured and filtering was performed on the average datasets in order to visualize the microdomains (figure 61).

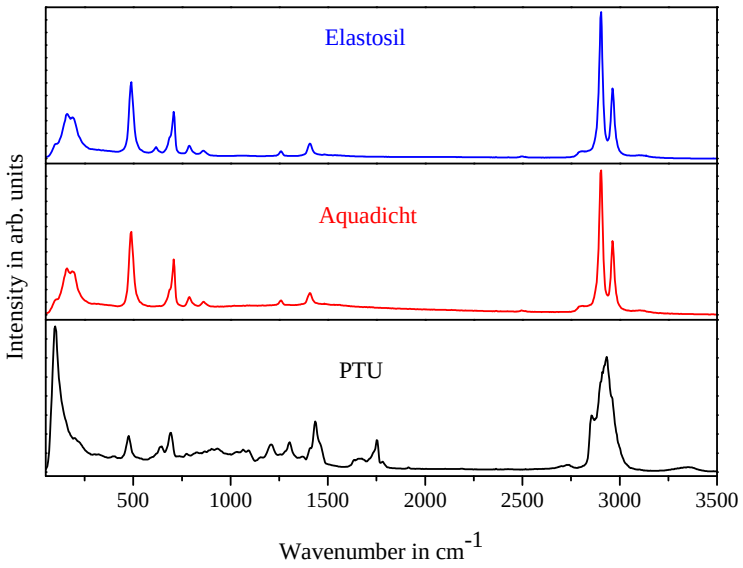

Figure 60: Raman-spectra of PTU and the two silicones, MTAS and ETAS. Besides the fingerprint region, MTAS and ETAS show nearly identical spectra, PTU shows significant differences.

The Raman-measurements shown in figure 61 reveal nearly identical spectra for the two silicones ETAS and MTAS. Small deviations were obtained within the fingerprint region in the range of lower wavenumbers. PTU has a significantly deviating spectrum wherefore the filtering of the datasets was easy to implement. Figure 61 shows the Raman-measurement of a silicone microdomain embedded into a PTU matrix. As the filtering was performed with respect to the silicone spectrum, the microdomain appears bright whereas the PTU is dark.

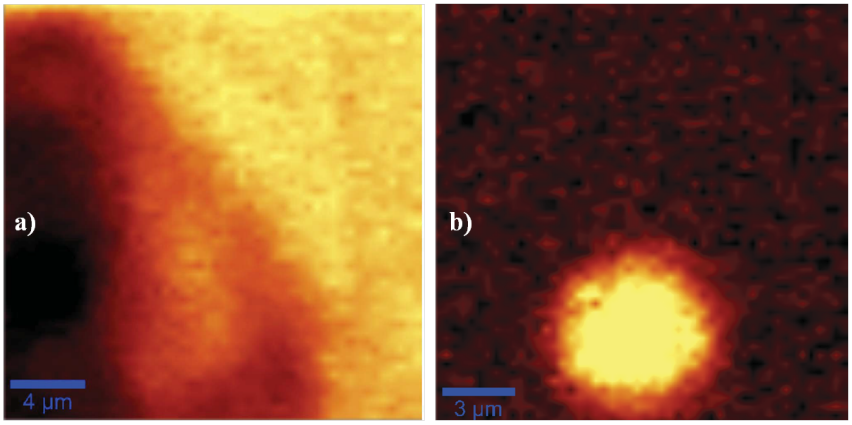

Figure 61: Filtered Raman-images of PTU and the two silicones. a) MTAS: no distinct microdomaines visible, transistion zone between the two polymers is blurred.b) ETAS: distinct microdomain embedded into the PTU matrix. The transition between the polymers is clearly distinguishable.

7.5 Surface characterization

As the surface plays the major role within the development of antifouling coatings, detailed information on the surface characteristics are necessary in order to evaluate its antifouling properties. As already stated, the convincing antifouling features of silicone-based coatings are a result of a suitable interaction between low surface-free-energy and low elastic modulus. The results obtained by tensile testing revealed a comparable high mechanical strength for the PTU/silicone-composites for what reason the investigation of the contact angle and the SFE with its polar and dispersive components is of major importance.

7.5.1 Contact angle experiment

In order to investigate the influence of the ZnO particles on the wettability of the PTU/PDMS-composites, contact angle experiments were performed and the corresponding mean values and standard deviations are illustrated in figure 62. For comparison, the contact value of PTU is provided in addition.
The measurements revealed, that the addition of ZnO particle led to slightly decreased contact angles. The initial value of 10 wt.% ETAS in PTU amounted to 110°, 1 wt.% s-ZnO led to a decrease to 100° which was not as pronounced for 1 wt.% t-ZnO where a value of 105° was obtained. The addition of 5 wt.% led to further decrease values as 5 wt.% s-ZnO reached 95° whereby 5 wt.% t-ZnO came down to 100°. regarding the particle morphology, it can be stated that the addition of s-ZnO had a more distinct influence on the contact angle of PTU/ETAS-composites as the decrease was less for t-ZnO particles.
A partially deviating behavior was obtained for the contact angle measurements of PTU/MTAS-composites. Compared to PTU/ETAS-composites, the initial contact

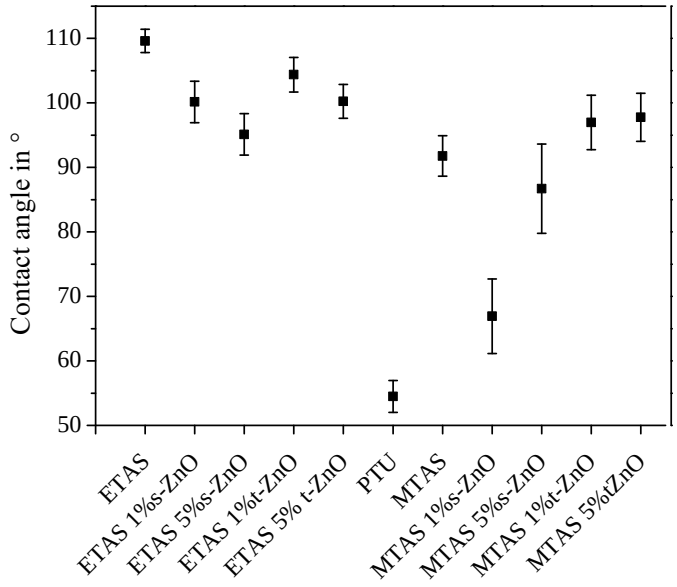

Figure 62: Influence of t-ZnO and s-ZnO on the contact angle of the PTU/PDMS composites. The addition of ZnO particles of both morphologies caused slightly decreased contact angles.

angle of around 95° was much lower. The addition of 1 wt.%s-ZnO led to another decrease down to below 70° which was not as pronounced for 5 wt.%s-ZnO at an angle of around 90°. Strongly deviating results were obtained for the additon of t-ZnO as both filling amount led to an increase to nearly 100°.

7.5.2 Topography

The surface roughness of the Two PTU/ silicone composites MTAS and ETAS was estimated for different ZnO filler amounts and morphologies by the confocal light microscope FA. NANO FOKUS. Height profiles were recorded and the mean roughness Ra was estimated according to DIN EN ISO 11562. In table 6, mean values of the measured Ra values and the corresponding standard deviations are shown.
The highest roughness were obtained for the PTU/silicone blends without additional ZnO, whereby the values amounted to 1.16 μm 0.818 μm for ETAS and MTAS, respectively. With the addition of ZnO particles, Ra was decreasing for all filler amounts and particle morphologies whereby the lowest value was obtained for 5 wt.% s-ZnO in MTAS.

Table 6: Roughness Ra of the different PTU/silicone composites with different ZnO filling amounts and morphologies.

ZnO content	Ra ETAS in μm	Ra MTAS in μm
0 wt.% ZnO	1.16 ± 0.22	0.818 ± 0.164
1 wt.% t-ZnO	0.46 ± 0.09	0.26 ± 0.10
1 wt.% s-ZnO	0.48 ± 0.14	0.30 ± 0.11
5 wt.% t-ZnO	0.46 ± 0.09	0.49 ± 0.15
5 wt.% s-ZnO	0.70 ± 0.25	0.23 ± 0.06

7.5.3 Surface free energy

The wetting behavior and the free surface energy of the different samples (pure PTU, pure silicone, PTU/silicone blends) was investigated by contact angle measurements at HZG with a Kruess DSA 100 device. For the evaluation of the polar and dispersive components, contact angles of three liquids with known surface tension (water 1000 mN/m, ethylene glycol with 47.5 mN/m, chlorobenzene with 33.6 mN/m) were measured and the OWKR method was applied for the evaluation of the respective fraction. Table 7 shows mean values of the FSE with its polar and dispersive fractions for PTU, ETAS and the polymer blend PTU/ETAS.

Table 7: Free surface energy of PTU, ETAS and the PTU/ETAS composite. The amounts of the polar and dispersive components are given, respectively.

Sample	FSE in mJ/m^2	Pol.in mJ/m^2	Disp. in mJ/m^2
PTU	35.8 ± 1.4	9.7 ± 3.6	26.1 ± 3.0
ETAS	20.9 ± 0.4	0.0 ± 0.0	20.9 ± 0.4
PTU/ETAS	20.9 ± 0.8	0.0 ± 0.1	20.9 ± 0.8

Pure PTU showed a high FSE of around 36 mJ/m^2 with a polar fraction of around 10 mJ/m^{2}and a dispersive fraction of 26 mJ/m^2. In contrast, ETAS had a low SFE of around 21 mJ/m^2 with no polar fraction. Considering the PTU/ETAS-blend, the values coincide perfectly with those of pure ETAS.

7.6 Immersion experiment

The fouling process on the PTU/PDMS composites was studied at Laboe harbor (Baltic Sea) and the outlet of the Schwentine river. The fouling progress was recorded weekly and an overwiev on the period of immersion is shown in figure 63 for Laboe and in figure 64 for the Schwentine. As reference, PTU as well as an

AlMg3 substrate were immersed and the growth was compared to the PTU/PDMS-composites.

7.6.1 Evaluation of fouling process in Baltic Sea

After three months of immersion in the Baltic Sea, all samples except PDMS were almost completely covered by algae, PDMS showed only a very small amount of attached organisms. Six months after immersion all surfaces, except for PDMS were fouled. Barnacles were found on all kind of surfaces, even on the well-known low-fouling and fouling-release silicone material. Three months later, the PTU and AlMg3 surfaces showed strong fouling of hard and soft foulers. PDMS was only covered by a thin layer of organisms. Isolated barnacles were attached. The PTU/ETAS and PTU/MTAS samples and their composites filled with ZnO particles were completely covered by biofoulers. After nine month there were no changes for the PTU and AlMg3 surfaces. The biofouling on PDSM increased slightly and an opposite trend within this period of time was found for all PTU/silicone-composites. After twelve months of immersion, fouling was most pronounced on the PTU surface where high amounts of barnacles and ascidiae were accumulated. A slightly lower amount of fouling was found on the PTU/silicone-composites (with and without particles). Additionally, the detachment of single barnacles from PTU/ETAS with 5Â wt% t-ZnO was observed. The lowest amount of fouling was recorded on the PDMS surface, which was constant within the last three month.

7.6.2 Evaluation of fouling process in freshwater surroundings

Comparing the growth within the first three months of immersion into the Baltic Sea and the river Schwentine, similar results were obtained as all samples showed a complete overgrow by green and brown algae.
After six months, the results from different water conditions started to diverge as the growth within the Schwentine river was strongly reduced compared to the first months. Additionally, the amount of fouling was remarkably reduced on all PTU/PDMS-composites.
Three months later, the growth was again increased. All surfaces were overgrown by mainly green algae and no difference appeared between all sample sunder investigation.
Strongly deviating results were obtained after 12 months of immersion. Overall, the growth was slightly reduced on all samples, but remarkable differences showed up between the different materials. Comparing PTU and ALMg3 to both PTU/PDMS composites, the growth on the latter named was slightly reduced. A much more pronounced difference was obtained for the PTU/PDMS-composites and those filled

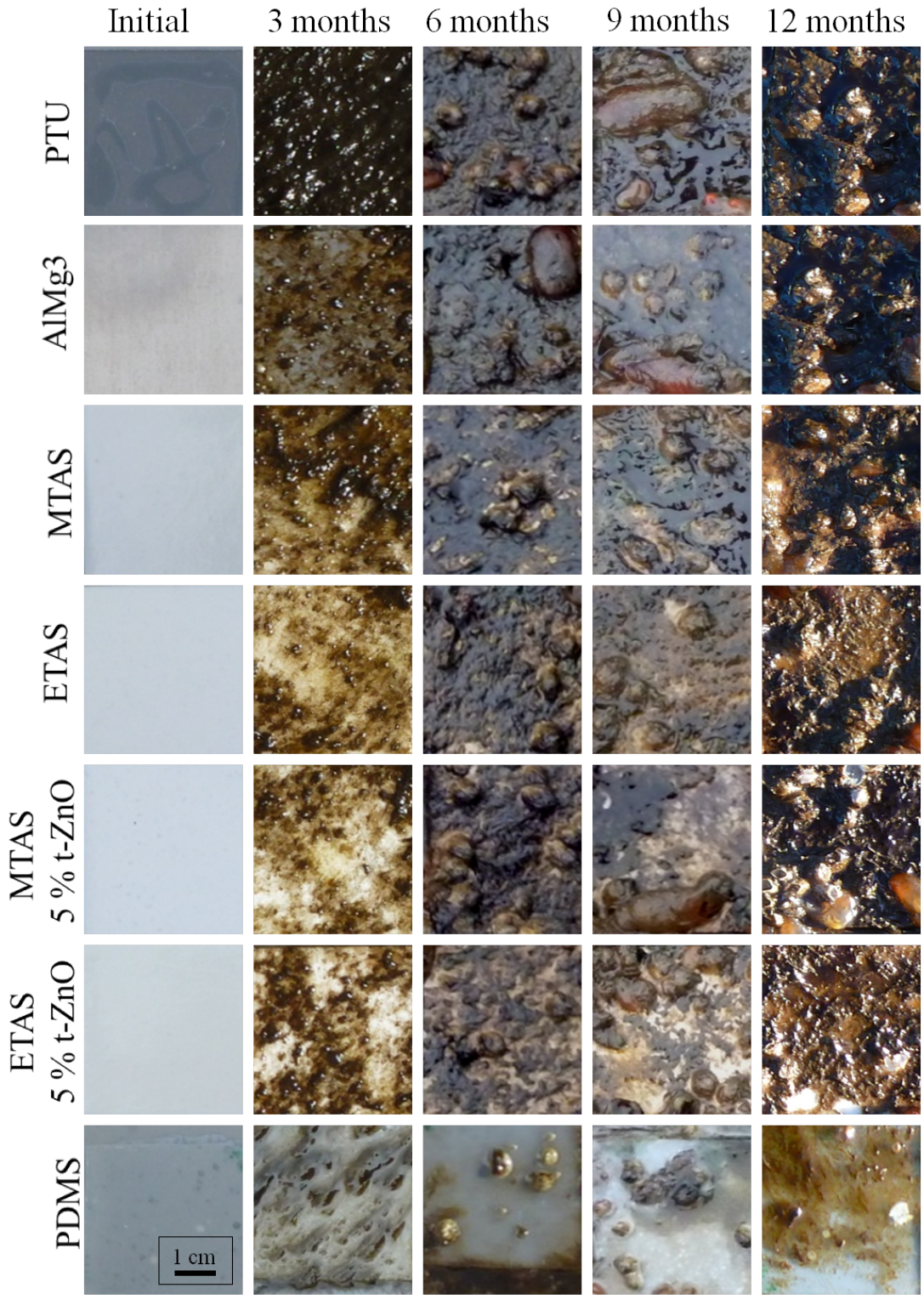

Figure 63: Fouling process over time on PDMS/PTU-composites in Laboe harbor. After 3 months, all samples except PDMS were completely fouled. The same results were found after 6 months of immersion, additional barnacles were settled on every surface. After 12 months, fouling was slightly reduced on PTU/silicone-composites when compared to PTU samples, barnacles and ascidiae were found on every surface. The lowest amount of fouling organisms was found on PDMS.

with ZnO particles. As underlined in figure 65, some surfaces remained nearly clear after 12 months within the Schwentine. These samples were those PTU/PDMS-composites based on the silicone ETAS combined with 1 wt.% and 5 wt.% ZnO particles. At this, the particle shape did not seem to make any difference as both t-ZnO and s-ZnO led to the same results. On the other hand, these observations could not be found for PTU/PDMS-composites based on the silicone MTAS.

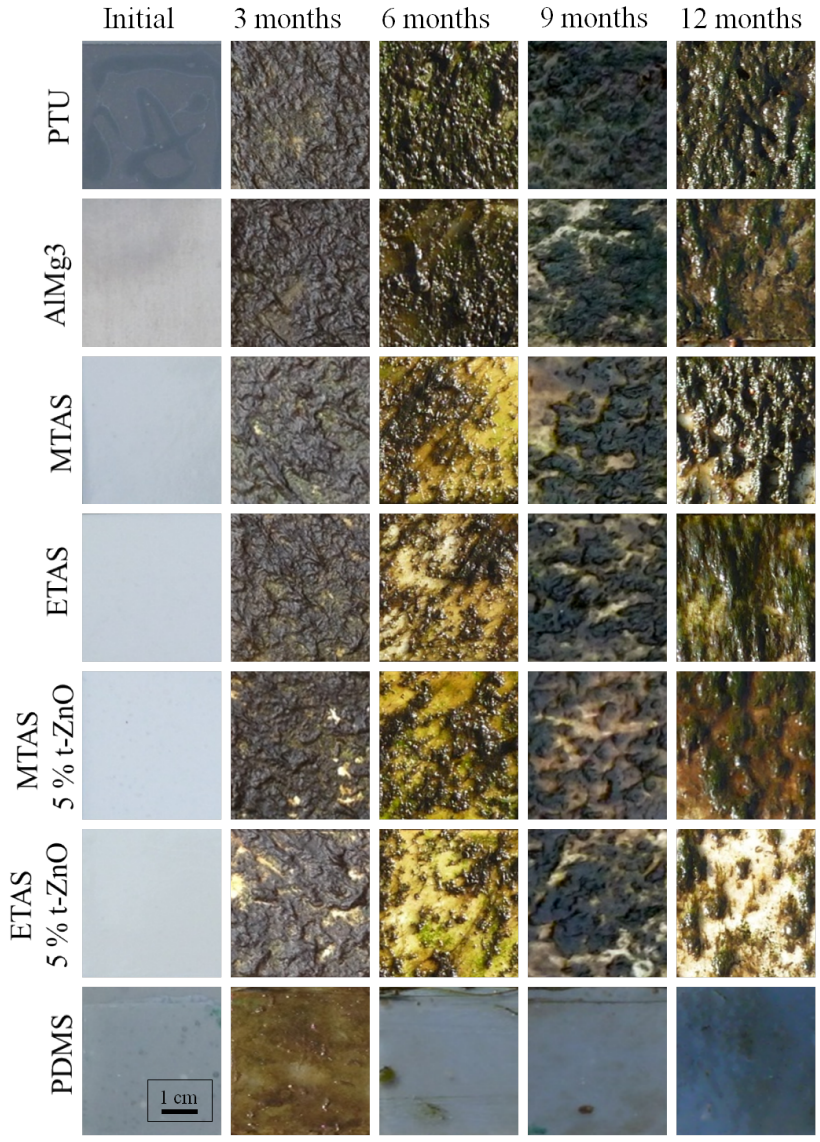

Figure 64: Fouling process over time on PDMS/PTU-composites in the river Schwentine. Within the first 9 months, the amount of fouling was alternating on PTU/silicone composites whereas it was constantly increased on PTU and AlMg3. 12 months after immersion, significant differences were found as those PTU/ETAS composites containing ZnO particles showed a strong reduction in attached organisms.

Figure 65: Fouled PTU/silicone-composites after 12 months of immersion in the river Schwentine. PTU and AlMg3 are shown as references. The sample surfaces with reduced fouling belong to PTU/ETAS composites with additional ZnO particles of both morphologies and concentrations. The sample size amounts to 80 mm * 80 mm.

7.7 Cleaning experiment

To evaluate the attachment of the marine organisms to the polymer surfaces and the easy-to-clean properties of the different materials a cleaning experiment was conducted. The setup of the cleaning experiment with a high pressure water blaster was chosen comparable to the commonly used cleaning procedure for ships.

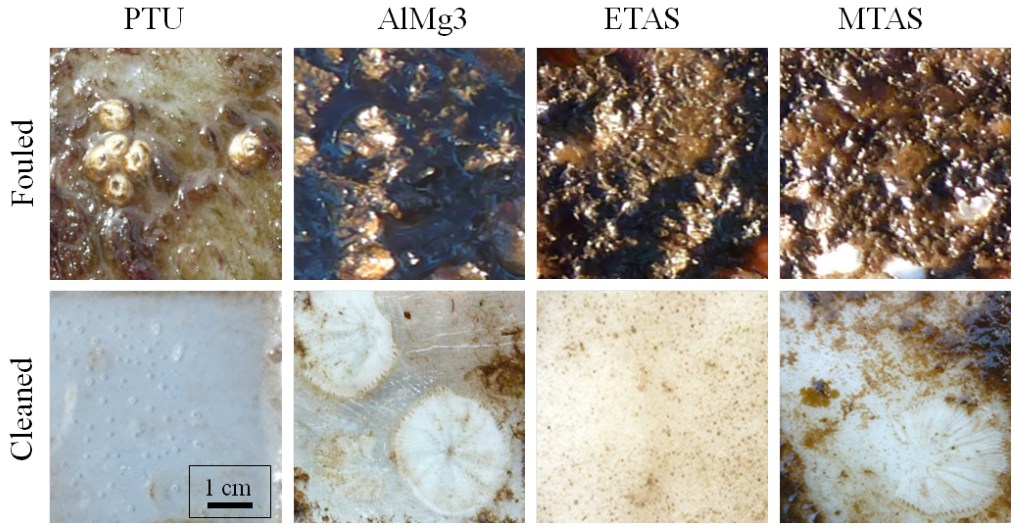

Figure 66: PTU/ZnO samples and the PVC reference after immersion of 12 months and after subsequent cleaning. The PVC sample showed a remarkable amount of barnacle cement accompanied by material degradation due to biocorrosion. the PTU surfaces were nearly completely cleaned, no residues of hard foulers and no effect of biocorrosion was obtained.

The high-pressure cleaning of PTU and AlMg3 showed that most of the attached organisms, even the hard fouling barnacles, were removed, but small residues of the cemented shell, which enable the attachment to the substrate were left behind. Regarding the PTU surface, these small residues were easily removed by hand. The clean surface was completely intact and there was no sign of biocorrosion. In contrast, these residues could not be mechanically removed from AlMg3 and the surface was obviously damaged by biocorrosion. Applying this cleaning procedure to PDMS led to complete removal of all attached organisms, but the surface was severely damaged by the water-blaster. Both surfaces of PTU/ETAS with 5Â wt% t-ZnO and without added particles were easily cleaned by water pressure and even the calceous residues of barnacles were completely removed. In contrast, the removal on all PTU/MTAS-composites was not as simple. Residues of cemented barnacle shells were found on every sample.

8 Discussion on PTU/silicone-composites

With the development of PTU/silicone blends it was aimed to develop a mechanically stable polymer composite with PTU as matrix and silicone microdomains which provide the necessary surface characteristics, e.g. hydrophobicity and low surface free energy. For the fabrication of PTU/silicone polymer blends, different silicones were evaluated with respect to their processability and their influence on mechanical and surface properties. Two main categories were chosen, one-component and two-component silicone systems. It was shown, that most two-component systems led to the formation of a thin liquid layer on top of the sample surface. Therefore they were not considered for following experiments. As a result, the one-component systems ETAS and MTAS were selected and their percentage share with respect to the PTU matrix was set to 10 wt.%. For additional reinforcement in mechanical and antifouling properties, ZnO microparticles were added to the composites. The amount was varied from 1 wt.% to 5 wt.% and for the evaluation of the morphologies influence, tetrapodal as well as spherical particles were investigated.

By the implementation of hydrophobic silicone microdomains on the surface a composite system was developed which combines the hydrophobicity of silicones and the mechanical stability of polyurethanes. To reach this goal, the production procedure of the composite was optimized with respect to maximum surface hydrophobicity by variation of the stirring time of the components. A of nearly 115 ° was reached when the unpolymerized composite was magnetically stirred for 30 min for both PTU/ETAS and PTU/MTAS. Further increase in mixing time resulted in decreasing water contact angles, which can be explained by the limited time for migration of ETAS microspheres before the viscosity of the polymerizing PTU matrix stopped this movement.

For the evaluation of the mechanical properties, tensile tests were performed on the PTU/silicone-composites. The dependency of the composites characteristics on the particular amount and morphology of ZnO filling particles was simultaneously investigated. It was shown, that PTU/silicone-composites exhibit high mechanical strength compared to pure silicone with a tensile strength of around 5 MPa and an elongation at fracture of nearly 100 %. The tensile strength of PTU/ETAS could almost reach 30 MPa combined with an elongation at fracture of 15 % which lays in the region of pure PTU with values of 60 MPa and 15 % for tensile strength and elongation at fracture, respectively. With only 10 wt.% of silicone, the mechanical properties of the PTU/ETAS composites are comparable with the pure matrix polymer PTU and therefore they are much more mechanically stable than silicone

material. This combination of material properties is highly preferable as the good fouling-release properties of silicone can be maintained while its disadvantage of mechanical instability can be compensated by the PTU matrix, whose mechanical robustness dominates the overall mechanical properties [37]. Nevertheless the combination of PTU with silicones results in reduced E-modulus of around 70 % compared to the mechanically stable pure PTU. Regarding the addition of ZnO particles into the composite, it was shown that the highest increase in mechanical properties could already be obtained for 1 wt.% particle addition. The E-modulus was increased up to 87 % for 1 wt.% s-ZnO compared to the pure matrix polymer. In addition, the tensile strength of PTU/ETAS without particles dropped to 46 % and was increased by the additon of 1 wt.% s-ZnO up to 63 %. This effect was not detectable for higher filler amounts of 5 wt.%. As stated by Niu et al. [31], these reduced mechanical properties for particle amounts above 1 wt.% may be a result of increased mixture viscosity and bubble formation within the curing composite. In addition, there can be a mechanically deteriorating effect due to particle agglomerations at higher filler amounts [31].

Aimed by Raman-spectroscopy, the formation of silicone microdomains within a PTU matrix was visualized. It was shown, that both silicones ETAS and MTAS formed a phase-separated structure. On the other hand, defined microdomains with a spherical shape were only detectable for ETAS-composites as MTAS led to the formation of blurred, undefined blocks. The phase separation of the two polymers can be attributed to the immiscibility of the single components [37]. A possible explanation for this effect could be the differences in surface free energy and also in the polar fractions of ETAS (0.0 mN/m) and PTU (9.7 mN/m). This is for the ETAS component a less favorable thermodynamic condition to form interfaces with PTU and the formation of interfaces with mostly apolar air is favorable. Assuming there would be no other limiting conditions within the polymer mixture a complete phase separation would occur. However this process is prematurely terminated by the increasing viscosity of the PTU matrix due to the ongoing polymerization reaction. On the other hand, the non-spherical domains formed by MTAS may be attributed to either too high viscosity or too low curing time of the silicone. For the first case, the viscosity would cause a hindered stirring which could led to inhomogeneous dispersion and size of the domains. On the other hand, a short curing time would cause the same effect as a homogeneous stirring would be prevented by insufficient time.

Regarding the surface characteristics, it was shown by contact angle measurements that the addition of ZnO particles to the PTU/silicone composites had a significant

influence on the wettability. With a contact angle of around 110 °, PTU/ETAS showed the highest obtained value which was continuously decreased down to below 100 ° with increasing amount of ZnO. An influence of the particle morphology could not be detected. On the other hand, a shape-dependency was obtained for the PTU/MTAS-composites. The initial contact angle of around 90 ° was strongly decreased to below 70 ° for 1 wt.%s -ZnO, a value of below 90 ° showed up for 5 wt.% s-ZnO. In contrast, both filling amounts of t-ZnO led to a slightly increased contact angle of around 95 °.
The decreased contact angles for PTU/ETAS-composites with additional ZnO filling particles can be explained by taking the surface roughness into consideration. The highest contact angle was obtained for PTU/ETAS which is in good accordance to the highest measured Ra value of 1.16 μm. With increasing filling amount, the contact angle decreased and also the surface roughness showed decreasing values to around 0.5 μm. As stated by Cassie and Baxter [46], an increased surface roughness would led to increased contact angles in the case of hydrophobic surfaces. The findings concerning contact angle and surface roughness with regards to PTU/ETAS-composites are therefore in good accordance with theoretical considerations.
For PTU/MTAS-composites, the explanation is not straightforward as a change to both higher and lower contact angles was obtained with the addition of ZnO particle. As the relation to the surface roughness is not easily possible here, a different explanation needs to be developed. One possibility might be the contact angle of PTU/MTAS itself. Showing a value of around 90 °, the surface is not clearly defined as either hydrophilic or hydrophobic.

The evaluation of the surface free energy by contact angle measurements and the OWKR method was performed in order to investigate whether the PTU/silicone-composites show the desired similar values as pure silicone. For that reason, pure PTU as well as pure ETAS were measured and compared to the composite. As already shown, PTU has a relatively high surface energy of around 36 mJ/m^2 with a polar fraction of around 10 mJ/m^2 and a dispersive fraction of around 26 mJ/m^2. On the other hand, the SFE of silicone amounts to 21 mJ/m^2 with a purely dispersive fraction. Regarding the PTU/ETAS-composite, it can be stated that the SFE is identical to pure ETAS. It could therefore be underlined, that the mechanical features of PTU were kept while the surface energy of silicone was adapted. The specific wetting behavior of PTU/silicone can be explained by applying the wetting model by Cassie and Baxter [46] where it is stated that surface protrusions as a result of surface roughness cause air filled gaps which stay unwetted [46], it can be assumed that the microdomains act similarly as protrusions whose distance is

small enough to avoid surface wetting in between. The model of Cassie and Baxter [46] shows that the wetting behavior not only depends on surface chemistry and emphasizes the important role of surface roughness for this phenomenon. Therefore the influence of ZnO particles on the surface topography was investigated by roughness measurements. It was shown, that the roughness decreased with increasing particle amount accompanied by a decrease in contact angle. This effect of decreasing roughness and contact angle is in good accordance to the wetting models by Cassie and Baxter [46]. They state, that the hydrophobic or hydrophilic properties of a surface can be increased by the introduction of roughness. The decrease in roughness itself as a consequence of ZnO addition may be attributed to catalytic effects of the particles [106]. Oxygen vacancies present in the lattice of ZnO as a result of their high temperature synthesis led to the formation of catalytic sites which can accelerate the polymerization of polymers [107, 106]. As a result, the migration time of the ETAS domains towards the surface may be reduced for what reason their amount at the surface and therefore the roughness of the composite decreases.

During the immersion experiment within the Baltic Sea at Laboe harbor and the river Schwentine, it was shown that the growth during 12 months differed strongly in both habitats. While the amount of fouling increased continuously and nearly as strong as on the two reference surfaces PTU and AlMg3 with time of immersion in the Baltic Sea, a fluctuating behavior was obtained in the freshwater surroundings. After a phase of homogeneous fouling within the first three months, the PTU/silicone-composites showed reduced fouling when compared to PTU and AlMg3 after six months. Again three months later, an increased growth appeared followed by a second decrease within the last three months. Additionally, comparing PTU/ETAS and PTU/MTAS after 12 months of immersion, it was found that PTU/ETAS with ZnO filler particles of both investigated shapes and amounts showed strongly reduced growth. Without filler addition, fouling on PTU/ETAS and PTU/MTAS composites was significantly increased.

Regarding the cleaning experiment for these surfaces originally immersed in salt water, strong differences became obvious. After water-blaster treatment small amounts of cemented residues from barnacles were found, but on PTU it was possible to remove those easily by hand and there was no indication to biocorrosion. Exactly the opposite was found on AlMg3. It was not possible to remove the residues of hard fouling organisms by hand and strong changes in the material due to biocorrosion were detected. In general AlMg3 and PU are well established materials used in ship building, respectively ship hull coating. Both are known to bear nearly no

antifouling properties [108]. The findings for PDMS immersed in both habitats were in accordance with literature. There has been only strongly reduced biofouling and this process was subject to periodic cycle due to the materials immanent self-cleaning properties [16, 37]. The mechanical limitations of silicones got obvious after the cleaning experiment. The PDMS surface was completely free of attached organisms, but there was some damage within the material. Comparable fouling behavior was also found for PTU/ETAS composite for both habitats. The addition of ZnO particles resulted in a strong reduction of biofouling in periodic cycle for the freshwater habitat, comparable to pure silicone, but the degree of biofouling was still on a higher level. This kind of behavior was not found within the salt water habitat, which can be explained by the fact, that in general the biofouling potential in salt water is much higher than in freshwater. The composite with or without ZnO particles of both morphologies were easily freed from attached organisms by high pressure cleaning. No residues of barnacles were found and the surface was still intact after the water-blaster treatment. This shows, that the mechanical stability and biocorrosion resistance of PTU was combined with the low-fouling and fouling-release properties of silicone [104, 28]. Although it was shown that the surface properties of PTU/ETAS were similar to those of pure ETAS, the obtained difference in the amount of fouling indicates that the bulk material properties contribute significantly to the fouling-release properties. The beneficial mechanical stability and biocorrosion resistance of the PTU matrix [104] is accompanied by a comparably high elastic modulus which is unfavorable for easy release of marine organisms [37]. The detailed investigations of surface properties, mechanical testings and the evaluation of the biofouling properties have shown, that the PTU/ETAS composite which contains 1 wt.% t-ZnO particles possesses superior properties. This material combination has shown the best hydrophobic properties, elongation at fracture and showed only slightly reduced performance for elastic modulus and tensile strength, compared to the best PTU/ETAS ZnO particle combination on these parameters. The immersion tests showed no clear advantage in fouling behavior of a distinct concentration or morphology of ZnO particles.

Summarizing, taking into account all relevant properties, it can be stated that PTU/ETAS containing 1 wt.% tetrapodal-shaped ZnO particles is a promising environmentally friendly, mechanically stable and long-lasting composite hybrid material for fouling-release coatings. The advantageous surface properties of silicone materials are utilized and at the same time their major drawbacks like low adhesion to the substrate, low mechanical stability and sensitivity to UV-light are overcome. This fouling-release composite material is best suited for large scale marine applications

like ship hulls and submerged maritime buildings. Fortunately, a low required filler amount is attractive for upscaling as it brings along side benefits like reduced costs and simplified application.

Chapter 8

PTU/ZnO composites as sustainable coatings for marine applications: a long-term field experiment

9 Coating of a multi purpose vessel

To test the up-scaling possibility of the coating system, a preliminary large scale long-term field experiment was conducted in cooperation with the shipping company Roerd Braren, Kollmar, Germany. The shipping company offered three test areas for coating on the ship hull of the multi purpose vessel *African Forest*. The vessel commutes between Antwerpen, Belgium and Douala, Cameroon. The velocity profile of this ship is quiet diverse, there are longer periods at a cruising speed of around 12 kn to 15 kn, interrupted by waiting times from hours to weeks to access harbors at the western coast line of Africa. The fouling pressure within those warm, sun-drenched and rich in nutrients marine environment is enormous. Therefore, effective antifouling measurements are essential. The ship owner reported incidents were the ship was forced to wait in the tropical ocean for up to four weeks after which the ship was not operational anymore due to biofouling. A harsh mechanical ship hull cleaning was necessary in order to be able to continue the travel. However, due to the underwater ship hull cleaning the conventional selfpolishing coating was

badly damaged and needed to be replaced after two years.

In detail test area 1 was located at the port side, the areas 2 and 3 were located at the propeller (figure 67) whereby the cavitational forces are much higher at the backside of the propeller as compared to the frontside. In contrast to test area 1, the test areas 2 and 3 were polished by abrasive paper directly before application of the different PTU/ZnO composites (0 wt.% t-ZnO, 1 wt.% t-ZnO, 5 wt.% t-ZnO and 1 wt.% t-ZnO with additonal 10 wt.% t-ZnO of red pigment).
As the samples evaluated in the aforegoing chapters were on the laboratory scale and occasionally processed in a way unsuitable for large scale applications, long-term filed experiments were conducted in collaboration with the shipping company Roerd Braren in Kollmar, Germany.

Figure 67: Experimental coating areas on the multi purpose vessel *African Forest*, kindly provided by the shipping company Roerd Braren. 1. Port side. 2. Propeller front side with high cavitational forces. 3. Propeller back side with low cavitational forces.

The coatings were hand-applied by foam-rolls at a component ratio of 58 % HDI to 42 % PETMP whereby the appropriate amount of t-ZnO particles was mixed into the PETMP component in advance. The temperature of the steely ship hull was 13 °C at an atmospheric temperature of 11 °C . The relative humidity of the adhesion promotor was 73.3 %. The coating was dried for around two days before exposure to seawater and the remaining hull was coated by conventional biocide-containing abrasive antifouling-coating.

After two years of traveling along the African west coast between Antwerpen, Belgium and Douala, Cameroon, Africa, the African Forest was brought back to the dry dock at Kollmar, Germany in order to renew the antifouling coating. This dry docking interval opened up the possibility to inspect the test areas after long term seawater exposure to different habitats (figure 68).

The ship hull with its testing areas was inspected and documented by photographs. Not only the degree of fouling was in focus, but also the cleaning properties and the polymer durability with respect to biocorrosion. Figure 68 shows test area 1 before exposure to seawater, after two years of immersion and after cleaning by polymer brushes.

9.1 Test area 1

Regarding the smoothness of the different PTU/ZnO composites, a remarkable difference was obtained between pure PTU, PTU with ZnO addition and PTU/ZnO composites with additional red pigment. The PTU surface appeared smooth, but the roughness of the underlying ship hull was still noticeable. On the other hand, the PTU/ZnO coating showed an increased roughness. A different surface was obtained for PTU/ZnO composites with 10 % red pigment as it appeared extremely smooth. Additionally, the roughness of the underlying ship hull was not visible anymore. In figure 68 the PTU/ZnO composites applied to test area 1 are shown before and after cleaning by polymer brushes.
After two years within seawater, the complete testing area 1 was covered by sessile barnacles (figure 68, b)). No differences were found between the tested PTU-composites.
After hand-cleaning with a brush, differences with respect to residues were found on the different PTU/ZnO composites. While no residues were found on PTU and PTU/ZnO with 10 % red pigment (figure 68, f)), PTU/ZnO composites with 1 wt.% and 5 wt.% particle addition showed small residues (figure 68, e)).
On the other hand, all surfaces from test area 1 were not affected by biocorrosion within the two years of immersion.

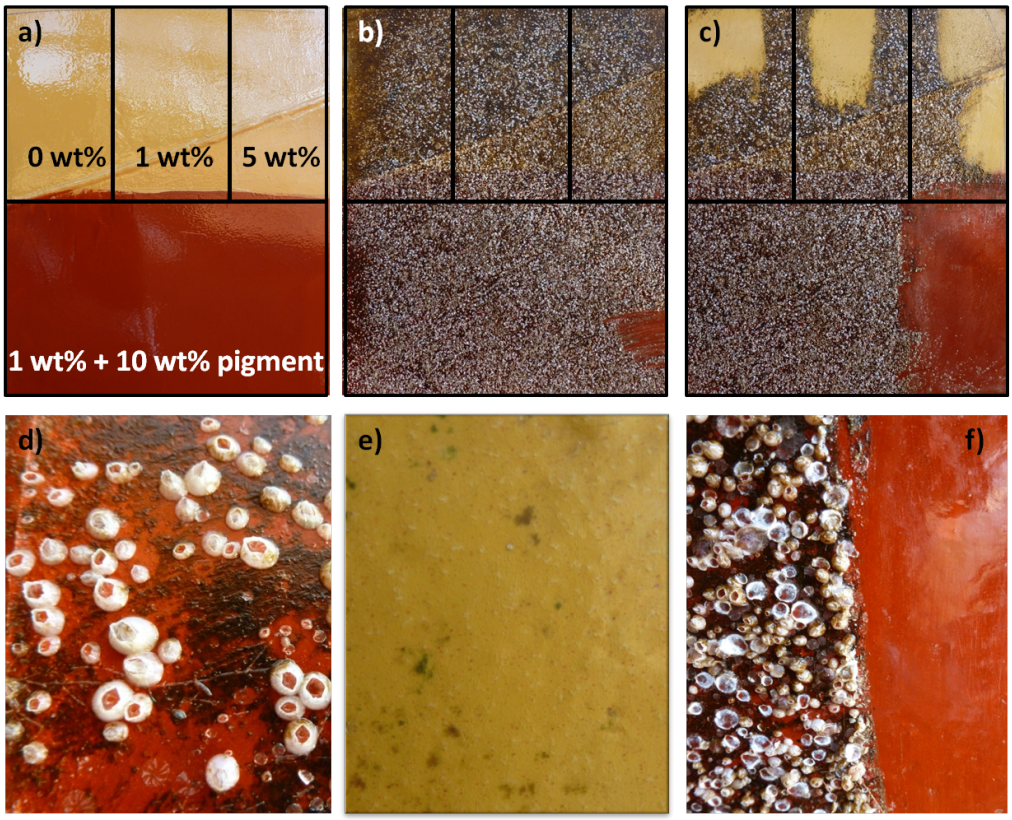

Figure 68: Overview of PTU coating area 1. a) Original PTU surface of area 1 before exposure to seawater. Indications of wt% show the amount of added t-ZnO particles, black frames define the respective areas. b) Coating area 1 after two years of exposure to seawater. The complete testing surface is homogeneously covered by barnacles. c) All four different PTU surfaces of area 1 after cleaning with a polymer brush. The coverage by barnacles could be easily removed, no residues remained on the surfaces. d) Close-up view of PTU surface with 1 wt.% t-ZnO and 10 wt.% red pigment covered by barnacles. e) Cleaned PTU surface with 1 wt.% t-ZnO, no residues were found and the surface was completely intact. f) Comparison of overgrown and cleaned PTU surface containing 1 wt.% t-ZnO and 10 wt.% red pigment. The surface was completely cleaned, no residues were found.

9.2 Testing areas 2 & 3

Regarding the coating of the propeller marked as testing area 2 and 3 in figure 67, the results obtained after two years of seawater suspension showed strong differences when compared to the coating of the ship hull. In figure 69, the front-side of the propeller is shown directly after coating and two years after two years of duty.

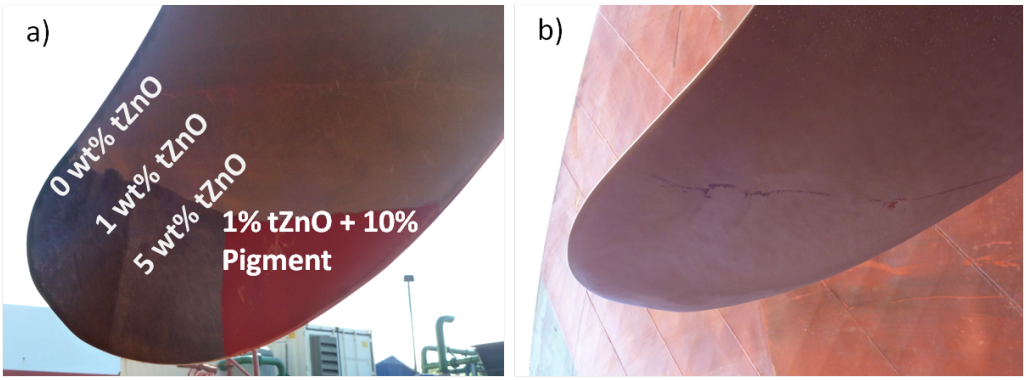

Figure 69: Overview of PTU coating area 2. The different PTU/ZNO coatings marked in a) are completely vanished after the two years of immersion.

The harsh conditions on the propeller led to complete delamination of the coating. Therefore no polymer material was left.

10 Discussion

Small-scale long-term immersion tests at the Baltic Sea and in freshwater surroundings have shown, that PTU/t-ZnO composites posses convincing low-fouling and easy-to-clean properties combined with a strong biocorrosion resistance [104]. These findings based on lab-scale experiments led to the assumption that this composite has enormous potential as an environmentally friendly, mechanically stable ship hull coating with low-fouling properties. To evaluate this field of application, a large-scale long-term immersion test under realistic conditions for a commercial seagoing ship was performed. The coating of a seagoing ship is challenging as it has to be homogeneously dispersed on a huge area. Therefore special application techniques strongly differing from those used in laboratory scale need to be implemented. Of special importance within these aspects is the reduction of biofouling and a durability of the coating for two to five years. All these demands have to be fulfilled under harsh mechanical, chemical and physical conditions.

Performing immersion tests on the commercial multi purpose vessel *African Forest* owned by the company Roerd Braren, Kollmar, Germany opened up the possibility

to test the up-scaling of the application of the PTU/tZnO-composite. Therefore, three coating areas were made available, one at the port-side and two at the front- and backside of the propeller where different PTU/ZnO-composites (0 wt.% t-ZnO, 1 wt.% t-ZnO, 5 wt.% t-ZnO and 1 wt.% t-ZnO with additonal 10 wt.% of red pigment) were applied. After an operation time of two years along the west coast of Africa, the vessel was docked and the test areas were inspected. Due to the fact, that no polymer coating was left on the testing areas at the propeller, only the testing area on the port-side of the ship will be discussed in detail.

Regarding the surface morphology of the different PTU/ZnO-composites, pure PTU showed a smooth surface but the underlying roughness of the ship hull was not compensated. This effect may be a result of the minor coating thickness. The increased roughness obtained for the PTU/ZnO coatings may be attributed to inhomogeneous particle distribution and the comparably low coating thickness. These results underline the enormous effect of the application technique on the quality of the coating.

In contrast, an extremely smooth surface was obtained for PTU/ZnO composites with 10 wt.% red pigment. In addition, the roughness of the underlying ship hull was not visible anymore. One explanation for this effect might be the increased viscosity of the composite caused by the addition of the pigment. This increased viscosity may lead to an increased coating thickness which compensates the roughness of the ship hull.

Regarding the accumulation of fouling species, it was completely covered by barnacles after two years of traveling along the African west coast. However, it has to be claimed that the attached barnacles were comparably small which is unusual for vessels traveling this route were the diversity of marine organisms and the fouling pressure is extremely high. This comparably low size of the barnacles may be a result of insufficient adhesion to the test coatings. With increasing barnacle size, the drag resistance of the ship is increased and therefore also the forces acting on attached organisms. In general, barnacles attack the underlying surfaces by material degradation to provide sufficient strength of attachment [109]. In case of PTU, no biocorrosion was observable underlining that this strategy of attachment enhancement was successfully prevented. At a certain barnacle size, the increased drag resistance may therefore be too strong and these hard-foulers are released from the surface.
The results obtained from cleaning with polymer brushes revealed a complete cleaning ability for PTU and PTU/ZnO-composites with 10 wt.% addition of red pigment whereas small residues were found on PTU/ZnO composites. These find-

ings are in good accordance to the already mentioned differences in roughness. At smooth surfaces like PTU, cleaning is easily implemented as it is not hindered by outstanding protrusions. In contrast, the roughness induced by ZnO filler addition causes small cavities where the removal of residues is more complicated.

Regarding the stability of PTU/ZnO-composites it was shown that no signs of biocorrosion were found after two years of immersion. This stability can be attributed to the high degree of crosslinking as a result of the polymeric structure of PETMP providing four reactive SH groups [86]. This structure is known to result in high tensile strength and enhanced abrasion resistance [89]. Beyond this, PTU provides an aliphatic structure which lacks UV-instable aromatic rings and therefore provides stability under natural conditions [29].
Previous work has shown that the addition of tetrapodal-shaped ZnO particles increased the mechanical properties in general and the adhesion to metal substrates in detail [104]. The easy-to-clean properties may be a result of the very smooth coating surface, especially found for PTU/ZnO/pigment-composites. This smooth surface can be achieved by two kinds of mechanisms. First, the polymer composite is able to smoothen the uneven topography of the ship hull and second the absence of volatile organic compounds results in a pore-free and very smooth surface.
Summarizing, it can be stated that the long-term field-experiment on the *African Forest* has shown, that the PTU/ZnO composite is suitable as a durable easy-to-clean coating for marine structures like ship hulls.

Chapter 9

Summary and Outlock

In this work, the fabrication of environmentally friendly and mechanically stable antifouling coatings for the marine sector was demonstrated. A two-component thermoset polythiourethane (PTU) was utilized as basic polymeric material which was modified in several varieties. Within this topic, the incorporation of tetrapodal-shaped ZnO micro- and nanoparticles (t-ZnO) in order to obtain mechanical reinforcement was of major importance [31]. In addition, the fabrication of phase-separated PTU/silicone composites with the aim to combine the mechanical features of PTU with the well-known fouling-release properties of silicones was successfully implemented.

Initial variations of the PTU components 1,6 Diisocyanatohexan (HDI) and Pentaerythritoltetrakis (3-mercaptopropionat) (PETMP) revealed, that mechanical and chemical characteristics were kept nearly constant up to 40 % off-stoichiometry. Larger deviations caused a loss of mechanical features as well as incompleteness of the polyaddition reaction. Long-term Immersion-experiments in the aquarium Geomar and the Baltic Sea showed that off-stoichiometric PTU variations towards lower elastic moduli did not influence the attachment of fouling organisms.

For mechanical reinforcement of the PTU matrix, PTU/ZnO composites (0 - 10 wt.% particles) were fabricated and they showed enhanced tensile response for t-ZnO incorporation as well as strongly increased adhesion to metal surfaces. In this context, the incorporation of hollow micro- and nanoparticles e.g. made from silicon would be very interesting for future work. Those particles could be of great

benefit for mechanical reinforcement of polymers as the hollow structure allows penetration of the polymer matrix which causes additional interlocking. Furthermore, the amount of anorganic material within the polymeric matrix would be reduced which would cause overall reduction in additional weight.

Raman-sopectroscopy, infrared spectroscopy and thermogravimetric analysis of the PTU/ZnO composites revealed, that the quantitative polyaddition of HDI and PETMP was not hindered by filler additions. Measurements of the surface free energy showed deviations between PTU and PTU/t-ZnO composites as the polar fraction was slightly decreased for PTU/t-ZnO composites whereas the dispersive fraction was comparable to pure PTU. Preliminary Immersion-experiments at Aquarium Geomar revealed significant reduction of biofouling on samples containing 5 wt.% t-ZnO compared to pure PTU and a PVC reference. These observations could neither be repeated in the Baltic Sea nor in the river Schwentine as all samples showed homogeneous fouling. However, high-pressure water-blaster experiments showed convincing easy-to-clean properties of the PTU/ZnO-composites as a complete residue-free surface cleaning was obtained in a realistic cleaning scenario. In addition, no signs of biocorrosion were found after more than one year of immersion underlining the suitability as mechanically stable and durable coating for highly stressed marine technologies.

Another aspect of this work focused on the mechanical reinforcement of the well-establish fouling-release material silicone. The incorporation of up to 10 wt.% t-ZnO caused strongly increased tensile features, but this was still below those values reached for PTU/t-ZnO composites. During long-term Immersion-experiments, a continuous fouling by was observed. After high-pressure water-blaster cleaning, all silicone/t-ZnO composites were damaged showing their lack of mechanical stability.

In order to overcome this lack of mechanical stability of silicones, PTU/silicone composites were fabricated and additionally reinforced by ZnO micro- and nanoparticles. Two one-component silicones (MTAS, ETAS) were incorporated and their proportion was set to 10 % by weight. Preliminary evaluations of the wetting characteristics revealed an optimum stirring time of 30 min which was utilized for all following experiments. Tensile tests showed high strength for PTU/silicone composites which were comparable to pure PTU. By t-ZnO incorporation, this tensile response was additionally increased while the beneficial wetting properties of silicones were preserved as contact angle measurements revealed a hydrophobic nature. The surface free energy of PTU/silicone composites was similar to pure silicone. These results underlined, that a composite was fabricated which has the

mechanical stability and adhesion features of PTU combined with the surface properties of the fouling-release material silicone. Long-term Immersion-experiments in the Baltic Sea showed a continuous fouling on all PTU/silicone composites and on those filled with ZnO particles of both morphologies and concentrations. Aimed by high-pressure water-jet cleaning, convincing easy-to clean features of PTU/ETAS composites were shown whereas the PTU/MTAS suffered from incomplete removal of barnacle cement. Regarding the samples immersed into the river Schwentine, PTU/ETAS composites with additional ZnO micro- and nanoparticles showed self-cleaning abilities as settled fouling species were completely washed-off after one year of immersion. In contrast, the PTU/ETAS composites without particle incorporation as well as all PTU/MTAS composites were continuously overgrown.

In the future, the comparison of thin film coatings to molded samples is of great importance as it is necessary to prove whether the outstanding features of the PTU/ETAS composites can be preserved. Another big topic is the cleaning of the samples under real conditions. On the one hand, it needs to be verified whether the speed of a moving ship is sufficient to remove settled organisms from the surface. This could be implemented by a water-channel with an adjustable speed and indirect measurement of the drag resistance. On the other hand, a transporting ship is always subjected to periodic fluctuations regarding the time spend in harbor and those within the sea. For this reason, a stationary sample setup with the possibility to simulate movements in a distinct time-sequence (e.g. one week) would be of great benefit.
In addition, the utilization of PTU/ETAS composites in different areas is of great interest. For example, sanitary seals made out of silicon suffer from the low surface energy of the polymer as it makes a proper adhesion to any surface nearly impossible. PTU/ETAS composites possess outstanding mechanical features as they combine a high elastic modulus and a high impact strength with appropriate chemical and wear resistance. Especially important for the planned application is the strong adhesion to many substrates like e.g. metals or glasses which can be provided by the PTU matrix.
The implementation of adapted techniques for the application of PTU/ETAS composites as coating on large scale is part of future work. This development would include a detailed analysis on the possibility to pre-mix the ETAS component with either HDI or PETMP in order to provide applicability out of the laboratory scale.

11 Acknowledgments

I want to thank Prof. Dr. Rainer Adelung for giving me the opportunity to be part of his fascinating working group for the last 3.5 years. It was a great pleasure to see his scientific enthusiasm and to start thinking in a new way.
I thank Prof. Dr. Helmut Föll, who was responsible for my first impression of the scientific world.
Dr. habil Yogendra Kumar Mishra was very helpful with the realization of the publications and I thank him for his supervision.
Furthermore, I want to thank Prof. Dr. Enrique Quiroga-Gonzales who was a superior adviser during my masters-thesis and who encouraged me to go my way.
Special thank goes to Dr. Martina Baum for her supervision during the last two years and for being such a great and inspiring personality. Besides fruitful work-related discussions and exciting travels to our sample-setup in Laboe, actions like our business trip to Magdeburg with overnight-stay in a tent stay unforgotten.
Another big thank goes to my long-term HiWi Lars Bumke. Besides the writing of two excellent thesis, he was a great help with all the laboratory work and his ideas and ways of thinking were of great benefit for the completeness of this work.
I thank Prof. Dr. Lorenz Kienle and especially his group member Gero Neubüser for the straightforward collaboration.
I thank Dr. habil. Oleg Lupan for his support, especially during the last months.
Furthermore, I want to thank the group of Prof. Dr. Christine Selhuber-Unkel for their collaboration. Special thanks go to Dr. Sören Gutekunst not only for scientific discussions but also for his happy nature.
Many thanks go to my bachelor- and master students who were all part of my work. Without their continuous contributions, the thesis in its present form would not exist.
I am thankful for the first two years I was allowed to share the office with Dr. Viktor Hrkac, Mathias Hoppe, Stefan Freitag and Grit Köppel. We had an amazing time within a great atmosphere which I would not like to miss in my life. Special thanks go furthermore to Dr. Sören Kaps who had always time for me and who was so enthusiastic by realizing any kind of setup.
I want to express my deepest respect to Dr. Arnim Schuchardt. Besides being a brilliant scientist, his positively insane and infectious personality cannot be expressed in words.
Furthermore, I want to thank all other members and ex-members of our working group, Sandra Nören, Sindu Shree, Fabian Schütt, Jorit Gröttrup, Daria Smazna, Leonard Siebert, Ingo Paulowicz, Melike Baytekin-Gerngross, Dr. Mark-Daniel Gerngross, Dr. Andreas Schütt, Dr. Jürgen Carstensen, Dr. George Popkirov,

Dr. Jan-Martin Wagner, Dr. Xin Jin, Emmanuel Ossei-Wusu, Christoph Ochmann and Jörg Bahr. Tim Reimer I have to thank for answering all my questions about chemistry. Dr. Ala Cojocaru as a great friend and colleague during the last years and I am especially thankful for the amazing time we spent in Moldova.
I thank Katrin Brandenburg and Beate Minten for their help with all the bureaucracy and especially for their reliability. For technical support I want to thank all members of the TF workshop. Special thanks go to Berndt Neumann not only for his patience with the realization of my ideas but also for his enthusiasm and encouragement about running.
Furthermore, I want to thank the group of Prof. Dr. Eckhard Quandt for the great collaboration. Claas Thede helped me a lot with the tensile testing machine and took always time to answer my questions. I thank Thomas etzing and Antonio Malave for introducing me to the PECVD device and for their continuous help and patience. I sincerely want to thank Till Jurgeleit, Erdem Yarar, Dr. Ali Tavassolizadeh and Dr. Andre Piorra for their great friendship during the last years and for the great time we spent together. I am very thankful to Dr. Christiane Zamponi for her enthusiasm for everything, for introducing me to the beauty of rowing and for all the funny hours we spent together.
Special thanks go to Volker Röbisch, Christoph Chluba, David Haffner, Sandra Nören and Maike Wegner. We shared the last nine years being not only classmates and colleagues, but also friends. Without these great people, I have to assume that my studies would not have been that successful.
My grateful thanks go to my highly appreciated friend, colleague, classmate and boyfriend Patrick Hayes for his continuous encouragement and for driving me crazy all the time.
Besides university, I want to thank my friends Imke Henningsen, Carolin Diekmann, Mira Kreye, Hanna Gerwinn, Sara El-Madani and Dr. Birgit Bayer for being always there for me and for making my life so enjoyable.
I want to thank the whole family Hayes. I am proud to be part of this crazy assemblage of people.
In the end, I want to thank my parents Hilde Hölken and Dr. Ulrich Hölken for being always so supportive and for the encouregement on any descision I made. I thank my brother Helge, especially for the time he spent on understanding and correcting my scientific work. I thank my sisters Petra Frei, Margit Ness and Astrid Hirche for being there for me at any time. Furthermore, I thank my nieces Kathleen and Ina and my nephews Leeor and Nepomuk for being such an enrichment in my life.

References

[1] Wei Peng Zhang, Yong Wang, Tian Ren Mao, Salim Bougouffa, Bo Yang, Cao Hui Luo, Gen Zhang, Wong Yue Him, Batang Zenon, Al-Suweilem Abdulaziz, Zhang Xi Xiang, and Qian Pei-Yuan. Species sorting during biofilm assembly by artificial substrates deployed in a cold seep system. *Scientific Reports*, 4:1–7, 1995.

[2] M. Legg, M.K. Yücel, I. Garcia de Carellan, V. Kappatos, C. Selcuk, and T.H. Gan. Acoustic methods for biofouling control: A review. *Ocean Engineering*, 103:237–247, 2015.

[3] Sibylle Abarzua and Sabiene Jakubowski. Biotechnological investigation for the prevention of biofouling. biological and biochemical principles for the prevention of biofouling. *Marine ecology progress series*, 123:301–312, 1995.

[4] On On Lee, Yong Wangand Renmao Tian, Weipeng Zhang, Chun Shum Shek, Salim Bougouffa, Abdulaziz Al-Suwailam, Zenon Batang, Wei Xu, Guang Chao Wang, Xixiang Zhang, Feras F. Lafi, Vladimir B. Bajic, and Pei-Yuan Qian. In situ environment rather than substrate type dictates micrmicro community structure of bbiofilm in a cold seep system. *scientific Reports*, 4:95–108, 2014.

[5] Sergery Dobretsov, Max Teplitski, and Valerie Paul. Quorum sensing in marine environment and its relationship to biofouling. *Biofouling*, 25:413–427, 2009.

[6] Maureen E Callow and James A Callow. *Marine biofouling: a sticky problem.* Biologist, 49, 2002.

[7] Shan Cao, JiaDao Wang, HaoSheng Chen, and DaRong Chen. Progress of marine biofouling and antifouling technologies. *Chinese Science Bulletin*, 56:598–612, 2010.

[8] MP Schultz, JA Bendick, ER Holm, and WM Hertel. Economic impact of biofouling on a naval surface ship. *Biofouling*, 27:87–98, 2011.

[9] David Carteau, Karine Vallée-Réhel, Isabelle Linossier, Francoise Quiniou, Romain Davy, Chantal Compère, Maxime Delbury, and Fabienne Fay. Development of environmentally friendly antifouling paints using biodegradable polymer and lower toxic substances. *Progress in Organic Coatings*, 77(2):485 – 493, 2014.

[10] Diego Meseguer Yebra, Sören Kiil, and Kim Dam-Johansen. Antifouling technology: past, present and future steps towards efficient and environmentally

friendly antifouling coatings. *Progress in Organic Coatings*, 50(2):75 – 104, 2004.

[11] S. Gollasch. The importance of ship hull fouling as a vector of species introductions into the north sea. *Biofouling*, 18:105–121, 2002.

[12] M. David and M. Perkovic. Ballast water sampling as a critical component of biological invasions risk management. *Marine Pollution Bulletin*, 49:313–318, 2004.

[13] Axel Rosenhahn, Sören Schilp, Hans Jürgen Kreuzer, and Michael Grunze. The role of inert surface chemistry in marine biofouling prevention. *Physical Chemistry Chemical Physics*, 12:4275–4286, 2010.

[14] Jeanette E. Gittens, Thomas J. Smith, Rami Suleiman, and Robert Akid. Current and emerging environmentally-friendly systems for fouling control in the marine environment. *Biotechnology Advances*, 31(8):1738 – 1753, 2013.

[15] Claude Alzieu. Environmental impact of tbt: the french experience. *The Science of the Total Environment*, 258:99–102, 2000.

[16] Yoichi Yonehara, Hiroshi Yamashita, Chikara Kawamura, and Kei Itoh. A new antifouling paint based on a zinc acrylate copolymer. *Progress in Organic Coatings*, 42:150 – 158, 2001.

[17] J.B. Kristensen, R.L. Meyer, and B.S. Laursen. Antifouling enzymes and the biochemistry of marine settlement. *Biotechnology Advances*, 26(5):471–481, 2008.

[18] M. Hoch. Organotin compounds in the environment, an overview. *Applied Geochemistry*, 16:719–743, 2001.

[19] Michele Ferrari, Alessandro Benedetti, Eva Santini, Francesca Ravera, Libero Liggieri, Eduardo Guzman, and Francesca Cirisano. Biofouling control by superhydrophobic surfaces in shallow euphotic seawater. *Colloids and Surfaces A: Physicochemical and Engineering Aspects*, 480:369–375, 2015.

[20] K. Schiff, D. Diehl, and A. Valkirs. Copper emissions from antifouling paint on recreational vessels. *Marine Pollution Bulletin*, 48:371–377, 2004.

[21] G.M. Douglas-Helders, C. Tan, and J. Carson. Effects of copper-based antifouling treatment on the presence of neoparamoeba pemaquidensis page, 1987 on nets and gills of reared atlantic salmon (salmo salar). *Aquaculture*, 221:13–22, 2003.

[22] L.D. Chambers, K.R. Stokes, and F.C. Walsh. Modern approaches to marine antifouling coatings. *Surface and Coatings Technology*, 201:3642–3652, 2006.

[23] Jason Fang, Antonios Kelarakis, Dongyan Wang, Emmanuel P. Giannelis, John A. Finlay, Maureen E. Callow, and James A. Callow. Fouling release nanostructured coatings based on pdms-polyurea segmented copolymers. *Polymer*, 51(12):2636 – 2642, 2010.

[24] Maja Wiegemann and Burkard Watermann. Biozidfreie bewuchsschutzmaßnahmen in der seeschiffahrt-forschungsstand und verfuegbare daten. *Rostock. Meeresbiolog. Beitrag*, 11:39–55, 2002.

[25] Katherine A. Dafforn, John A. Lewis, and Emma L. Johnston. Antifouling strategies: History and regulation, ecological impacts and mitigation. *Marine Pollution Bulletin*, 62:453–465, 2011.

[26] Manoj K. Chaudhury. Surface free energies of alkylsiloxane monolayers supported on elastomeric polydimethylsiloxanes. *Journal of Adhesion Science and Technology*, 7:669–675, 1993.

[27] Elisabete Almeida, Teresa C. Diamantino, and Orlando de Sousa. Marine paints: The particular case of antifouling paints. *Progress in Organic Coatings*, 59:2–20, 2007.

[28] Pascal Buskens, Marielle Wouters, Corne Rentrop, and Zeger Vroon. A brief review of environmentally benign antifouling and foul-release coatings for marine applications. *Journal of Coatings Technology and Research*, 10:29–36, 2013.

[29] Jelena Pavlicevic, Milena Spirkova, Oskar Bera, Mirjana Jovicic, Branka Pilic, Sebastian Balos, and Jaroslava Budinski-Simendic. The influence of zno nanoparticles on thermal and mechanical behavior of polycarbonate-based polyurethane composites. *Composites: Part B*, 60:673–679, 2014.

[30] Farzana Hussain, Mehdi Hojjat, Masami Okamoto, and Russell E.Gorga. Polymer-matrix nanocomposites, processing, manufacturing, and application: An overview. *Journal of Composite Materials*, 40:1511–1575, 2006.

[31] L.N. Niu, M. Fang, K. Jiao, L.H. Tang, Y.H. Xiao, L.J.Shen, and J.H. Chen. Tetrapod-like zinc oxide whisker enhancement of resin composite. *Journal of Dental Research*, 2010.

[32] C. Wan, H. Tan, S. Jin, H. Yang, M. Tang, and J. He. Highly conductive al-doped tetra-needle-like zno whiskers prepared by a solid state method. *Mater. Sci. Eng. B*, 150:203–207, 2007.

[33] Y.K. Mishra, S. Kaps, A. Schuchardt, I. Paulowicz, X. Jin, D. Gedamu, S. Freitag, M. Claus, S. Wille, A. Kovalev, S. Gorb, and R. Adelung. Fabrication of macroscopically flexible and highly porous 3d semiconductor networks from interpenetrating nanostructures by a simple flame transport approach. *Particle and Particle systems characterization*, 30:775–783, 2013.

[34] Xin Jin, Jan Strueben, Lars Heepe, Alexander Kovalev, Yogendra K. Mishra, Rainer Adelung, Stanislav N. Gorb, and Anne Staubitz. Joining the unjoinable: Adhesion between low surface energy polymers using tetrapodal zno linkers. *Advanced Materials*, 24(42):5676–5680, 2012.

[35] Xin Jin, Michael Götz, Sebastian Wille, Yogendra Kumar Mishra, Rainer Adelung, and Cordt Zollfrank. A novel concept for self-reporting materials: Stress sensitive photoluminescence in zno tetrapod filled elastomers. *Advanced Materials*, 2012.

[36] H. Papavlassopoulos, Y. K. Mishra, S. Kaps, I. Paulowicz, R. Abdelaziz, M. Elbahri, E. Maser, R. Adelung, and C. Röhl. Toxicity of functional nano-micro zinc oxide tetrapods: Impact of cell culture conditions, cellular age and material properties. *PLOS ONE*, 9:1342–1347, 2014.

[37] Stacy Sommer, Abdullah Ekin, Dean C. Webster, Shane J. Stafslien, Justin Daniels, Lyndsie J. VanderWal an d Stephanie E.M. Thompson, Maureen E. Callow, and James A. Callow. A preliminary study on the properties and fouling-release performance of siloxane-polyurethane coatings prepared from poly(dimethylsiloxane)(pdms) macromers. *Biofouling*, 26:961–972, 2010.

[38] D.G. Davies and G.G. Geesey. Exopolysaccharide production in biofilms: substratum activation of alginate gene expression by pseudomonas aeruguinosa. *Appl Environ Microbiol*, 59:860–867, 1995.

[39] Martin Wahl. Marine epibiosis. i. fouling and antifouling: some basic aspects. *Marine ecology progress series*, 58:175–189, 1989.

[40] A. Jain and N.B. Bhosle. Biochemical composition of the marine conditioning film: implications for bacterial adhesion. *Biofouling*, 25:13–19, 2009.

[41] I. Thome, M. E. Pettitt, M. Callow, J. Callow, M. Grunze, and A. Rosenhahn. Conditioning of surfaces by macromolecules and its implication for the

settlement of zoospores of the green alga ulva linza. *Biofouling*, 28:501–510, 2012.

[42] James A. Callow and Maureen E. Callow. Trends in the development of environmentally friendly fouling-resistant marine coatings. *nature communications*, 1251:1–10, 2011.

[43] J. A. Callow and M. E. Callow. *The Ulva Spore Adhesive System*. Biological Adhesives, Springer Berlin, 2006.

[44] Luigi Petrone. Molecular surface chemistry in marine bioadhesion. *Advances in Colloid and Interface Science*, 195-196(0):1 – 18, 2013.

[45] Kei Kamino. *Biological Adhesives, Barnacle Underwater Attachment*. Springer Berlin Heidelberg, 2006.

[46] A. B. D. Cassie and S. Baxter. Large contact angles of plant and animal surfaces. *Nature*, 155:21–22, 1945.

[47] R. Wenzel. Surface roughness and contact angle. *Ind. Eng. Chem*, 28:988–994, 1936.

[48] Daniel Owens and RC Wendt. Estimation of the surface free energy of polymers. *Journal of applied polymer science*, 13:1741–1747, 1969.

[49] Jan Genzer and Kirill Efimenko. Recent development in superhydrophobic surfaces and their relevance to marine fouling: a rewiev. *Biofouling*, 22:339–360, 2006.

[50] T. Young. An essay on the cohesion of fluids. *Phil. Trans. R. Soc. Lond*, 95:65–87, 1805.

[51] Robert Edward Baier. Surface behaviour of biomaterials: The theta surface for biocompatibility. *Journal of Materials science Materials in Medicine*, 17:1057–1062, 2006.

[52] Krishnan E. Chawla. *Composite materials: Science and Engineering*. Springer, 1998.

[53] Henry G. Schwartzberg and Richard W. Hartel. *Physical Chemistry of Foods*. Marcel Dekker, 1992.

[54] Rafael S. Peres, Elaine Armelin, Carlos Aleman, and Carlos A. Ferreira. Modified tannin extracted from black wattle tree as an environmentally friendly antifouling pigment. *Industrial Crops and Products*, 65(0):506–514, 2014.

[55] M.A. Champ. A rewiev on biofouling regulatory strategies, pending actions, related costs and benefits. *Sci Total Environ*, 258:21–71, 2000.

[56] R.L. Townsin. The ship hull fouling penalty. *Biofouling*, 19:9–15, 2003.

[57] Mao-Sheng Cao, Wei-Li Song, Wei Zhou, Da-Wei Wang, Ji-Li Rong, Jie Yuan, and Simeon Agathopoulos. Dynamic compressive response and failure behavior of fiber polymer composites embedded with tetra-needle-like zno nanowhiskers. *Composite Structures*, 92(12):2984 – 2991, 2010.

[58] Sergey Dobretsov, Hairong Xiong, Ying Xu, Lisa A. Levin, and Pei-Yuan Qian. Novel antifoulants: Inhibition of larval attachment by proteases. *Marine Biotechnology*, 9(3):388–397, 2007.

[59] Maria Salta, Julian A. Wharton, Yves Blache, Keith R. Stokes, and Jean-Francois Briand. Marine biofilms on artificial surfaces: structure and dynamics. *Environmental Microbiology*, 15:2879–2893, 2013.

[60] CM Waters and BL Bassler. Quorum sensing: cell-to-cell communication in bacteria. *Annu Rev Cell Dev Biol*, 21:319–346, 2005.

[61] Andrew J Scardino and Rocky de Nys. Mini review: Biomimetic model and bioinspired surface for fouling control. *Biofouling*, 27:73–86, 2011.

[62] Beibei Wang, Gang Wang, and Hui Wang. Synthesis and electrochemical investigation of hollow hierarchical metal oxide microspheres for high performance lithium-ion batteries. *Electrochimica Acta*, 156(0):1 – 10, 2015.

[63] Partha Majumdar and Dean C. Webster. Preparation of siloxane-urethane coatings having spontaneously formed stable biphasic microtopographical surfaces. *Macromolecules*, 38:5857–5859, 2005.

[64] Gerhard W. Becker and Dietrich Braun. *Kunststoff Handbuch Polyurethane*. Carl Hanser Verlag München Wien, 1993.

[65] Ian Clemitson. *Castable Polyurethane Elastomers*. Taylor and Francis Group, LLC, 2008.

[66] Junghwan Shin, Hironori Matsushima, Justin W. Chan, and Charles E. Hoyle. Segmented polythiourethane elastomers through sequential thiol-ene and thiol-isocyanate reactions. *Macromolecules*, 42:2394–3301, 2009.

[67] James E. Mark, Dale W. Schaefer, and Gui Lin. *The Polysiloxanes*. Oxford University Press, 2015.

[68] Emel Yilgör and Iskender Yilgör. Silicone containing copolymers: Synthesis, properties and applications. *Progress in polymer science*, 39:1165–1195, 2014.

[69] Y. K. Mishra, G. Modi, V. Cretu, V. Postica, O. Lupan, T. Reimer, I. Paulowicz, V. Hrkac, W. Benecke, and L. Kienle. Direct growth of freestanding zno tetrapod networks for multifunctional applications in photocatalysis, uv photodetection and gas sensing. *ACS Appl. Mater. Interfaces*, 7(26):14303–14316, 2015.

[70] Zhong Lin Wang. Zinc oxide nanostructure: growth, properties and applications. *Journal of Physics: Condensed Matter*, 16:829–858, 2004.

[71] R.F. Zhou, X.Y. Xu, H.T. Feng, D.Yan, H.J. Li, S. Cheng, and P.X. Yan. Morphology-controlled synthesis, growth mechanism, and optical properties of zno nanocombs/nanotetrapods. *Advanced Materials Research*, 97:960–964, 2010.

[72] Thessicar E. Antoine, Yogendra K. Mishra, James Trigilio, and Rainer Adelung. Prophylactic, therapeutic and neutralizing effect of zinc oxide tetrapod structures against herpes ssimple virus type-2 infection. *Antiviral Research*, 96:363–375, 2012.

[73] Tawatchai Charinpanitkul, Pat Nartpochananon, Thornchaya Satitpitakun, Jenifer Wilcox, Takafumi Setoand, and Yoshio Otani. Facile synthesis of tetrapodal zno nanoparticles by modified french process and its photoluminescence. *Journal of Industrial and Engineering Chemistry*, 18:469–473, 2012.

[74] C. Ronning, N. G. Shang, I. Gerhards, H. Hofsäss, and M. Seibt. Nucleation mechanism of the seed of tetrapod zno nanostructures. *Journal of Applied Physics*, 98(3):1–5, 2005.

[75] Hongqiang Wang, Caihong Li, Haigang Zhao, Ru Li, and Jinrong Liu. Synthesis, characterization, and electrical conductivity of zno with different morphologies. *Powder Technology*, 522(0):40–44, 2012.

[76] H.H.K. Xu, T.A. Martin, J.M. Antonucci, and F.C. Eichmiller. Ceramic whisker reinforcement of dental resin composites. *Journal of Dental Research*, 78:706–712, 1999.

[77] Hua Lei, Tao Xu, and Chuantao Gao. Characterization of the dispersion of tetrapod-like nano-zno whiskers in acrylic resin and properties of the nanocomposite coating system. *Journal of Coa*, 7:91–97, 2010.

[78] Chi Ma, Erfan Chen, Ting Sun, Shan Shi, and qinghong Fang. Preparation and characterization of tetrapod-shaped zno whisker filled polyurethane cross-linked epoxy/polyurethane damping composites. *Journal of Reinforced Plastics and Composites*, 31:1564–1575, 2012.

[79] Anran Zeng, Yuying Zheng, Yong Guo, Shangchang Qiu, and Lei Cheng. Effect of tetra-needle-shaped zinc oxide whisker (t-znow) on mechanical properties and crystallization behavior of isotactic polypropylene. *Materials & Design*, 34(0):691 – 698, 2012.

[80] Matthias Mecklenburg, Arnim Schuchardt, Yogendra K. Mishra, Sören Kaps, Rainer Adelung, Andriy Lotnyk, Lorenz Kienle, and Karl Schulte. Aerographite: Ultra lightweight, flexible nanowall, carbon microtube material with outstanding mechanical performance. *Advanced Materials*, 24:3468–3490, 2012.

[81] H. Iwanaga, M. Fujii, and S. Takeuchi. Growth model of tetrapodal zinc oxide particles. *Journal of Crystal Growth*, 134:275–280, 1993.

[82] S. Takeuchi, H. Iwanaga, and M. Fujii. Octahedral multiple-twin model of tetrapod zno crystals. *Philosophical Magazine A*, 69:1125–1129, 1994.

[83] Motoi Kitano, Takeshi Hamabe, and Sachiko Maeda. Growth of large tetrapod-like zno crystals ii. morphological considerations on growth mechanism. *Journal of Crystal Growth*, 108:277–284, 1991.

[84] Iris Hölken, Stefan Schröder, and Rainer Adelung. Characterization of silicon nanolayers deposited by plasma enhanced chemical vapor deposition on 3-d zno templates for hollow silicon microstructures. *IFMBE Proceedings*, 55:30–34, 2015.

[85] Helmut Guenzler and Michael Heise. *IR-Spektroskopie: eine Einführung*. VCH Verlagsgesellschaft mbH, Weinheim, 1975.

[86] Krzysztof Strzelec, Natalia Baczek, Sylwia Ostrowska, Karolina Wasikowska, Maagorzata Iwona Szynkowska, and Jacek Grams. Synthesis and characterization of novel polythiourethane hardeners for epoxy resins. *Comptes Rendus Chemie*, 15(11-12):1065 – 1071, 2012.

[87] Wolfgang Demtroeder. *Laserspektroskopie 2, Experimentelle Techniken*. Springer, 1986.

[88] Manfred Hess, Herbert Meier, and Bernd Zeh. *Spektroskopische Methoden in der organischen Chemie*. Georg Thieme Verlag, 2005.

[89] D.K. Chattopadhay and Dean C. Webster. Thermal stability and flame retardancy of polyurethanes. *Progress in Polymer Science*, 34:1068–1133, 2009.

[90] Peter J. Goodhew, John Humphreys, and Richard Beanland. *Electron microscopy and analysis*. Taylor and Francis, 2001.

[91] Roger Brown. *Handbock of Polymer Test: Short-Term Mechanical Tests*. Rapra Technology Limited, 2002.

[92] Amit Bandhyopadhyay and Susmita Bose, editors. *Characterization of Biomaterials*. Elsevier, Oxford, 2013.

[93] A.W. Adamson. *Physical chemistry of surfaces*. Wiley, New York, 1982.

[94] EV Gorb and SN Gorb. Physicochemical properties of functional surfaces in pitchers of the carnivorous plant nepenthes alata blanco (nepenthaceae). *Plant Biology*, 8:841–848, 2006.

[95] Ewa A. Papaj, Douglas J. Mills, and Sina S. Jamali. Effect of hardener variation on protective properties of polyurethane coating. *Progress in Organic Coatings*, 77(12, Part B):2086 – 2090, 2014. Studies of Coating and Polymer Films.

[96] D.K. Chattopadhyay and K.V.S.N. Raju. Structural engineering of polyurethane coatings for high performance applications. *Progress in Polymer Science*, 32:352–418, 2007.

[97] R. Oliveira, J. Azeredo, and P. Teixeira. The role of hydrophobicity in bacterial adhesion. *BioLine*, 8:11–22, 2011.

[98] Mercedes Camps, Aude Barani, Gérald Gregori, Agnès Bouchez, Brigitte Le Berre, Christine Bressny, Yves Blache, and Jean-Francois Briand. Antifouling coatings influence both abundance and community structure of colonizing biofilms: a case study in the northwestern mediterranean sea. *Applied and environmental microbiology*, 80:4821–4831, 2014.

[99] M. Chen, Y. Qu, L. Yang, and H. Gao. Structures and antifouling properties of low surface energy non-toxic antifouling coatings modified by nano-sio2 powder. *Sci. China Ser. B Chem.*, 51:848–852, 2008.

[100] R. Holland, T. M. Dugdale, R. Wetherbee, A. B. Brennan, J. A. Finlay, J. A. Callow, and Maureen E. Callow. Adhesion and motility of fouling diatoms on a silicone elastomer. *Biofouling*, 20 (6):323–329, 2004.

[101] Xin Jin, Sören Kaps, Xinwei Xu, Iris Hölken, Kristin Mess, Rainer Adelung, and Yogendra K. Mishra. Study of tetrapodal zno-pdms composites: A comparison of fillers shapes in stiffness and hydrophobicity improvements. *PLOS ONE*, 9:1–7, 2014.

[102] Linnea K. Ista, Maureen E. Callow, John A. Finlay, Sarah E. Coleman, Aleec C. Nolasco, Robin H. Simons, James A. Callow, and Gabriel P. Lopez. Effect of substratum surface chemistry and surface energy on attachment of marine bacteria and algal spores. *Applied and environmental microbiology*, 70 (7):4151–4157, 2004.

[103] Natalia Filip, Amanda Pustam, Veronica Ells, Kathleen M.T. Grosicki, Jin Yang, Ikenna Oguejiofor, Cory D. Bishop, M. Edwin DeMont, Truis Smith-Palmer, and Russell C. Wyeth. Fouling-release and chemical activity effects of a siloxane-based material on tunicates. *Marine Environmental research*, 116:41–50, 2016.

[104] Iris Hölken, Mathias Hoppe, Yogendra Kumar Mishra, Stanislav N. Gorb, Rainer Adelung, and Martina Baum. Complex shaped zno nano- and microstructure based polymer composites: Mechanically stable and environmentally friendly coatings for potential antifouling applications. *Physical Chemistry Chemical Physics*, 18:7114–7123, 2016.

[105] Iris Hölken, Mathias Hoppe, Martina Baum, and Rainer Adelung. Functional ecofriendly coatings for marine applications. *IFMBE Proceedings*, 55:250–253, 2015.

[106] Xue-Yong Ma and Wei-De Zhang. Effects of flower-like zno nanowhiskers on the mechanical, thermal and antibacterial properties of waterborne polyurethane. *Polymer Degradation and Stability*, 94(7):1103 – 1109, 2009.

[107] Lamia Saad and Mary Riad. Characterization of various zinc oxide catalysts and their activity in the dehydration de hydrogenation of isobutanol. *Journal of the Serbian Chemcial Society*, 73:997–1109, 2008.

[108] Geoffrey Swain. Redefining antifouling coatings. *Journal of Protective Coatings & Linings*, 16:26–35, 1999.

[109] M. Eashwar, G. Subramanian, P. Chandrasekaran, and K. Balakrishnan. Mechanism for barnacle-induced crevice corrosion in stainless steel. *Corrosion*, 48:608–612, 1992.

12 List of Publications

In order of authorship appearance and chronological sequence

1. **Iris Hölken**, Mathias Hoppe, Yogendra Kumar Mishra, Stanislav N. Gorb, Rainer Adelung, Martina Baum. *"Complex shaped ZnO nano- and microstructure based polymer composite: Mechanically stable and environmentally friendly coatings for potential antifouling applications".* Phys Chem Chem Phys. 18:7114 -7123, (2016).

2. **Iris Hölken**, Mathias Hoppe, Rainer Adelung, Martina Baum. *"Functional ecofriendly coatings for marine applications".* IFMBE Proc. 55:250-253 (2015).

3. **Iris Hölken**, Stefan Schröder, Rainer Adelung. *"Characterization of silicon nanolayers deposited by plasma enhanced chemical vapor deposition on 3-d zno templates for hollow silicon microstructures."* IFMBE Proceedings, 55:30-34 (2015).

4. **Iris Hölken**, Janno Jacobsen, Oleg Lupan, Volkan Filiz, Yogendra K. Mishra, Rainer Adelung, Martina J. Baum. *"Ecofriendly Polyurethane/silicone/ZnO composites as mechanically durable biofouling-release coatings. "*, submitted.

5. **Iris Hölken**, Gero Neubüser, Vasile Postica, Oleg Lupan, Martina Baum, Lars Bumke, Lorenz Kienle, Rainer Adelung1. *"Sacrificial template synthesis and properties of 3-D hollow-silicon microstructures."*, submitted.

6. Vasile Postica, **Iris Hölken**, Viktor Schneider, Victor Kaidas, Oleksandr Polonskyi, Vasilii Cretu, Ion Tiginyanu, Franz Faupel, Rainer Adelung, Oleg Lupan. *"Multifunctional device based on ZnO:Fe nanostructured films with enhanced UV and ultra-fast ethanol vapour sensing"* Materials Science in Semiconductor Processing. 49 20-33 (2016.)

7. Sebastian Wille, **Iris Hölken**, Galina Haidarschin, Rainer Adelung, Matthias Kern *"Biaxial flexural strength of new Bis-GMA/TEGDMA based composites with different fillers for dental applications."*, submitted.

8. Mohamed Kheir, Heinz Kreft, **Iris Hölken**, Reinhard Knöchel. *"On the physical robustness of RF on-chip nanostructured security."* Journal of Information, 19 4-5 (2014.)

9. Mohamed Kheir, Heinz Kreft, **Iris Hölken**, Reinhard Knöchel. *"Modeling, Methodologies and Tools for Molecular and Nano-scale Communications."*, *RF Nanostructured Security*, Springer nanocom (2014).

10. Xin Jin, Mao Deng, Sören Kaps, Xinwei Zhu, **Iris Hölken**, Kristin Mess, Rainer Adelung, Yogendra Kumar Mishra. *"Study of Tetrapodal ZnO-PDMS Composites: A Comparison of Fillers Shapes in Stiffness and Hydrophobicity Improvements."* PLoS ONE, 9 1-6 (2014).

11. Sören Gutekunst, **Iris Hölken**, Christine Selhuber, Rainer Adelung. *"Mikroporöses Polymertemplat für in vitro und in vivo Anwendungen"*, Granted patent, EP 15 16 6793.

13 List of supervised Bachelor- and Masterthesis

1. *"Influence of ceramic particles on the mechanical characteristics of different polymeric materials."* Master thesis, Patrick Harry Möseler, 2013.

2. *"Untersuchung der Haft- und Zugfestigkeit von tetrapodalen Zinkoxid-Kompositlacken auf Polyurethanbasis."* Bachelor thesis, Sascha Sachau, 2013.

3. *"Polyethylenterephthalat mit tetrapodalem ZnO."* Bachelor thesis, Lars Bunke, 2013.

4. *"Einfluss von sphärischem und tetrapodalem Zinkoxid sowie Zirkoniumoxid auf die mechanischen Eigenschaften von Polythiourethan."* Bachelor thesis, Carsten Hänel, 2014.

5. *"Untersuchung der chemischen und mechanischen Eigenschaften von variierenden Polythiourethan Stöchiometrien."* Bachelor thesis, Lea Katharina Jessen, 2014.

6. *"Einfluss von verschiedenen Zinkoxid-Mikrostrukturen auf mechanische und chemische Eigenschaften von Polythiourethan."* Bachelor thesis, Andreas Tonitzki 2014.

7. *"Stöchiometrievariation von Polythiourethan und der Einfluss von tetrapodalem Zinkoxid."* Bachelor thesis, Lukas Nickel, 2014.

8. *"Einfluss von tetrapodalem Zinkoxid auf die mechanischen Eigenschaften verschiedener Klebstoffe."* Bachelot thesis, Gerhard Wolfgang Niehus, 2014.

9. *"Einfluss der Oberflächenrauheit und verschiedener Zinkoxidmikrostrukturen auf die reflexiven Eigenschaften von Duroplasten."* Bachelor thesis, Marvin Faulhaber, 2015.

10. *"Einfluss der Materialwahl und Partikelgeometrie auf die Eigenschaften von Verbundwerkstoffen mit Anwendungspotenzial in der restaurativen Dentaltechnik."* Master thesis Galina Haidarschin, 2014.

11. *"Hydrogenated amorphous silicon thin films by plasma-enhanced chemical vapor deposition in argon diluted silane - Characterization and applications."* Master thesis, Stefan Schröder, 2015.

12. *"Mechanisch belastbare, umweltverträgliche fouling release Beschichtungen auf der Basis von Polythiourethan/Silikon-Kompositen."* Master thesis, Janno Jacobsen, 2015.

13. *"Influence of Zinc oxide on the mechanical parameters of several fiber reinforced polymers."* Master thesis, Thorben Waldmann, 2015.

14. *"Mechanical and chemical characterization of ZnO particle/polymer composites with potential of application as adhesion agent for Ti-6Al-4V components fabricated by metal injection molding."*, Bachelor thesis, Mona Milena Mintken, 2015.

15. *"Hollow silicon structures by plasma enhanced chemical vapor deposition for Li-Si batteries."* Master thesis, Lars Bunke, 2016.

14 Eidesstattliche Erklärung

Ich erkläre, dass ich meine Dissertation *Mechanically stable and environmentally friendly polymer/particle composites for the application as low-fouling coating in the marine sector* selbstständig und ohne Benutzung anderer als der angegebenen Hilfsmittel angefertigt habe und dass alle Stellen, die wörtlich oder sinngemäss aus Veröffentlichungen entnommen wurden, als solche kenntlich gemacht sind. Die Arbeit hat bisher in gleicher oder ähnlicher Form oder auszugsweise noch keiner Prüfungsbehörde vorgelegen und enstand unter Einhaltung der Regeln guter wissenschaftlicher Praxis der Deutschen Forschungsgemeinschaft.